Veðurstofa Íslands
Report

Ragnar Stefánsson, Françoise Bergerat, Maurizio Bonafede, Reynir Böðvarsson, Stuart Crampin, Kurt L. Feigl, Frank Roth, Freysteinn Sigmundsson, Ragnar Slunga

PRENLAB-TWO – first annual report
April 1, 1998 - March 31, 1999

VÍ-G99016-JA05
Reykjavík
August 1999

Veðurstofa Íslands
Report

Ragnar Stefánsson, Françoise Bergerat, Maurizio Bonafede, Reynir Böðvarsson, Stuart Crampin, Kurt L. Feigl, Frank Roth, Freysteinn Sigmundsson, Ragnar Slunga

PRENLAB-TWO - first annual report
April 1, 1998 - March 31, 1999

VÍ-G99016-JA05
Reykjavík
August 1999

Contents

1 Summary by coordinator 4

2 Main achievements as reported by the responsible institutions 9
- 2.1 IMOR.DG: Icelandic Meteorological Office, Department of Geophysics . . 9
- 2.2 UUPP.DGEO: Uppsala University, Department of Geophysics 9
- 2.3 UEDIN.DGG: University of Edinburgh, Department of Geology and Geophysics 10
- 2.4 GFZ.DR.DBL: Stiftung GeoForschungsZentrum Potsdam - Solid Earth Physics and Disaster Research - Earthquakes and Volcanism 10
- 2.5 NVI: Nordic Volcanological Institute 10
- 2.6 CNRS.TT: Centre National de la Recherche Scientifique, Delegation Paris B - Département de Géotectonique 11
- 2.7 UBLG.DF: University of Bologna, Department of Physics 11
- 2.8 CNRS.DTP: Centre National de la Recherche Scientifique, UPR 0234 - Dynamique Terrestre et Planétaire 11

3 Summary of scientific achievements by subprojects and tasks 12
- 3.1 Subproject 1: Monitoring crustal processes for reducing seismic risk 12
  - 3.1.1 Task 1: Database development and service for other scientists . . . 13
  - 3.1.2 Task 2: Enhancing the basis for alerts, warnings and hazard assessments 16
  - 3.1.3 Task 3: Modelling of near-field ground motions in catastrophic earthquakes in Iceland 17
  - 3.1.4 Task 4: Mobile stations for shear-wave splitting monitoring 17
  - 3.1.5 Task 5: Extending the alert system functions by real-time research 19
  - 3.1.6 Task 6: To prepare the SIL system and the alert system for use in other risk areas 19
  - 3.1.7 References 19
- 3.2 Subproject 2: Applying new methods using microearthquakes for monitoring crustal instability 20
  - 3.2.1 Task 1: Investigation and monitoring of stable/unstable fault movements 20
  - 3.2.2 Task 2: Statistical and adaptive analysis of space/time distribution of microearthquakes 33
  - 3.2.3 Task 3: Investigation of variations of relative crustal velocities . . . 39
  - 3.2.4 Task 4: Implementation of these new methods in a second EU country with high seismic risk 39
  - 3.2.5 References 39

3.3 Subproject 3: Shear-wave splitting to monitor in situ stress changes before earthquakes and eruptions 41
3.3.1 Task 1: Continuous monitoring of shear-wave splitting 41
3.3.2 Task 2: Analysis of shear-wave splitting measurements 46
3.3.3 Task 3: Establish shear-wave splitting map of Iceland 46
3.3.4 Task 4: Calibrate techniques and behaviour if and when changes are identified 46
3.3.5 Meetings 47
3.4 Subproject 4: Borehole monitoring of fluid–rock interaction 48
3.4.1 Task 1: Logging in borehole Nefsholt 49
3.4.2 Tasks 2, 3 and 4: Cross correlation of logs of the same type of this campaign to those from earlier campaigns, to search for changes in the rock physical parameters and the physical state of the rock around the borehole; Comparison of changes in logs of different type; and Comparison of changes in logs with changes in seismicity, fault plane solutions, shear-wave splitting, gravity, borehole strainmeter readings, crustal deformation, etc., to investigate if changes found in the borehole can be related to anomalies detected with other methods and if they can be related to the preparation of seismic activity. 52
3.4.3 Acknowledgements 63
3.4.4 References 63
3.5 Subproject 5: Active deformation determined from GPS and SAR 66
3.5.1 Subpart 5A: SAR interferometry study of the South Iceland seismic zone 66
3.5.2 Subpart 5B 67
3.5.3 Achievements 69
3.5.4 References 70
3.6 Subproject 6: Effects of stress fields and crustal fluids on the development and sealing of seismogenic faults 71
3.6.1 Task 1: Determine the paleostress fields associated with the test areas from fault-slip data 71
3.6.2 Task 2: Reconstruct the current stress fields associated with the test areas using: a) inversion of large sets of focal mechanisms of earthquakes, b) seismotectonic analysis of individual faults, c) geodetic analysis of present-day crustal displacements 73
3.6.3 Task 3: Investigate the potential effects of fluid pressure on the probability of faulting 78
3.6.4 Task 4: Make analytical and numerical studies of the nucleation and development of the seismogenic faults and fault populations . 78
3.6.5 Task 5: Make a detailed analysis of the Tjörnes fracture zone test site and its vicinity 79
3.6.6 Task 6: Analyze the fracture properties of Icelandic rock in the laboratory and to make theoretical, observational and experimental studies on the sealing of seismogenic faults with application to the test areas in Iceland 79
3.6.7 Meetings 84
3.6.8 Reference 84
3.7 Subproject 7: Theoretical analysis of faulting and earthquake processes . . 85

3.7.1 Subpart 7A: Ridge-fault interaction in Iceland employing crack models in heterogeneous media 85
3.7.2 Subpart 7B: Modelling of the earthquake related space–time behaviour of the stress field in the fault system of southern Iceland . 91

4 Papers directly associated with PRENLAB-2 116
4.1 Subproject 1 116
4.2 Subproject 2 117
4.3 Subproject 3 118
4.4 Subproject 4 118
4.5 Subproject 5 118
4.6 Subproject 6 119
4.7 Subproject 7 121

Summary by coordinator

The PRENLAB-2 project started in April 1998. It was a continuation of the PRENLAB project lasting from March 1, 1996, to February 28, 1998.

Meetings and workshops:

- A whole day planning workshop was organized during the XXIV EGS General Assembly in Nice, France, April 20-24, 1998.
- A PRENLAB-2 workshop was held in Húsavík, Iceland, July 30, 1998, attended by participants of the project in addition to several Icelandic and other European geophysicists, who are active in research related to the Húsavík fault. The workshop was also attended by representatives from the Húsavík community. The main topics of the workshop were to discuss the probability of a possibly impending destructive earthquake near Húsavík and action to be taken for research in the area as well as for enhancing the basis for providing warnings by increased monitoring.
- A third workshop was held on March 31, 1999, during the tenth biennial EUG meeting in Strasbourg, France.
- Papers related to progress and results of the project were presented at the above-mentioned workshops. Among other conferences where progress of PRENLAB-2 was presented were the XXVI ESC General Assembly in Tel Aviv, Israel, August 23-28, 1998, and the Early Warning Conference (EWC98) in Potsdam, Germany, September 7-11, 1998. At both of these meetings the coordinator presented ongoing work.

The project got a good start, based on a workprogramme where the various subprojects were detailed in subtasks. All the subprojects were started in accordance with the detailed programme, and all the subprojects have been carried out successfully in accordance with the general outlines in the workprogramme. Referring to the time schedule presented in the workprogramme for carrying out the individual tasks there are some slight modifications in the estimated end time for a few tasks, but in all cases there has been complemented by more work and more achievements in other tasks. The course of events in the earth made such modifications feasible and necessary. An earthquake sequence in the Hengill-Ölfus area in SW Iceland (Figure 1) and associated deformation lead to concentration of the PRENLAB-2 activity in this area which, because of these events, became the most significant part of the natural laboratory for the time being.

Among achievements of great significance for the project and for its outcome following can be mentioned:

- Most significant extension of the observational network is that continuous monitoring of deformation has been initiated in Iceland by the installation of continuous

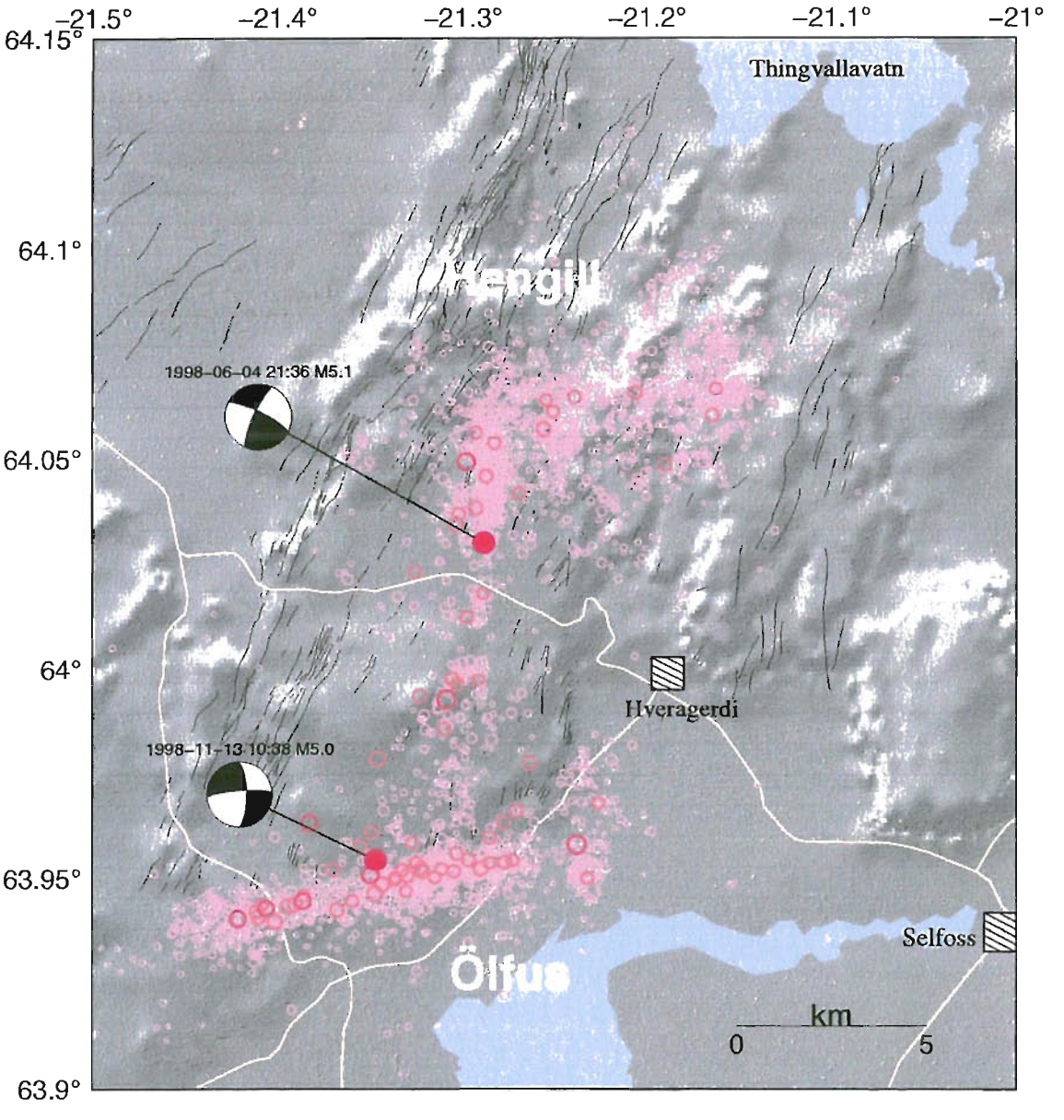

Figure 1. *The Hengill-Ölfus area is between the South Iceland seismic zone to the east, and the Reykjanes seismic zone and rift zone to the west. To NW goes the western volcanic zone. In this area there has been high seismic activity since 1994, which culminated in two earthquakes of magnitude 5 in 1998. These two earthquakes and related observed earth activity created research conditions which were of enormous significance for the progress of many parts of the PRENLAB-2 project.*

GPS at 4 sites in an area of high seismic activity in SW Iceland, the Hengill-Ölfus area (Figure 2). These four stations are linked to observations of two former continuous GPS stations, which create a reference base for the local deformation monitoring. Observations and research within the PRENLAB-2 project of this activity, and the need to understand what is going on in this area, made it possible to obtain funds to start this innovating work. On the other hand the continuous GPS measurements provide new constraints in using the activity in this area as a basis for modelling earthquake processes.

- The Hengill-Ölfus area has become a very significant test area for the PRENLAB-2 project. The reason is basically the very high seismic activity in this area since 1994. The seismic activity is a result of one hand the strain caused by transversal motion along the EW plate boundary in SW Iceland and on the other hand fluid expansion source near the center of the Hengill volcanic complex. It has been possible to carry out deformation measurements of various kinds to keep track of the deformation in addition to very detailed observations of frequent seismic swarms and individual earthquakes up to 5.1 in magnitude. Frequent observations by the SAR technology since 1993 show a steady uplift of 1.5 cm/year above a postulated pressure source at 7 km depth. The horizontal deformation is observed by GPS measurements, which have shown well constrained displacements related to individual earthquake sequences in two cases. The stress modifications related to both of these earthquakes have been observed. Thus an earthquake cycle has been observed from the start time of build-up of stress on June 4, 1998, in a large area towards concentration of stress in a focal region and foreshocks of an earthquake that occurred on November 13, 1998. After the earthquake of November 13, it was then observed how an E-W fault zone served as a stress guide, and how a sequence of earthquakes was observed related to that guide. This has consequences for modelling large South Iceland seismic zone earthquakes which occur in sequences of earthquakes reaching magnitude 7.

- Very significant progress in observing relation between shear-wave splitting delay and deviatoric stress build-up has resulted in a successful stress forecast. On basis of experience in studying shear-wave splitting time patterns in the very active Hengill-Ölfus area in SW Iceland a successful stress forecast was issued. After a general information about increase in stress in the Hengill area in SW Iceland at end-October 1998 a definite stress forecast was issued by Stuart Crampin of the PRENLAB-2 project, on November 10, 1998. This forecast said that an earthquake of magnitude 5-6 could occur anytime between the issuing of the forecast (M=5) and the end of February 1999 (M=6) if stress kept increasing. An earthquake of magnitude 5 occurred near the center of the region included in the forecast on November 13. Although this kind of forecast is far from being a complete earthquake prediction this is a step forward for short-term warnings. It does not in itself specify the epicenter of the earthquake. In this case the most likely epicenter could be guessed based on former activity, i.e. to complete an ongoing seismic cycle. The earthquake itself had foreshock activity, which in fact defined the most likely epicenter for the earthquake, and also indicated that it was impending within short. Of course it is always a question if a sequence of small earthquakes is a foreshock activity or not. However, the pattern of foreshock activity in this case and methods for automatic evaluations of observations which are ongoing on basis of the collected data, give hopes that procedures can be developed to complete such a stress forecast by observations

which aim at finding the place and the time of the earthquake nucleation before it ruptures.

- There has been significant progress in utilizing microearthquakes to study faulting processes. An automatic process has been developed to relate small earthquakes with individual fractures within an earthquake fault system on basis of very accurate relative location procedure and on basis of fault plane solutions. This opens the possibility to use microearthquakes to observe stable motion within a complicated fault system, changes of stresses and stress directions and earthquake nucleation. In seismology microearthquakes are mostly considered or treated as chaotic feature. By work in this field in the PRENLAB projects we are gradually discovering causality which in a physically understandable way relates the microearthquakes to each other and to larger events. Among significant indications of this mostly methodological study is that small earthquakes, also at depths near the base of the seismogenic crust, show similarity with hydraulic fracturing and changes in pore pressure that may have strong influence of the periodicity of and triggering of seismic activity.

- The current stress fields near the earthquake zones in North Iceland and in SW Iceland have been calculated by inverting a large number of fault plane solutions of the SIL system for stress. The average direction of extension was observed to be N66°E for the Tjörnes fracture zone in North Iceland and N143°E for the area around the South Iceland seismic zone. This is in good agreement with the postulated pattern of the general divergent plate motion in Iceland. This result is also a significant base for studying the spatial and temporal variations in stress directions, which are related to uneven transversal plate motion and fluid intrusions, and thus to earthquake occurrence.

- Significant results have been obtained in geodetical and geological studies near the Húsavík-Flatey transform fault zone in northern Iceland. A model has been created mainly on basis of repeated GPS measurements which describes the fault system as a locked system down to a depth of 10 km but with a right-lateral transversal motion of 5 mm/year below that depth along the fault, i.e. the same sense of motion expected in a large earthquake on the Húsavík fault. Thus stress seems to be fast built up by time increasing the probability of a large earthquake in this area. Studies of aspect ratio of fluid filled veins studied in exposed parts of the Húsavík-Flatey fault zone indicate that fluid overpressure above the minimum compressive principal stress is 20MPa.

- Modelling work has been ongoing within some of the subprojects to explain observations of various kinds. A model has been developed to explain the historical earthquake sequence of the South Iceland seismic zone. This is a simple model assuming that the earth is a homogeneous halfspace and the plate divergency is constant, and that all the strain energy or stress build-up comes from the plate motion. The stress build-up in elastic lithosphere caused by magma upwelling from a medium with different rheological parameters has been modelled and studied with respect to earthrealistic conditions. A model has been proposed, based on modelling results and observations, which assumes that a significant part of the stress build-up before earthquakes comes from heat energy from the mantle. It is probable that basaltic fluids extracted from the Iceland mantle plume at depth of less than 100 km play a significant role, not only in triggering earthquakes in Iceland but also a significant role in the stress build-up. Work has started to develop such a model.

The results of the very multidisciplinary approach of the project are described in following chapters. The work has been described in many papers, which are listed there. But results have also been presented at the following meetings besides the PRENLAB-2 workshops earlier described:

- The EU-Japan workshop on seismic risk, Chania, Crete, Greece, March 24-26, 1998.
- XXIII EGS General Assembly, Nice, France, April 20-24. 1998.
- XXVI ESC General Assembly, Tel Aviv, Israel, August 23-28, 1998.
- Early Warning Conference (EWC 98), Potsdam, Germany, September 7-11, 1998.
- Tenth biennial EUG meeting, Strasbourg, France, March 28 - April 1, 1999.
- Results and progress are described at the PRENLAB webpage:
  http://www.vedur.is/ja/prenlab/

Main achievements as reported by the responsible institutions

2.1 IMOR.DG: Icelandic Meteorological Office, Department of Geophysics

IMOR.DG coordinates the PRENLAB-2 project and is responsible for Subproject 1, *Monitoring crustal processes for reducing seismic risk.* The commitments of the first year of PRENLAB-2 workprogramme have been fulfilled as detailed below.

The coordinator and contractor is Ragnar Stefánsson. IMOR.DG is responsible for a significant extension of the seismic network, of build-up of the new continuous GPS network, and others available for the project, and for operating these networks. It has done extensive work in extending, refining and standardizing the earthquake databases as well as related databases on slow changes, where continuous borehole strainmeters are most significant, together with the emerging continuous GPS measurements. It serves the other subprojects with data from these databases. It is continuously working on with mapping of active faults, in studying seismicity patterns, in enhancing the alert system in Iceland, for developing and testing new algorithms and methods to cope with steadily increasing data acquisition and for enhancing the data automatic evaluation processes. It cooperates closely with all the other subprojects, and through its coordination all the subprojects were well linked together.

Work has been carried out according to the time schedule of the workprogramme, although there has been more achieved in the data collection than planned, both because of significant earthquake sequences that had to be very well observed and because the observational system has expanded more than had been planned, also because of these earthquakes.

2.2 UUPP.DGEO: Uppsala University, Department of Geophysics

UUPP.DGEO is responsible for Subproject 2, *Applying new methods using microearthquakes for monitoring crustal instability.*

The contractor Reynir Böðvarsson, UUPP.DGEO, has fulfilled its commitments in the first year schedule of the workprogramme. Very significant results have been developed in Task 1: *Investigation and monitoring of stable/unstable fault movements* as detailed in Chapter 3. Task 2: *Statistical and adaptive analysis of space/time distribution of microearthquakes* has mainly been aimed to group evaluations of microearthquakes for inversion in time and space on stresses and stress changes. This task is well on schedule. Software has been prepared to handle Task 3: *Investigation of variations of relative crustal velocities.* Only Task 4 has not been carried out in the way, which was planned. The task is implementation of these new methods in a second EU country with high seismic risk. The plan was to implement these methods within the Seismological Laboratory, University

of Patras in Greece. However, the leading scientist in Patras, which was a contact person in this cooperation moved to a new position in Athens, and it has not been successful so far to re-establish the practical contact for carrying out the implementation. On the other hand the necessary preparations for being able to apply the SIL procedures at other sites have been in good advance by the contractor, both in cooperation with Subproject 1 but also in connection with the build-up of a SIL system in Sweden. The build-up of the SIL system in Sweden has to be considered a great advance for the subproject and will further make it more feasible to export the SIL procedures to other sites.

In all tasks above the closest cooperator was IMOR.DG. There has also been cooperation with UEDIN.DGG in using microearthquakes for studying shear-wave splitting.

2.3 UEDIN.DGG: University of Edinburgh, Department of Geology and Geophysics

UEDIN.DGG was responsible for Subproject 3, *Shear-wave splitting to monitor in situ stress changes before earthquakes and eruptions.* The contractor is Stuart Crampin. UEDIN.DGG has fulfilled its commitments in the workprogramme as a whole. Howeves frequent earthquakes in the Hengill-Ölfus area in SW Iceland made it significant to change the emphasis of individual tasks to be carried out. This is reflected in Chapter 3, in detailing the work carried out. It is described in 4 tasks which are to some extent different from the definitions in the workprogramme. All the problems addressed in the workprogramme are however addressed in the work carried out. The emphasis on continuous survey of shear-wave splitting at a few stations in SW Iceland and stress forecasts based on that was a significant and correct modification, which are significant for the success of Subproject 3 and for the PRENLAB project as a whole. It is to be noted that considerably less money has been spent for this project during the first year than half of what is available for all the project. The reason for this is shift in emphasis in carrying out the different tasks, because of the high seismic activity in SW Iceland, and stress forecasts which were carried out. This led to some shift of working hours and other costs to the later half of the project.

In all tasks above there was a close cooperation with IMOR.DG as concerns basic evaluation of and in providing data and applying the forecasts.

2.4 GFZ.DR.DBL: Stiftung GeoForschungsZentrum Potsdam - Solid Earth Physics and Disaster Research - Earthquakes and Volcanism

GFZ.DR.DBL is responsible for Subproject 4 as a whole, *Borehole monitoring of fluid–rock interaction.* Commitments of the workprogramme have been satisfactorily fulfilled. Tasks 1-4 are in direct continuation of the loggings carried out during the PRENLAB project, and have been successfully continued during PRENLAB-2, significant results obtained and reported. Task 5 starts in the second year of PRENLAB-2.

2.5 NVI: Nordic Volcanological Institute

NVI is responsible for Subproject 5, *Active deformation determined from GPS and SAR.* NVI has fulfilled its commitments in the workprogramme, with some modifications in the

carrying out the individual tasks.

The Subproject was divided into two Subparts, 5A and 5B.

Subpart 5A, *SAR interferometry study of the South Iceland seismic zone*, was managed by associated contractor Kurt Feigl of the CNRS.DTP in close cooperation with Freysteinn Sigmundsson, contractor of NVI. Subpart A has been carried out with some modifications as compared to the workprogramme. In accordance with the high seismic activity in the Hengill-Ölfus area at the western end of the South Iceland seismic zone, the main emphasis was on observing this activity with the SAR technology.

Subpart 5B, *GPS measurements of absolute displacements*, was managed by the contractor Freysteinn Sigmundsson of NVI, in cooperation with Páll Einarsson, subcontractor, Science Institute, University of Iceland, and with IMOR.DG. The work has basically been carried out in accordance with workprogramme although there was some reorientation of priorities in accordance with obtained results and because of necessary concentration of activities to the Hengill-Ölfus area because of the intensive seismic and deformation processes there.

2.6 CNRS.TT: Centre National de la Recherche Scientifique, Delegation Paris B - Département de Géotectonique

CNRS.TT is responsible for Subproject 6, *Effects of stress fields and crustal fluids on the development and sealing of seismogenic faults*, and has fulfilled its commitments in the workprogramme. All the tasks have been carried out in accordance with the time table, by the contractor Francoise Bergerat of CNRS.TT, and the subcontractors Jacques Angelier of the CNTRS.TT, Ágúst Guðmundsson of the University of Bergen, Norway, Thierry Villemin of the Université de Savoie, France and Philip Meredith, University College London, United Kingdom, and their coworkers.

2.7 UBLG.DF: University of Bologna, Department of Physics

UBLG.DF was responsible for Subproject 7, *Theoretical analysis of faulting and earthquake processes*. This Subproject is divided in two Subparts, 7A and 7B.

Subpart 7A, *Ridge-fault interaction in Iceland employing crack models in heterogeneous media*, is managed by contractor Maurizio Bonafede of UBLG.DF. Subpart 7A has been carried out in accordance with the workprogramme, by the contractor and his coworkers at the same institute.

Subpart 7B, *Modelling the earthquake related space-time behaviour of the stress field in the fault system of southern Iceland*, was managed by associated contractor Frank Roth of GFZ.DR.DBL (see 2.4). Close cooperation was with IMOR.DG. Subpart 7B has been carried out in accordance with the workprogramme.

2.8 CNRS.DTP: Centre National de la Recherche Scientifique, UPR 0234 - Dynamique Terrestre et Planétaire

See 2.5.

Summary of scientific achievements by subprojects and tasks

3.1 Subproject 1: Monitoring crustal processes for reducing seismic risk

Coordinator/contractor:
Ragnar Stefánsson
Department of Geophysics
Icelandic Meteorological Office
Bústaðavegur 9
150 Reykjavík
Iceland
Tel: +354-560-0600
Fax: +354-552-8121
E-mail: ragnar@vedur.is

Reseachers:
Kristján Ágústsson
E-mail: kri@vedur.is
Þóra Árnadóttir
E-mail: thora@vedur.is
Pálmi Erlendsson
E-mail: pe@vedur.is
Gunnar B. Guðmundsson
E-mail: gg@vedur.is
Páll Halldórsson
E-mail: ph@vedur.is
Steinunn S. Jakobsdóttir
E-mail: ssj@vedur.is
Einar Kjartansson
E-mail: eik@vedur.is
Sigurður Th. Rögnvaldsson
E-mail: sr@vedur.is
Þórunn Skaftadóttir
E-mail: thorunn@vedur.is
Bergþóra S. Þorbjarnardóttir
begga@vedur.is
Barði Þorkelsson
E-mail: bardi@vedur.is
All at Department of Geophysics
Icelandic Meteorological Office

3.1.1 Task 1: Database development and service for other scientists

3.1.1.1 Task 1.1: Data collection

Much more work was carried out in data collection and data evaluation than anticipated when the workprogramme was prepared.

This was partly due to general extensions of the applied monitoring systems, but partly due to very high seismic and deformation activity in the Hengill-Ölfus area in SW Iceland (Figure 1). Enormously significant data were collected in this area which contain earthquake premonitory activity and short-term precursors to earthquakes, especially in June 1998 and in November 1998. The data collection and evaluations carried out in relation to this activity are of basic significance in understanding crustal processes leading to earthquakes, for modelling motions in an earthquake and for modelling the observed large-scale stress modifications that were caused by the two earthquakes.

The extension of the SIL seismological acquisition and evaluation system, the SIL system, has continued during the year. The number of operating SIL stations was increased from 33 to 37.

Quite often during high earthquake activity the incoming data of small earthquakes is so high in the SIL system that the communication system and the computers have problems to cope with the data stream, and jams were created, which sometimes could delay the data, so the system evaluation was delayed. This could even lead to loss of data. As it is very significant to gather earthquake data down to the smallest earthquakes, that provide information about crustal conditions, it was necessary to design and implement more effective procedures for doing this. For this purpose a new compresssion algorithm was developed for the system, i.e. the bit compression. This algorithm compresses the data very effectively at the site stations and the compressed data go directly into the evaluation procedures at the SIL center, much faster than the earlier procedures.

A new format for saving the digital earthquake waveform data will be described shortly in following:

The output of the seismometer digitizer is a series of integer values. The sample-to-sample variation is usually much less than the maximum values, which for most of SIL stations are between +/-3276800. In the AH format which was used by the SIL software, each value is stored in 32 bits.

A reduction in size of the data files of approximately a factor of 5 is achieved by storing the sample-to-sample variation in packed, variable size integers.

The access to data is thus much faster than to data that is compressed using general purpose compression programs such as gzip or compress and the files are typically 2-3 times smaller.

This new bit-compress format (bc) was incorporated into the data aqusition in the SIL system during the autumn of 1998. The software on each station writes in ascii files in format that is called the SIL format. The program bc-tool can convert these files to the bc format and back. All information in the headers is preserved.

The bc files are then transfered to the SIL center (currently using uucp). All files from each day are kept together, with a directory for each station. An index file that contains a list af all waveforms for each day is maintained.

The index files are stored on binary form, and are sorted by the programs that read them. A major performance bottleneck in previous version resulted from sorting index files on ascii form, each time that waveform data arrived.

The new software is able to keep up with much larger levels of earthquake activity

than previous software. Because the routines that read and uncompress the data are very fast and files are small, performance of all programs that use the data has been improved.

A build-up of continuous GPS monitoring at 4 sites in SW Iceland is a significant step forward for the PRENLAB-2 project data collection. It is significant for the watching the presently high seismic rate and deformation rate in the area. Four stations were installed in the Hengill-Ölfus area as shown in Figure 2.

The project of building the continuous GPS measurements is a collaboration between IMOR.DG, NVI, and the Science Institute, University of Iceland, with significant support from PRENLAB-2. The funding for purchasing the equipment comes from the Icelandic government and the Reykjavík Municipal District Heating Service. The high activity in the Hengill-Ölfus region, and the significant research that currently is being carried out there made it possible to obtain Icelandic funding to buy equipment for this purpose.

The instruments used are Trimble 4700 CORS dual frequency receivers and Trimble Choke Ring antennas, for the best data quality.

The data is collected onto a PC computer using the Trimble software Universal Reference Station (URS). The Trimble 4700 receivers are a new product, so communication software for remote downloading is still not available from Trimble. We are currently investigating options for downloading the data via phone lines, for real-time monitoring, but may have to write our own software for that. Currently operators are driving out to the stations once a week and copying data onto a laptop, and bringing it back to Reykjavík for processing. The station at OLKE is in a remote area and the data is collected onto the receiver, as it is not connected to a computer yet.

The data processing is done at IMOR.DG, using the Bernese version 4.0 software from University of Berne. We are using data from the IGS station Reykjavík (REYK) as a reference station. The data from the network and results will be made available via the internet. The URL is http://www.vedur.is/ja/gps.html.

A station for continuous monitoring of conductivity at depth in the crust by MT method was installed at the SIL station HAU, at the eastern end of the South Iceland seismic zone, and the data acquistion is merged with the SIL data acquisition. Changes of conductivity in the crust may provide significant information about conditions in the seismic zones.

3.1.1.2 Task 1.2: Data access

Work which started within the PRENLAB project of creating an earthquake database with easy accesss has continued and accelerated during PRENLAB-2. The database structure used is INGRES.

This database now contains SIL network seismic data since 1991 which can be accessed through the Internet, by search in a simple relational database table. This table has hypocenter and magnitude information on all SIL measured earthquakes since July 1991 that have been manually checked, approximately 140000 earthquakes. Search options for area, magnitude and time are provided.

The preparatory work for a general easy accessible relational database for all seismic data is completed and the inclusion of data in the database is in good progress.

Included in the database is already now or will be within short:

- Information based on historical information. This information has been gathered over the years and will be inserted into the database.

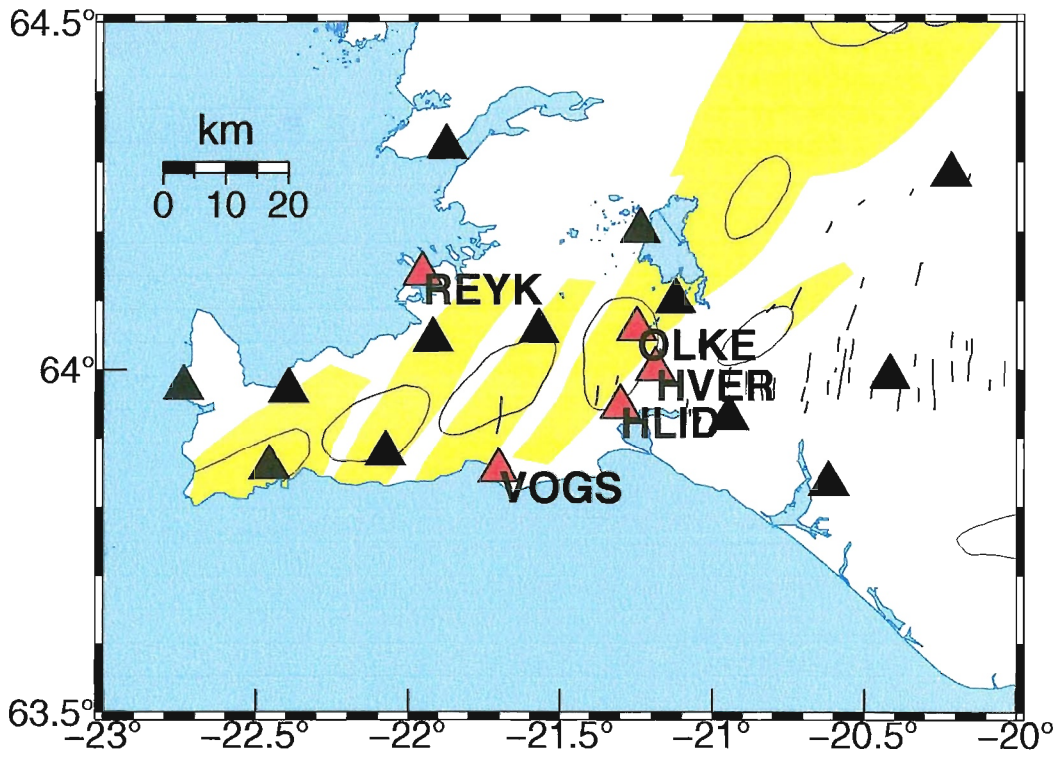

Figure 2. *The figure shows the location of the new GPS network in SW Iceland, for continuous monitoring of deformations. Red triangles show the continuous GPS stations and the black triangles are the SIL seismic stations in the area.*

- Information on instrumentally measured earthquakes from 1926 to 1991. Available parameter data for earthquakes during the period 1926-1973 has been extracted from catalogues and is currently being inserted into relational database tables. Information on earthquakes that were felt but not recorded is also inserted into the tables.

- Information on SIL parameter data, 1991-present. The data have been checked and updated to ensure compatible processing from different recording systems. The insertion of parameter data, both observed and derived, into relational database tables is nearly up-to-date. Information on approximately 140000 earthquakes is now accessible through a standardized SQL database.

- Information on station parameters, such as coordinates, instrument characteristics and time corrections at each respective time of measuring. Relational database tables have been developed.

Beside preparing this general database much work has been carried out in providing the various other subprojects with earthquake data, in accordance with the progress of the research work.

3.1.2 Task 2: Enhancing the basis for alerts, warnings and hazard assessments

This work has been carried out in relation to providing information and warnings about ongoing activity. It has been linked with increased probability of the occurrence of large earthquakes, on one hand in SW Iceland and on the other hand near the Húsavík earthquake fault in North Iceland.

Very much work which concerns all aspects of Task 2 has been devoted to the Hengill-Ölfus area in SW Iceland. An earthquake sequence has been ongoing in this region since 1994, related on one hand to E-W transversal motion across the plate boundary, and on the other to an expansion source at 8-10 km depth below the Hengill area. The largest earthquakes of this sequence took place on June 4, 1998, magnitude 5.1, and on November 13, 1998, magnitude 5. The sequence of events, as observed seismologically and geodetically related to the time period of these events is of enormous significance for understanding, build-up of stress before earthquakes and for understanding the nucleating process or the short-term precursor activity before earthquakes (Figure 3) (Ágústsson 1998, Rögnvaldsson et al. 1998, Tryggvason et al. 1999).

After the earthquake of June 4, 1998, and the following earthquake sequence and deformation, stress was modified up to 50 km distance to east and west from the epicenter, along the E-W plate boundary. This appeared in widespread seismic activity, but also in increases in shear-wave splitting delay time, which lead to earthquake forecast (Crampin et al. 1999).

Work which is concerned with the possibility of an impending large earthquake, i.e. earthquake of magnitude 7, near the town Húsavík in North Iceland, was discussed at a special PRENLAB-2 workshop in Húsavík, July 30, 1998. Work is going on under several subprojects with risk related research in this region. Subproject 1 has besides providing seismological data, taken initiative in planning new observations to be made in the area, on basis of the results of ongoing work. The objective is to provide observations which can create a better basis for modelling of the Húsavík earthquake, for an improved hazard

assesssment and for better real-time monitoring possibly involving short-term warnings (Stefánsson et al. 1998).

Work is ongoing within Subproject 1 regarding the Tjörnes fracture zone in general (Rögnvaldsson et al. 1998).

3.1.3 Task 3: Modelling of near-field ground motions in catastrophic earthquakes in Iceland

The M=5.1 earthquake June 4, 1998, on Hellisheiði, in the Hengill area provided excellent geodetic and seismic data for modelling of near-field displacements in the largest earthquake in the area since 1955.

A large earthquake swarm started in the Hengill area on June 3, 1998, and culminated with a M=5.1 earthquake on June 4, 1998, at 21:37 GMT, followed by thousands of aftershocks. Geodetic measurements were being done by the National Energy Authority at the time of the earthquake and repeated measurements begun on June 5, 1998. The data were processed by Sigrún Hreinsdóttir at the Science Institute and NVI, using the IGS station in Reykjavík as a reference station, and CODE orbits. That provided the surface displacements in the ITRF96 reference frame.

The surface displacements have been used by Þóra Árnadóttir at IMOR.DG to construct a dislocation model for the earthquake. The dislocation model is a rectangular fault with uniform slip model in an elastic half-space. The best fit model found by nonlinear optimization algorithm, is a vertical N-S fault with 30 cm right-lateral strike slip motion and 15 cm dip-slip motion, down to west. The fault is about 11 km long, and extends from the surface down to about 2 km depth. The location of the fault model fits well with the location and focal mechanism of the main shock and locations of aftershocks, although these are not used to constrain the model. The model fits about 96% of the data signal (Figure 3).

The main shock ruptured a N-S structure, and could therefore be similar to historical events that have occurred in the South Iceland seismic zone, where a M=7 event is currently anticipated. As there is no instrumental data for the large historical events it is important to study these recent earthquakes, to better understand the mechanism of the larger events.

Preparations are ongoing for modelling near-field ground motions expected in large South Iceland seismic zone earthquakes on basis of the result of the modelling above, on basis of strong motion records and records of the SIL network for the earthquake of June 4, described above, and on basis of historical documentation of near-field destruction in historical South Iceland seismic zone earthquakes.

3.1.4 Task 4: Mobile stations for shear-wave splitting monitoring

The objective of this task is to investigate more in detail the shear-wave splitting effects of the crust and the spatial distribution of the observed anisotropy. 7 three-component mobile seismometers of ORION type were borrowed for this purpose from Uppsala University. The seismometers were operated as a dense network near to the SIL station SAU for this purpose, from May 13 to July 5, 1998, and again from July 23 to August 13. This is in the middle of the South Iceland seismic zone and it is very significant for future use of shear-wave splitting methods in this earthquake prone area to carry out this study. Data were collected for this period and preparations are going on to evaluate these data. It has taken some work to merge these data with the SIL data evaluation system algorithms.

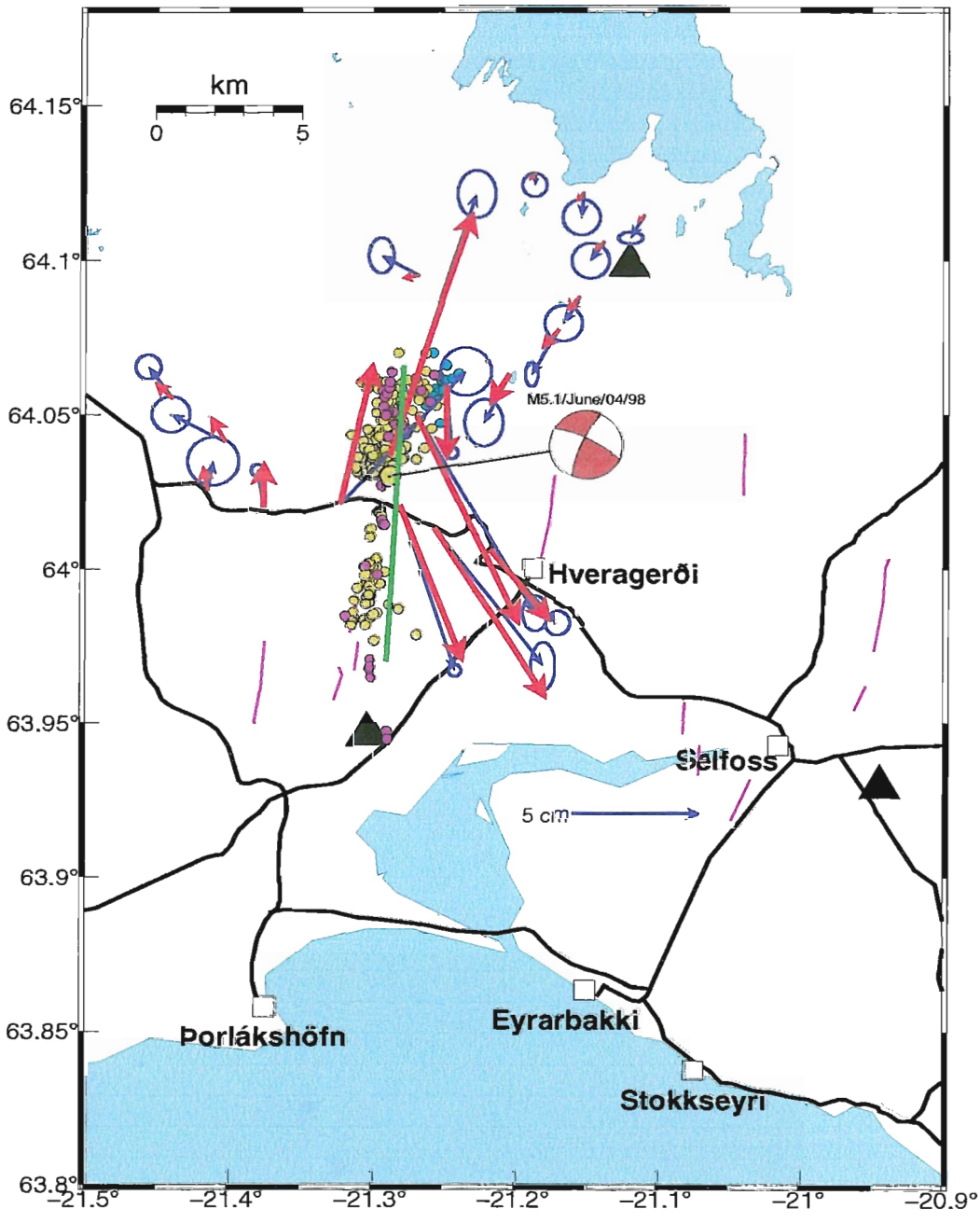

Figure 3. *The figure shows the surface projection of the best fit model (green line), and the observed and calculated displacements. The observed displacements are shown in blue with 95% confidence ellipses. The calculated displacements are shown in red. The figure also shows the main shock location and focal mechanism, and the locations of the earthquakes on June 3 (light blue), June 4 (yellow) and June 5 (pink).*

This is necessary for best results, and so the high level evaluation processes of the SIL system can be utilized in full. The course of events in the Hengill-Ölfus area has delayed somewhat to finish up this project.

3.1.5 Task 5: Extending the alert system functions by real-time research

Although this task is planned for the second year of the project it has, however, been going on to some degree following the course of seismic events in the Hengill-Ölfus area, and in efforts to try to provide useful warnings for a possibly large impending earthquake.

3.1.6 Task 6: To prepare the SIL system and the alert system for use in other risk areas

The main objective here was to prepare the SIL system for possibly implementing it at Patras in Greece led by Subproject 2. This has not started because the contact in Patras failed. However, considerable work has been carried out to enhance the SIL system functions (Böðvarsson et al. 1999), as described under Task 1 above. It can also be mentioned here that installation of SIL type network in Sweden includes many refinements based on experiences in operating and continuously developing the SIL system in Iceland (Böðvarsson et al. 1999).

3.1.7 References

Ágústsson, K. 1998. Jarðskjálftahrina á Hellisheiði og í Hengli í maí-júlí 1998. *Greinargerð Veðurstofu Íslands* VÍ-G98040-JA06. Report, Icelandic Meteorological Office, Reykjavík, 35 pp.

Rögnvaldsson, S.Th., Þ. Árnadóttir, K. Ágústsson, Þ. Skaftadóttir, G.B. Guðmundsson, G. Björnsson, K.S. Vogfjörð, R. Stefánsson, R. Böðvarsson, R. Slunga, S.S. Jakobsdóttir, B. Þorbjarnardóttir, P. Erlendsson, B.H. Bergsson, S. Ragnarsson, P. Halldórsson, B. Þorkelsson & M. Ásgeirsdóttir 1998. Skjálftahrina í Ölfusi í nóvember 1998. *Greinargerð Veðurstofu Íslands* VÍ-G98046-JA09. Report, Icelandic Meteorological Office, Reykjavík, 19 pp.

Tryggvason, A., S.Th. Rögnvaldsson & Ó.G. Flóvenz 1999. Three-dimensional imaging of the P- and S-wave velocity structure and earthquake locations beneath Southwest Iceland. *J. Geophys. Res.*, submitted.

Crampin, S., Volti, T. & R. Stefánsson 1999. A successfully stress-forecast earthquake. *Geophys. J. Int.*, in press.

Stefánsson, R., S.Th. Rögnvaldsson, P. Halldórsson & G.B. Guðmundsson 1998. PRENLAB workshop on the Húsavík earthquake, July 30, 1998. *Greinargerð Veðurstofu Íslands* VÍ-G98032-JA04. Report, Icelandic Meteorological Office, Reykjavík, 5 pp.

Rögnvaldsson, S.Th., Á. Guðmundsson & R. Slunga 1998. Seismotectonic analysis of the Tjörnes fracture zone, an active transform fault in North Iceland. *J. Geophys. Res.* 103, 30117-30129.

Böðvarsson, R., S.Th. Rögnvaldsson, R. Slunga & E. Kjartansson 1999. The SIL data acquisition system - at present and beyond year 2000. *Phys. Earth Planet. Inter.* 113, 89-101.

3.2 Subproject 2: Applying new methods using microearthquakes for monitoring crustal instability

Contractor:

Reynir Böðvarsson
Department of Geophysics
Uppsala University
Villavägen 16
S-752 36 Uppsala
Sweden
Tel: +46-471-182378
Fax: +46-471-501110
E-mail: rb@geofys.uu.se

Researchers:

Ragnar Slunga
Department of Geophysics
Uppsala University
Villavägen 16
S-752 36 Uppsala
Sweden
Tel: +46-471-182378
Fax: +46-471-501110
E-mail: ragnar@geofys.uu.se

Björn Lund, Ph.D. student
E-mail: bl@geofys.uu.se
Zaher Hossein Shomali, Ph.D. student
E-mail: hs@geofys.uu.se
Both at Department of Geophysics
Uppsala University

Reynir Böðvarsson is 40% funded by EC and Ragnar Slunga 20%.

3.2.1 Task 1: Investigation and monitoring of stable/unstable fault movements

3.2.1.1 Methods

The microearthquake analysis which is used in this task consists of inversion for fault plane solutions by use of spectral amplitudes and first motion directions (Slunga 1981, Rögnvaldsson and Slunga 1993, 1994), and multievent location based on high accuracy relative timing of the phase arrivals (Slunga et al. 1995). Both these algorithms are in routine use at the Icelandic seismological network within the PRENLAB-2 project. The multievent analysis aiming at inversion for the rock stress tensor is discussed in Task 2.

The fault plane solutions do not consist of a unique fault plane solution for each event, but of a number of different fault plane solutions consistent with the observed spectral amplitudes and first motion directions. In addition each acceptable fault plane solution consists of two possible fault planes oriented such that the slip direction on one of the

plane is normal to the other plane. Together this complicates the task to achieve a clear picture of what crustal deformation (fault movements) the microearthquakes are part of.

In a number of cases the relative locations of closely spaced similar microearthquakes have shown that such events often are situated on a plane which can be interpreted as the fault plane. This interpretation has also a sound physical basis as a slip on part of a fault will increase the instability at neighbouring areas if we have a rather similar rock stress tensor over the fault prior to the slip.

The most simple interpretation of a group of microearthquakes is to look for microearthquakes located along a plane and having acceptable fault plane solutions where one of its two possible fault planes coincides with the spatial plane. If one also requires that the slip directions on the plane are similar the process may be used to achieve a single fault slip solution for each microearthquake on the plane. The range of acceptable fault plane solutions has been reduced with no remaining ambiguity for the events of the consistent group.

In practice one will expect complications as the range of acceptable fault plane solutions may be large and random fits may occur. We will here give examples of multievent microearthquake where this procedure for reducing the ambiguity of the fault plane solutions have been used.

3.2.1.2 The microearthquakes of the example

In Figure 4 a map of the epicenters and a depth section of the hypocenters are shown. The events have been located with the multievent location algorithm based on relative timing of the arrivals. The figure includes 470 events during November 13, 1998. The events are distributed with rms less than 800 m from a plane striking N77°E dipping 87°. This group of events are mainly aftershocks to a ML=5 earthquake. The ML values are in the range 0.5-2.0 for most of the events.

Surface fractures in the area have roughly N-S directions. In Figure 5 the fit of the fault plane solutions to N-S fault orientation is illustrated by showing the fault plane out of the acceptable fault plane solutions being closest to a vertical N-S fault orientation. Thus for each event only one fault plane is shown as a circular "coin". The median angular deviation of these planes is 11° from the vertical N-S orientation.

It is, however, obvious that far from all events have acceptable fault plane solutions fitting a N-S striking plane. As a comparison Figure 6 is a similar figure but now illustrating the fit to a N79°E striking plane. The median deviation is here 13° and it is obvious that many events are not consistent with such a fault plane orientation.

Figure 7 shows the fault plane solutions (double-couple source moment tensors) as in Figure 5 but represented by the subsidiary directions of compression and tension with the method proposed by Slunga et al. 1984. Note that the horizontal stress directions are very consistent and dominated by SW-NE compression. If we look on the source moment tensors along the direction of compression (Figure 8), one can see that the events have a small normal faulting component in addition to the generally dominating strike-slip component.

3.2.1.3 Automatic relating of the earthquakes to individual fractures

We applied an automatic version of grouping the events based on their locations (a plane) and the consistency of their acceptable fault plane solutions (plane orientation similar to the spatial plane and similar slip directions).

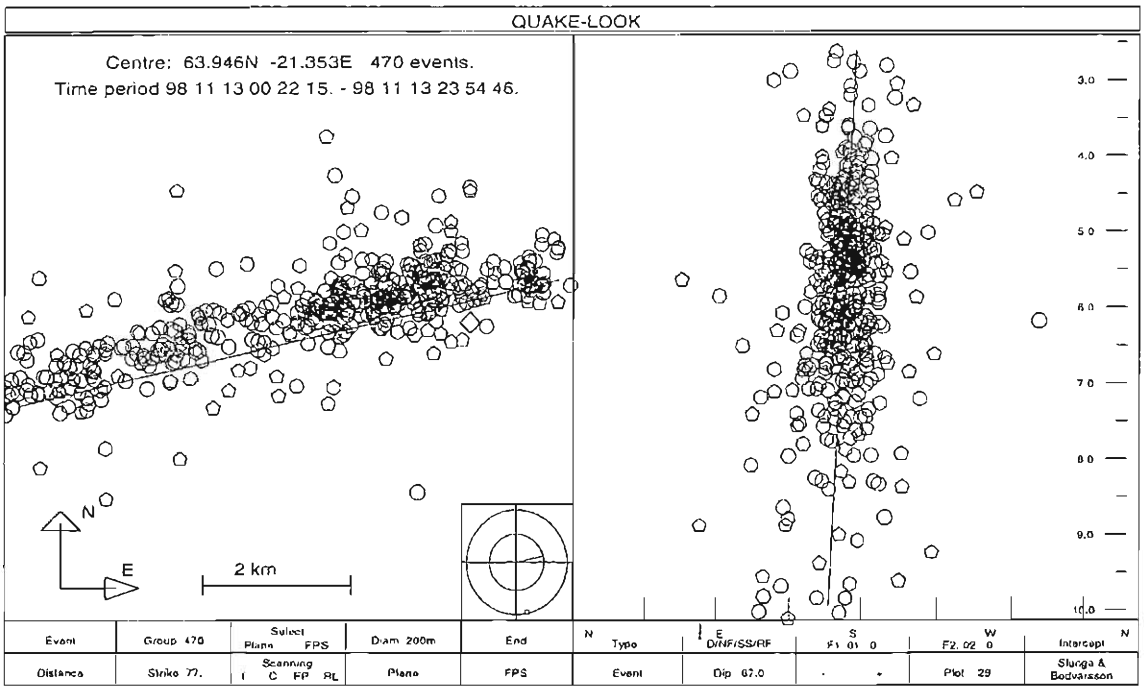

Figure 4. *A number of this type of figures will be shown. The left part is an epicentral map. The right part is a horizontal view, the depths are given by the numbered scale where the numbers give the depth in kilometers. The left and right figure show the same events. In this figure each microearthquake are marked by a polygon. The diamond in the left figure with slightly thicker line is the station BJA. The sizes of the event polygons have a diameter of 200 m. The horizontal direction of the view to the right is N77°E, as given in the strike box of the figure and also marked in the little circles at lower right in the left map. The plane having best rms fit to the events is marked on both parts. To the left its position at the surface is marked and we are looking along this plane in the right figure. These 470 events are mostly aftershocks to a magnitude 5 earthquake.*

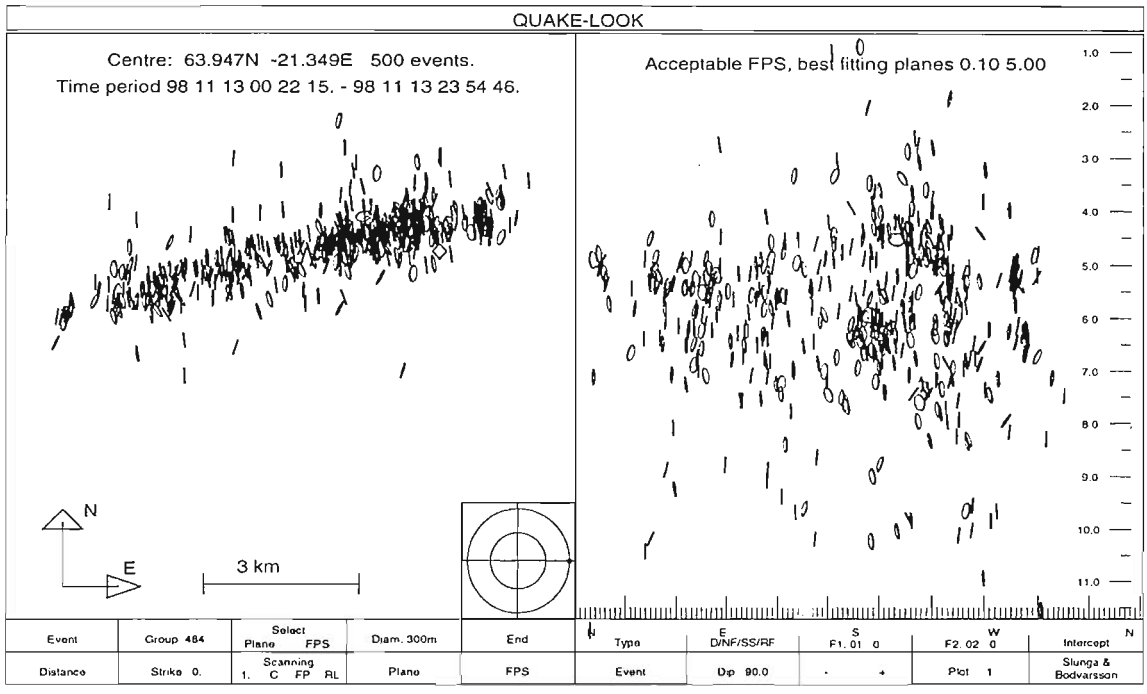

Figure 5. *The events of Figure 4 are shown as "coins". For each event the orientation of the coin is that of the one of the acceptable fault planes for each event which is closest to a N-S striking vertical plane. Note that not all events have such acceptable fault planes.*

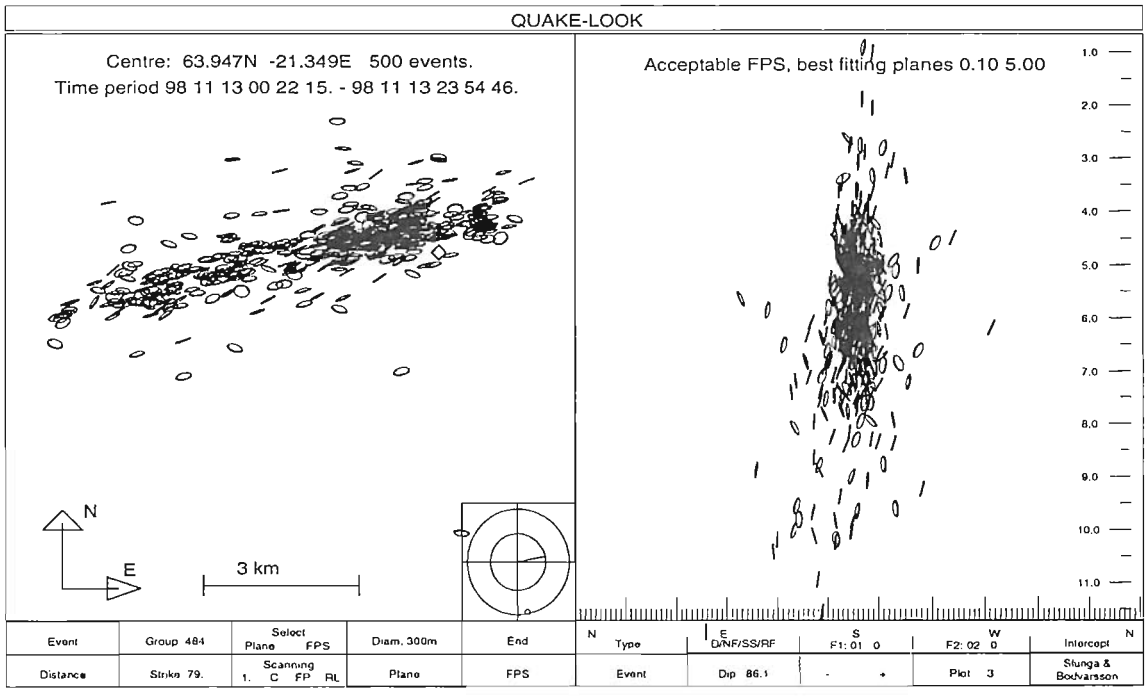

Figure 6. *The same as Figure 5 but with fit to a N79°E striking vertical plane. Note again the frequent bad fits.*

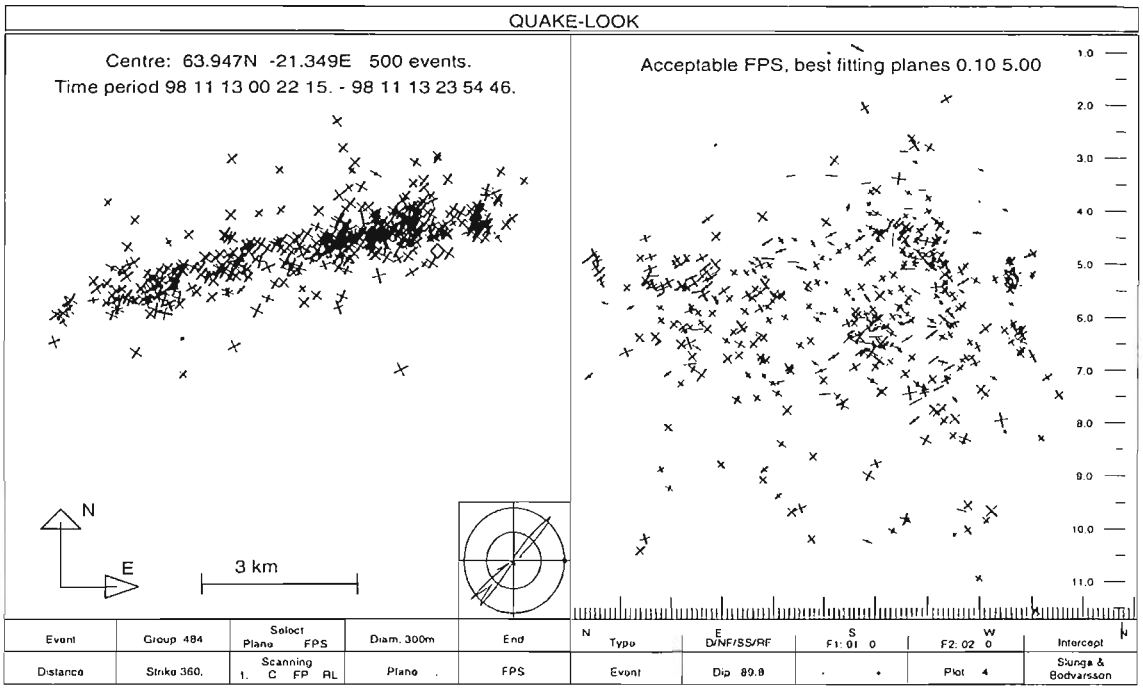

Figure 7. *This figure illustrates the double-couple source moment tensors of the fault plane solutions. The representation is the same as in Slunga et al. 1984, and the thick line shows the subsidiary compression and the thin line shows the subsidiary extension. The distribution of the horizontal compressions (the thick lines of the left map) are shown in the small circle. The right part shows the unscaled frequency (number of events), the left part is scaled according to seismic moment.*

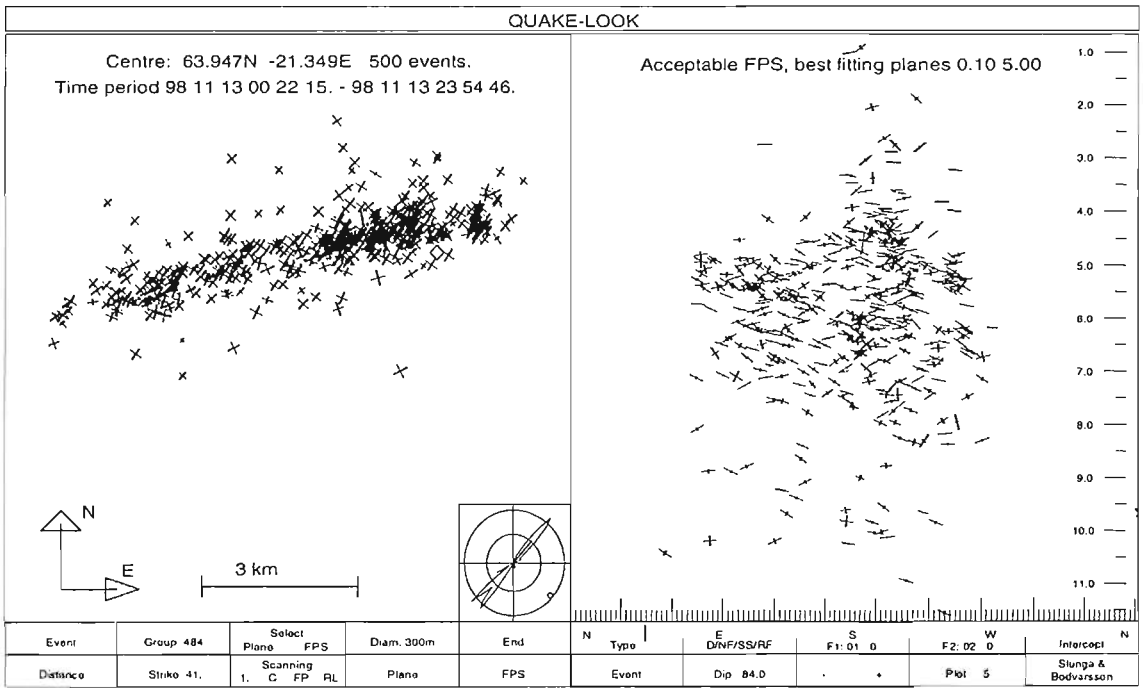

Figure 8. *The same as Figure 7 but with a view along the typical direction of horizontal compression. The typically vertical directions of the compression in the right part indicate the presence of normal faulting in addition to the dominating strike-slip.*

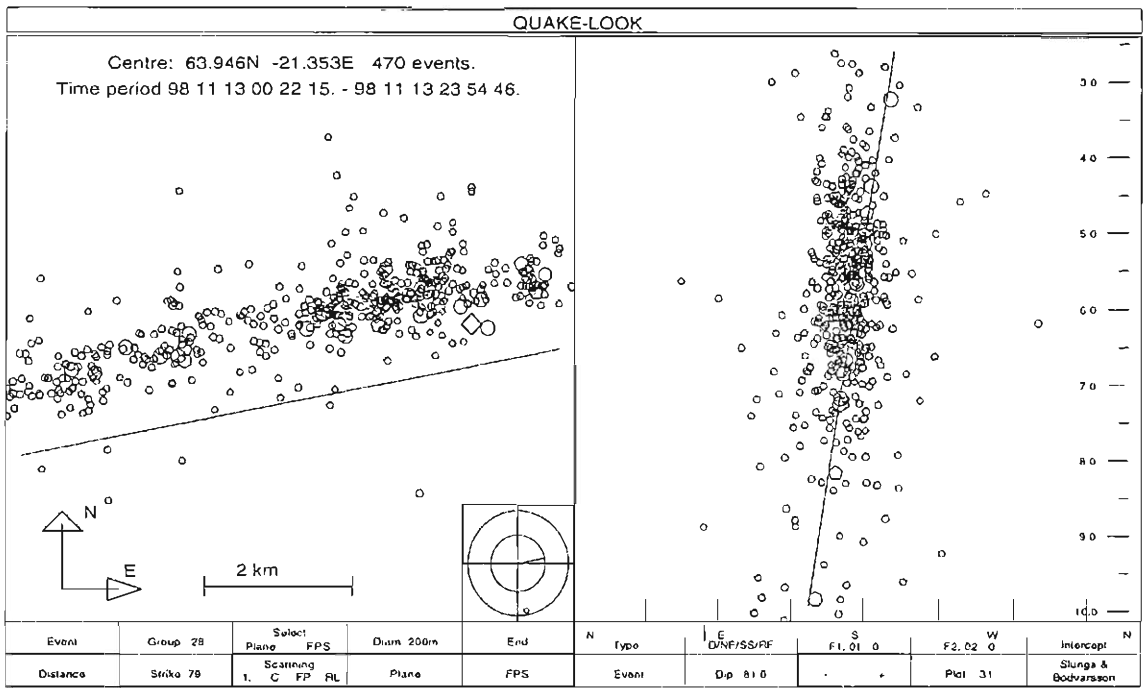

Figure 9. *The 28 events of the largest group found by the automatic grouping algorithm are marked as larger circles. The smaller circles are the remaining events. At depths above 5 km most events are north of this fracture.*

Of the 470 events within the group the automatic algorithm included 115 events within 15 groups. For each of these 115 events we thus have a proposed unique fault plane.

The largest group consists of 28 events and is shown in Figure 9. This group has a plane striking W-E and goes through the total group at depths exceeding 5 km.

The fault planes of the 115 accepted events are shown in a series of figures. As is seen in the left map of Figure 10 we have along the W-E extension of the group a number of fault planes with that strike. The W-E plane is then cut by several rather N-S striking almost vertical faults. There are also N-S striking more horizontal faults. The N-S vertical fractures are spaced about 1 km apart in the area of highest activity. This is reasonable as compared to surface N-S lineaments.

As is seen in the right parts of Figures 11 and 12 some of the groups define fractures that seem to delimit the seismic activity during this day. One must remember that the analysis is statistical and some events may well have been assigned wrong fault planes.

When we look along W-E direction (Figure 13) we see that at 5 km depth the W-E almost vertical fracture is connected to a less vertical fracture extending upwards towards the north. Most of the activity above this depth is clustered around this less vertical fracture.

Figure 14 shows the first events of the day. The W-E fault is active over the whole depth range. The following period is dominated by activity on other fractures (Figure 15). Then after a period with activity on both the W-E fracture and other fractures a period comes with mostly events on N-S fractures (Figure 16).

The automatic grouping of the events removes the ambiguity of the fault plane solutions. In Figure 17 the double-couple source moment tensors are illustrated with the method by Slunga et al. 1984. The subsidiary compressions and extension are illustrated by the thick and thin lines of each event. Again the most obvious feature is the

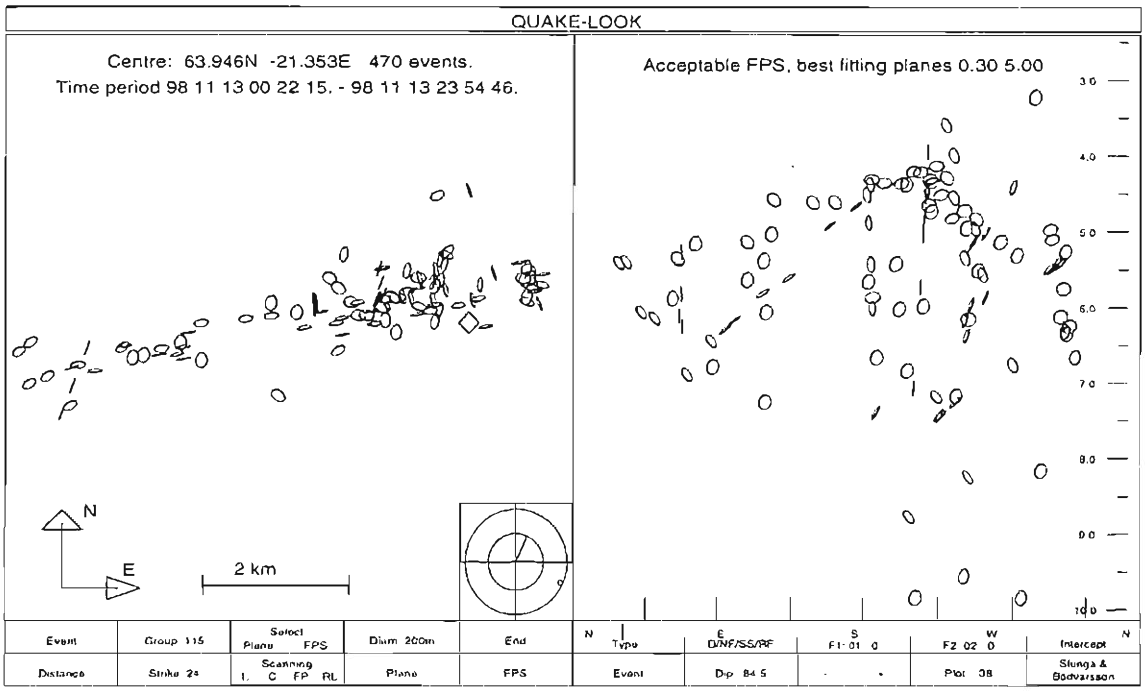

Figure 10.

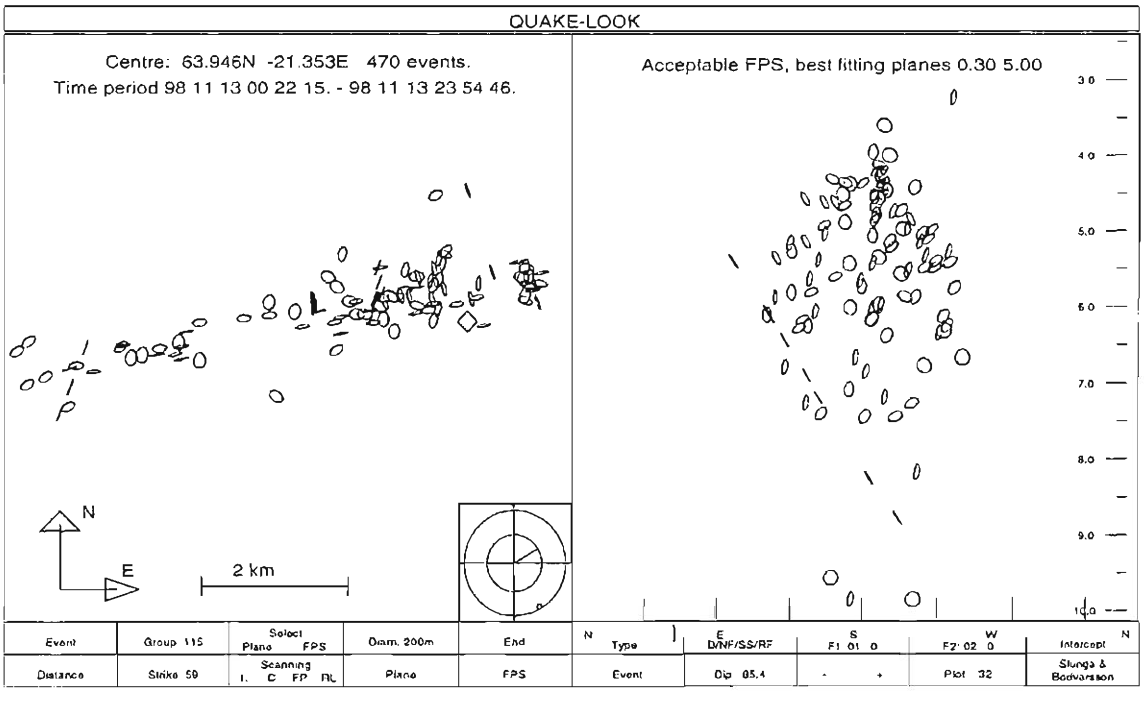

Figure 11. *The figure shows the 115 events included in the 15 fracture groups given by the automatic algorithm. Each event is given as a "coin" oriented as the fault plane of that event. A lot of events have faults striking roughly N80°E (among them the 28 events of the largest group). Several N-S fractures are also shown with a typical spacing of 1 km. In the view to the right (N59°E) is illustrated how one of the groups rather well delimit the activity.*

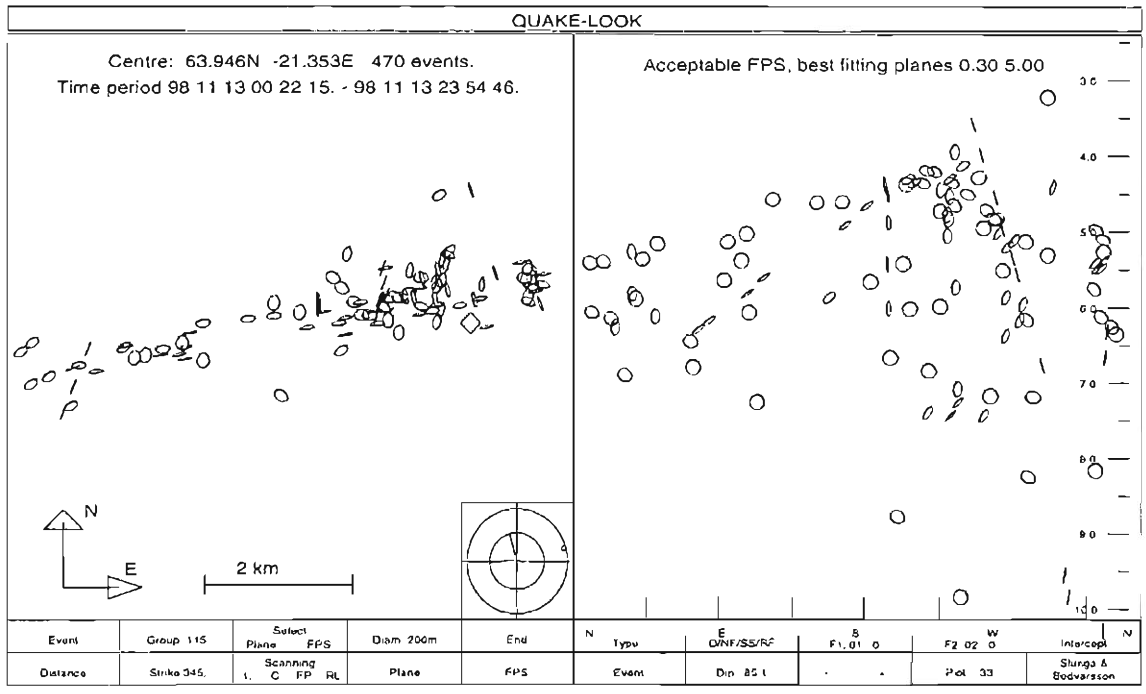

Figure 12. *The same as previous figure but with a view N15° W to the right. Again some of the fractures (groups) seems to delimit the activity which is a slight support for the physical relevance of the assumed fractures. Note that the small marks at the peripheries of the coins indicate the slip direction of the visible side. The thicker part of each coin is closer to the viewer than the thin line edge.*

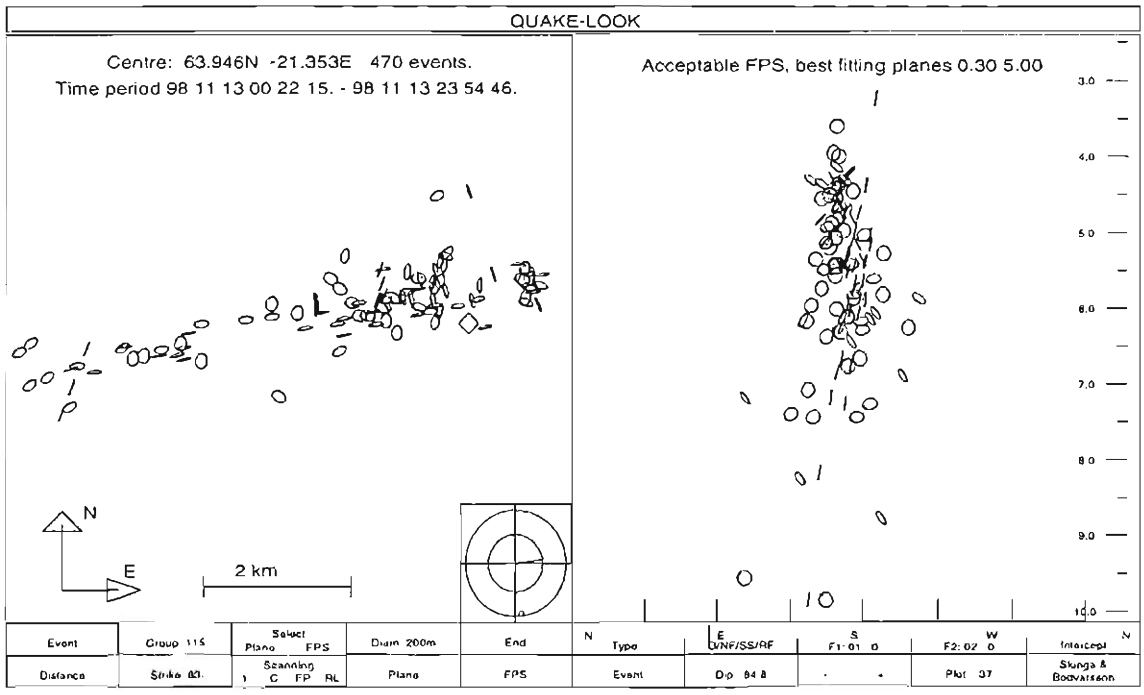

Figure 13. *The same as previous figures but now viewing N83° E. We see that at 5-5.5 km depth two W-E fractures with different dip directions are intersecting. The N-S activity is following another fracture above 5 km depth.*

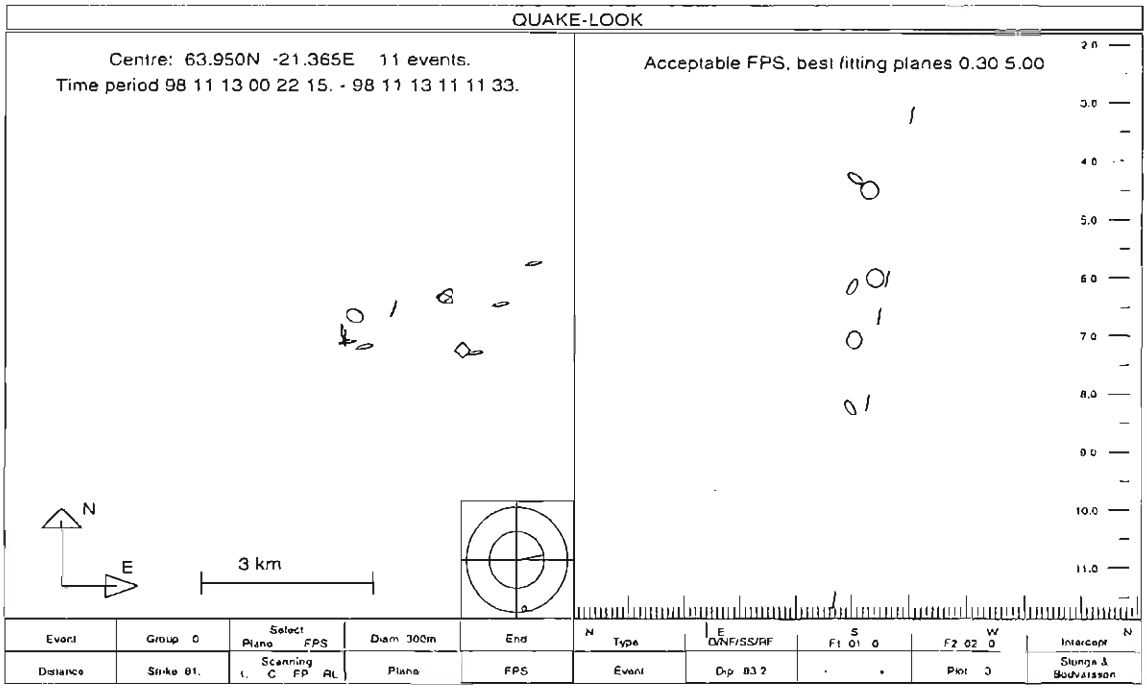

Figure 14. *The acitvity during the first hour after the main shock. The W-E fracture is active but with only small slip events.*

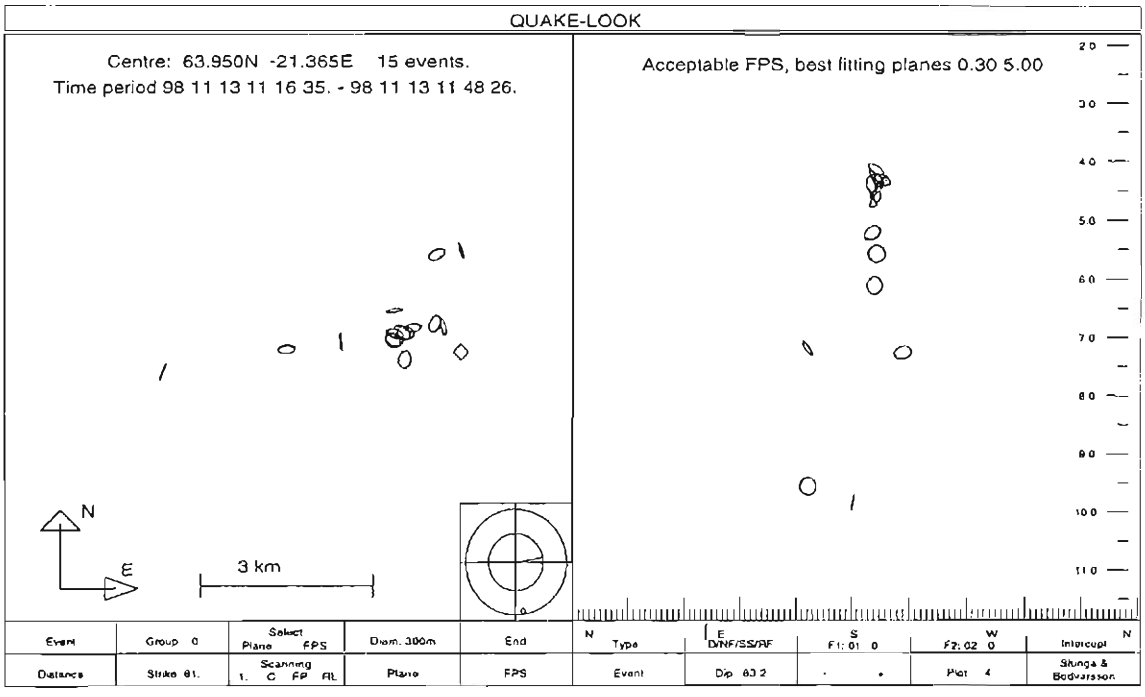

Figure 15. *As Figure 14 but for the following time interval. Now only few events are on the W-E fracture.*

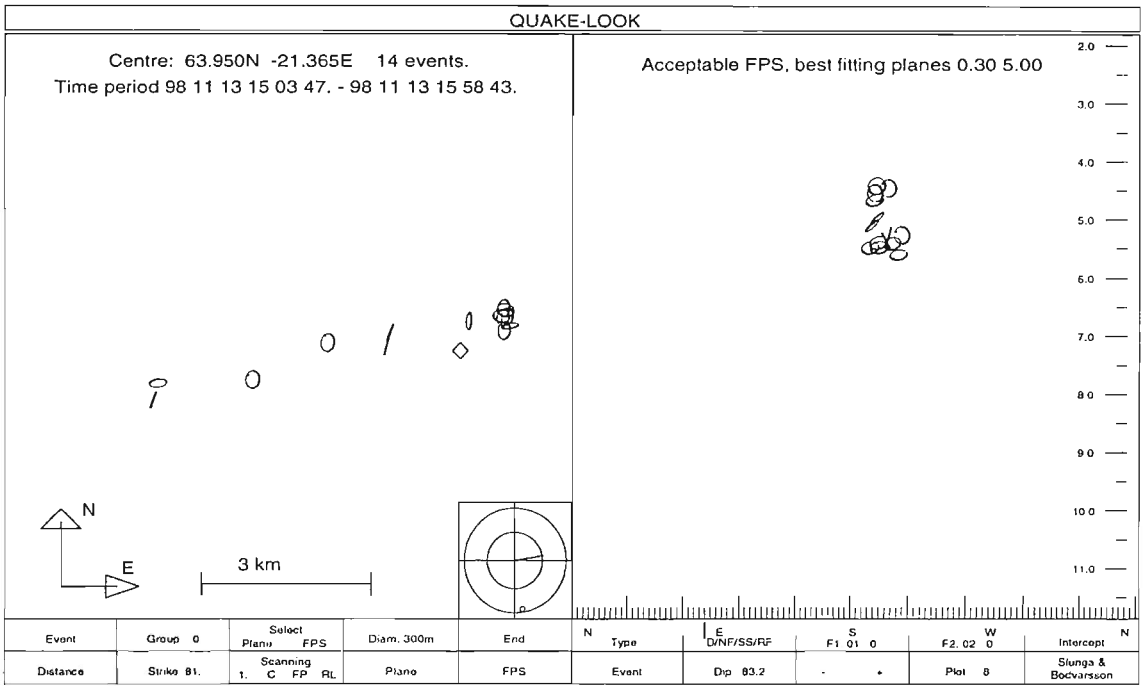

Figure 16. *As previous figures but showing a later interval with almost no events on the dominating W-E fracture.*

high consistency of the horizontal stress release. The vertical picture again appears more varying.

3.2.1.4 Discussion of picture of the seismic activity given by the automatic grouping

The sizes of the fractures have typically dimensions of several kilometers both laterally and vertically. The number of events on the same fracture is mostly only 6-9 and the estimated fault radii are mostly less than 200 meters. In Figure 18 we see a view of the earthquakes within the dominating W-E group. The events are fairly well spread over the fracture. The sizes are the real sizes as given by the corner frequency estimates (Rögnvaldsson and Slunga 1993). Even if the total number of events during this day is 5 times more the surfaces of the events will not cover the whole fracture area. The time order of the events over the area is rather random, not like a domino game. Figure 19 shows the same events as Figure 18 but now scaled according to slip size (the area of the event circles are proportional to slip size). The conclusion is that the size of the seismic slip during this day is very unevenly distributed over this fracture and that the activity starts at several places not neighbouring to each other.

3.2.1.4.1 Similarity to hydraulic fracturing

If the pore pressure is increased in a rock mass the pore pressure will first increase along certain fractures with highest permeability. If there remains shear stress over this fracture the pore pressure increase will trigger seismic events at locked asperities. The pore pressure will also increase in fractures crossing the main fracture and trigger slip on those fractures. This activity is initially expected to occur close to the first fracture and later spread out.

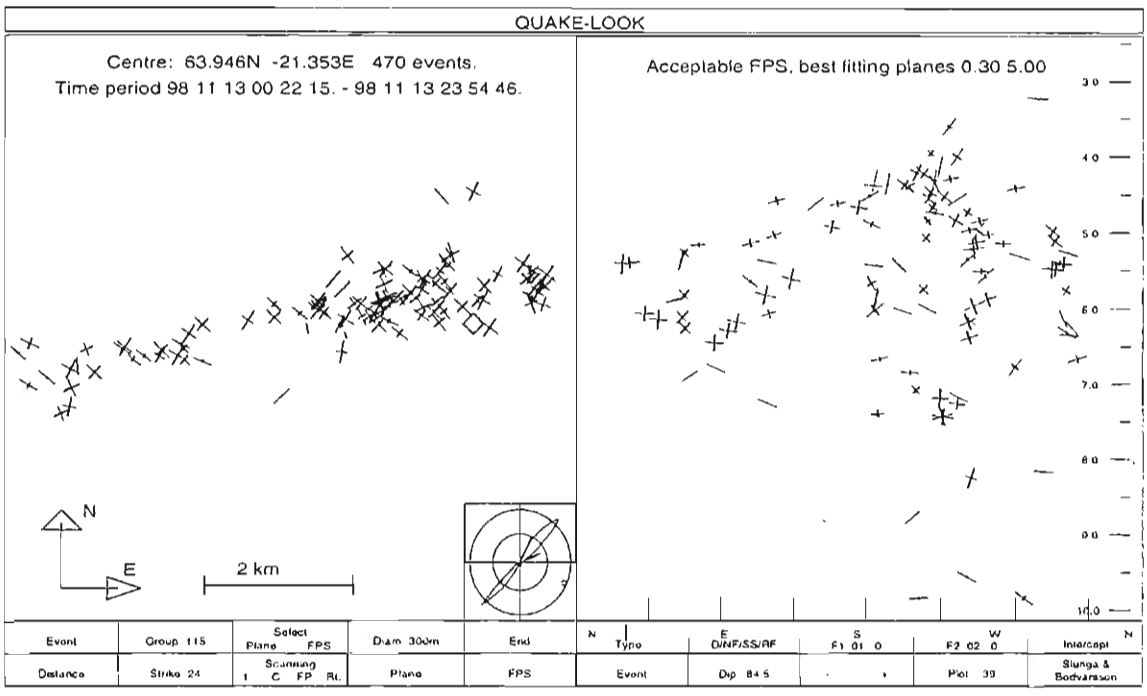

Figure 17. *This figure is similar to Figure 8 but now showing the nonambigous fault plane solutions for the 115 events included in the fracture groups. Note the still very consistent horizontal subsidiary compressions (the distribution in the small circle). The vertical view to the right is more scattered.*

The pattern we see here with a seismic activity spread along a main fracture and with activity on crossing fractures is very similar to what can be observed during hydraulic fracturing of rock masses through water injection. Thus it is possible that increase in pore pressure is affecting the period of seismic activity.

3.2.1.4.2 Stable and unstable fault slip

The seismicity is the unstable slip on the fracture. Stable brittle slip is not seismicly observed but is a possible cause to seismic activity at different places over a fault area within a short-time window. The reason is simple that if a fault starts to slip stably as a whole it is likely that some asperities will remain locked, accumulate stress concentration due to surrounding fault slip, and then break seismicly when the stress is too large. The size of the slip depends then on the strength of the locked part. In Figure 19 showing the peak slips of the events on the possibly primary fault there are three events having significantly larger slip. The peak slips of those events are 3-7 mm. The first events on this fracture have all small peak slips, less than 1 mm. Then the deep 3 mm event appears while smaller slip events continue to occur at "normal" (4-7 km) depth. After 7 hours the upper 3 mm event occurs and after 10 hours the 7 mm event comes. This picture is in reasonable agreement with what one might expect if the fracture started to slip stably at the time of the main event. Possibly the deeper part has started to slip earlier or at a higher rate.

It is of course not the purpose of this simple example to reach any conclusion, the reason of presenting this discussion is to indicate what eventually will come out if more extensive and intensive analysis of this type continues in the area.

The assumption of a general stable slip process triggering seismic events at asperities

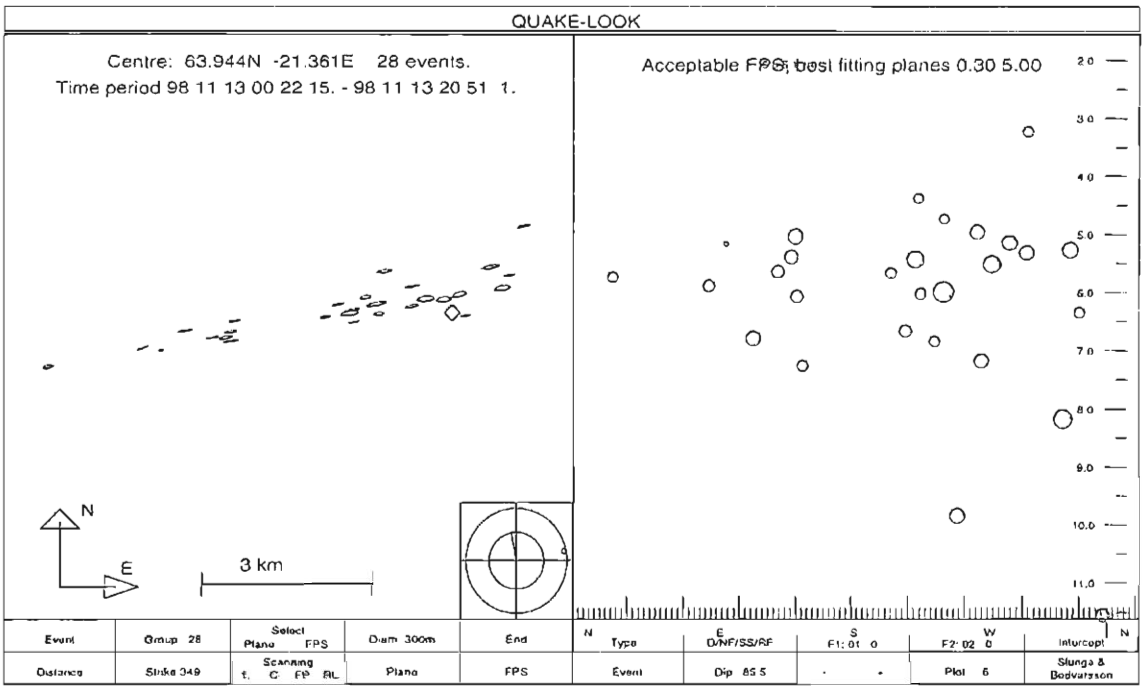

Figure 18. *This figure shows the 28 events of the largest group striking N79° E. The view to the right is normal to this strike (N21° W). The sizes are now not scaled but the true ones as estimated from the corner frequencies. The slip directions (marks at the peripheries) are not perfectly consistent but the slips are mainly in the same direction. Note that the fracture surface is not covered by these events which may indicate stable slip between the events.*

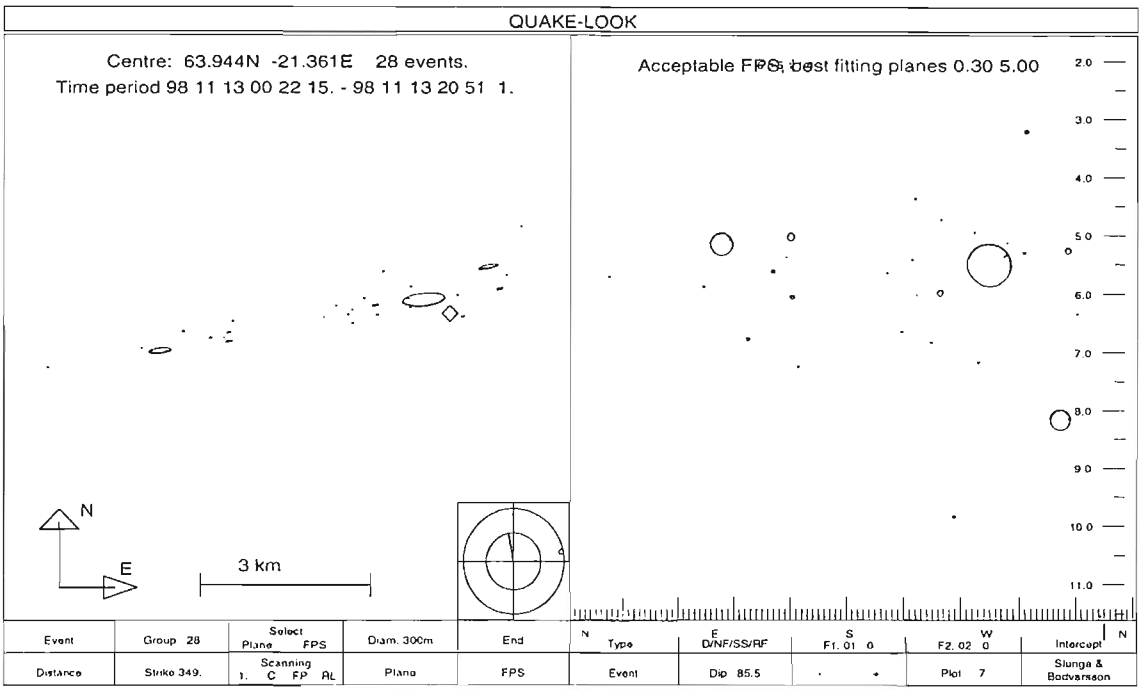

Figure 19. *As Figure 18 but now the events have been scaled according to slip size. The largest slip is 7 mm, the next largest are around 3 mm. The diameters of the event "coins" are proportional to the slip size. Note that the three largest events (slips) have very consistent slip directions. If the slip on this fault has been constant over the whole area most of the slip must have been stable (non-seismic).*

indicates that the stable slip over this single fracture during the day is at least 7 mm which is the largest slip of a single event on the fracture. One must, however, remember that it may be possible that the 7 mm event was already prestressed and was triggered by a smaller stable slip. This is, however, something that can be analyzed, a 7 mm movement on a large fault area will affect the stability in its close surroundings and can be expected to be consistent with occurrences and mechanisms of the surrounding microearthquake.

3.2.1.4.3 The time developement of the slip sizes on the different fractures

Only six of the 15 fracture groups contain events having peak slips exceeding 1.5 mm. Of these 4 shows a rather strict decay of the slip sizes with the largest slips within 2 hours of the main shock. One group has a rather irregular time development with the largest slip event about 5 hours after the main shock. This is one of the N-S striking fractures. Only the largest group, 28 events on the W-E fracture, shows a rather clear increase in the slip sizes with time and with the largest slip event at the end of the day and at the east end of the fault (east of the main event which is on a N-S fracture on the north side of the W-E fracture).

The N-S group having an unclear slip development with time is far from vertical and is at the east end of the activity. It may be that this activity is affected by the possibly increasing slip on the W-E fracture where the slip increases with time.

The activity prior to this day migrated from west along a western extension of the activity of Figure 4. Together with the indications that the W-E fault started to slip at the time of the main event it seems possible that the main event was associated with some locking of the W-E fracture of the 28 events.

3.2.1.5 Conclusions

There are several indications that the automatic grouping of the events applied after multievent location (based on relative timing) and after single-event fault plane solutions (based on spectral amplitudes and first motion directions) results in groups of events associated with fractures that may be real. It is not possible to come to definite conclusions from only one investigation of this type. The PRENLAB project produces however much more data, this example was based on only one day of activity. As not only the grouping algorithm is automatic, but also the fault plane solution algorithm and the multievent algorithm there are no real problems to submit all data to such a detailed analysis as given here. This little study is part of the preliminary work of how to implement this multievent analysis to all data. The point is not whether the tentative possible results of this example are true or not. The point is that studies like this do not demand a lot of work. When all data are interpreted in this way it is likely that altogether the significance will increase so there will be obvious results and not only indications.

Although there seems to be no chaos among the small earthquakes (for instance the very high horizontal stress consistency) the picture seems to be complicated as so many small fractures are involved. However, with use of computers the complexity is no real problem as it easily can be handled.

The coming work will partly go to develop the type of studies here to routine algorithms for analyzing all data, and partly to analyze the physical interaction of the different fracture slips. The hope is that the physical interaction will be of great help in reducing the uncertainty of the tentative interpretations.

3.2.2 Task 2: Statistical and adaptive analysis of space/time distribution of microearthquakes

Rather than only working with hypocenters of single earthquakes we chose to relate the statistical analysis with stress tensors derived from number of microearthquakes limited in time and space. Before applying the stress tensor inversion we pre-process the dataset to minimize the time/space span but ensuring stable stress tensor solution. For this we have developed a algorithm based on correlation of spectral amplitudes.

3.2.2.1 Spectral amplitude correlation

The SIL network frequently records swarms of microearthquakes where the individual events in the swarm occur very close to each other and often the events can be interpreted as occurring on the same fault. Assuming that this interpretation is correct and that the events in the swarm have similar slip directions, the radiation patterns from these events will be very similar. We should thus be able to observe strongly correlated amplitude and polarity recordings from the events in such a swarm.

We investigated amplitude recordings from a swarm of microearthquakes in Ölfus in SW Iceland. Since the events were not always registered by the same number of stations, or had the same number of phases registered at the stations, we picked out stations and phases common to the two events we wanted to compare. Shown in Figure 20 is a comparison of four events. Event number nine, in the lower right corner, is compared to itself and to events six to eight. For each event pair we sorted the logarithm of common phases according to ascending order of event nine's amplitudes and then plotted the two events common amplitudes next to each other. Since event nine is compared to itself in the lower right the amplitude pairs are exactly the same height. For the other three plots

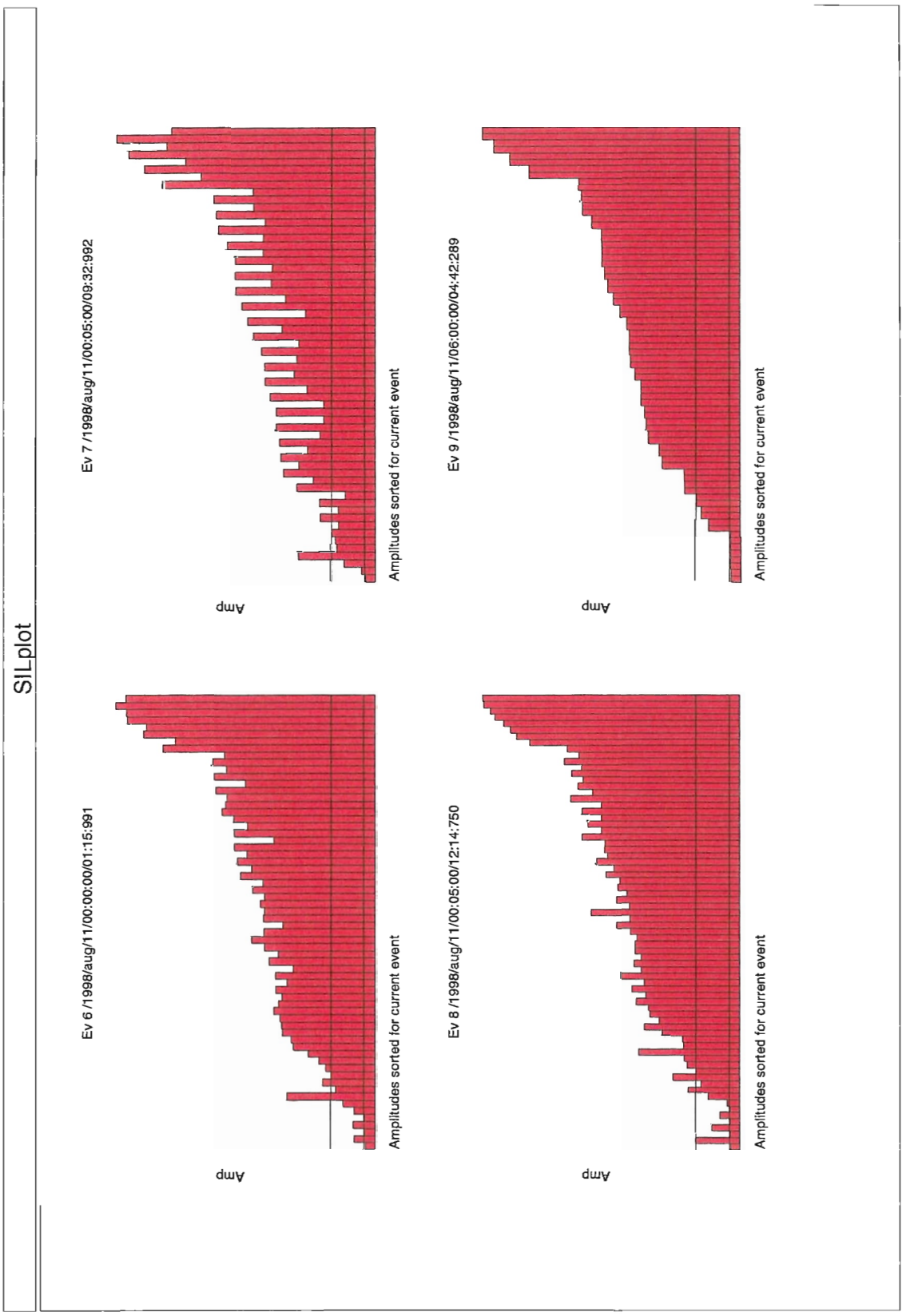
SILplot
Ev 7 /1998/aug/11/00:05:00/09:32:992
Amp
Amplitudes sorted for current event
Ev 9 /1998/aug/11/06:00:00/04:42:289
Amp
Amplitudes sorted for current event
Ev 6 /1998/aug/11/00:00:00/01:15:991
Amp
Amplitudes sorted for current event
Ev 8 /1998/aug/11/00:05:00/12:14:750
Amp
Amplitudes sorted for current event

Figure 20.

we see that the amplitude pairs are not identical but that there is great similarity in the shapes of the amplitudes. Figure 21 shows the logarithm of the amplitudes compared in a XY-plot. Again the events are compared to event nine, we plot the amplitudes of event nine on the x-axis and the amplitudes of the other event on the y-axis. Comparing event nine with itself thus gives a straight line, lower right, and the comparisons with other events give more scatter but we see that there is considerable correlation between the four events.

Figure 21 shows that the scatter in the amplitude data increases at smaller amplitudes and in order to reduce the effect of small amplitudes, with low signal to noise ratios, we studied the amplitude distributions from 1505 earthquakes occurring in the study area during 1998. We found that there is a rapid decrease in amplitude below, approximately, the lower 5% level in the number of amplitudes. We thus decided to set lower amplitude limits at the 5% level, corresponding to amplitudes of $4.4 \cdot 10^{-11}$ for P-waves and $1.0 \cdot 10^{-10}$ for S-waves.

A cross-correlation algorithm was constructed which calculates the linear correlation coefficient for all pairs of events in a dataset. Only common amplitudes above the threshold are included in each correlation, and the logarithms of the amplitudes are used in order to down weight the importance of the amplitudes at the closest station, which would otherwise dominate the correlation. Events with very few stations tend to correlate too well and we use a weighting scheme that puts low weight on events with less than 20 common phases. Figure 22, lower part, shows the matrix of correlation coefficients for our dataset, in order of time. Once the correlation coefficients have been calculated we proceed with grouping of the events. We group events having correlation coefficients higher than, typically, 0.9 or 0.95. In order to find homogeneous groups we also require that the events in the group have a certain fraction of their correlation coefficients with all other events in the group above a limit, usually 70%–80%. We also utilize a weighting scheme not to obtain groups with very few events. Figure 22, upper part, shows the same correlation matrix after grouping of the events. In the figure we have used a correlation limit of 0.9 and a fraction of 80%.

3.2.2.1.1 Composite focal mechanisms

The groups obtained by the amplitude correlation contain closely located events with very similar radiation patterns. This suggests that we could calculate a well constrained, composite focal mechanism for the events by stacking amplitude and polarity observations. The focal mechanism thus obtained would give more accurate information about the nodal plane orientations and slip directions, however, the dynamical parameters would be a mere average of the events in the group. We implemented an algorithm that normalizes the amplitudes of the individual earthquakes to the median amplitude for the event. These normalized amplitudes are then stacked, for each phase on all available stations, and the the final result is renormalized with the median of the event medians. Polarities are stacked at each station and the median polarity used as the correct one at the station. In our test group the composite mechanism was calculated from amplitudes at 11 stations and using seven polarities, to be compared to the individual events median of eight stations and two polarities. This work is still in progress but preliminary results show that the optimal fault plane solution obtained from the composite event show very good agreement with the estimate of the fault plane orientation from relative location.

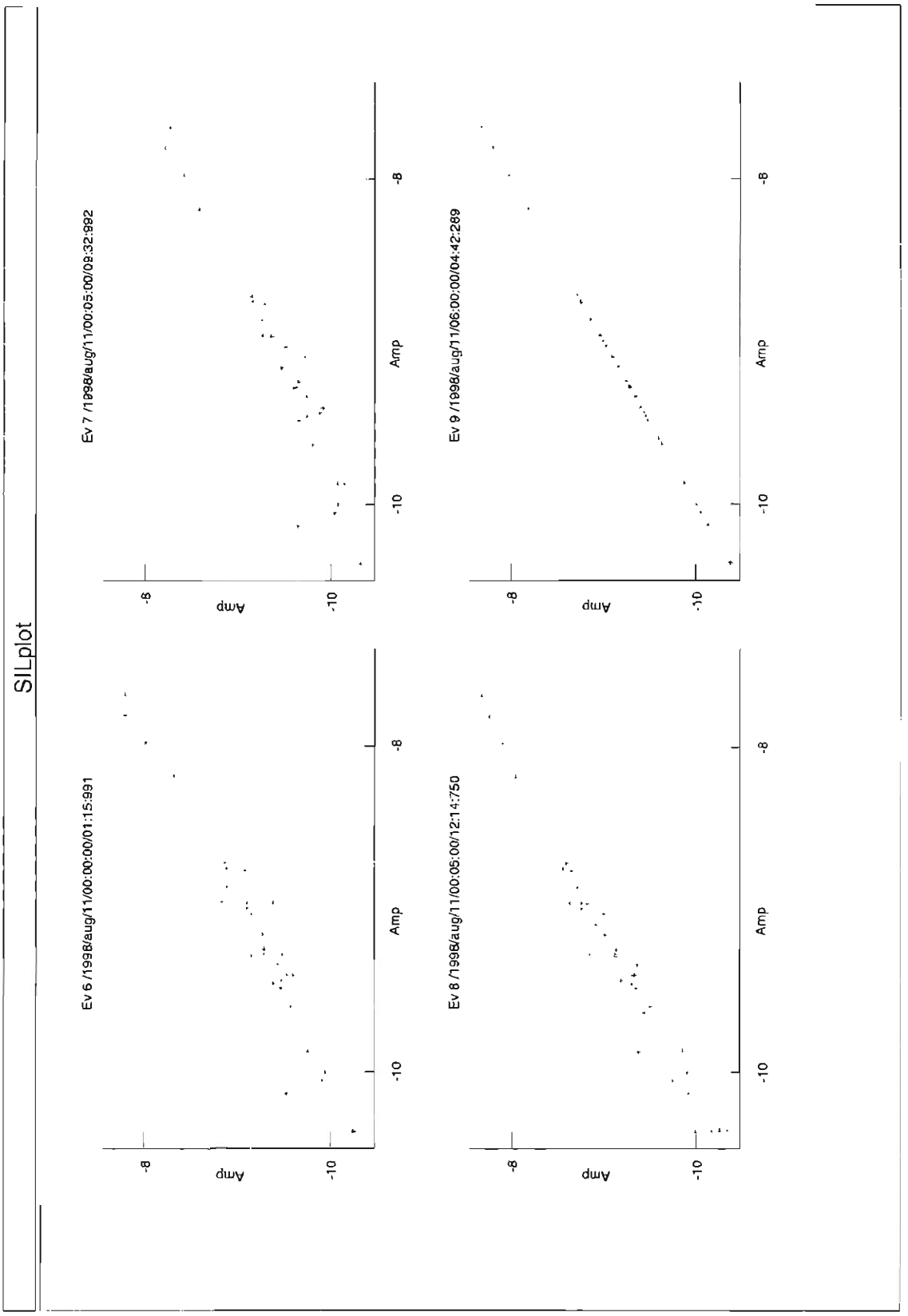
SILplot
Ev 7 /1998/aug/11/00:05:00/09:32:982
Ev 9 /1998/aug/11/06:00:00/04:42:289
Ev 6 /1998/aug/11/00:00:00/01:15:991
Ev 8 /1998/aug/11/00:05:00/12:14:750
Amp
-8
-10

Figure 21.

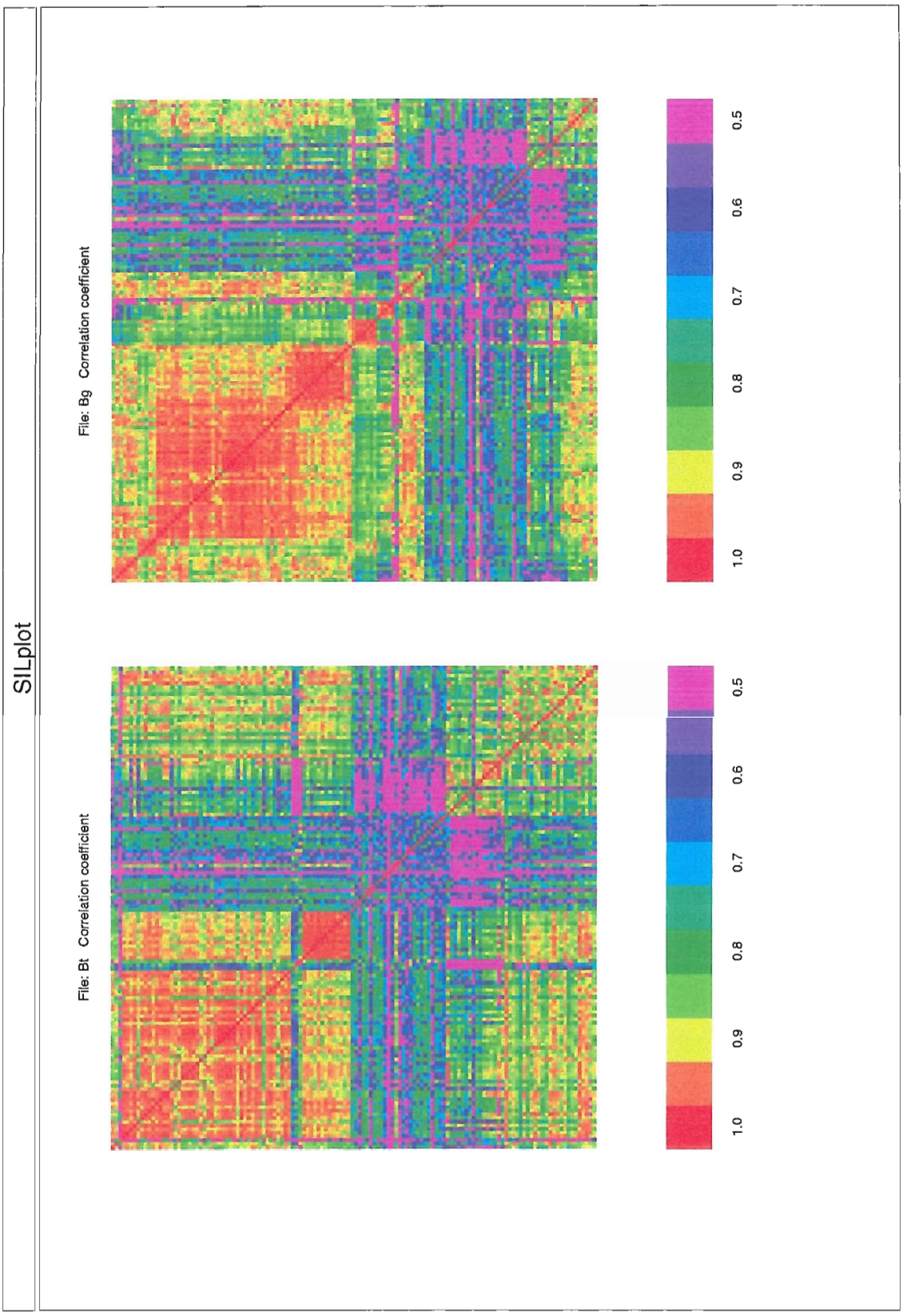
SILplot
File: Bg Correlation coefficient
File: Bt Correlation coefficient
0.5
0.6
0.7
0.8
0.9
1.0

Figure 22.

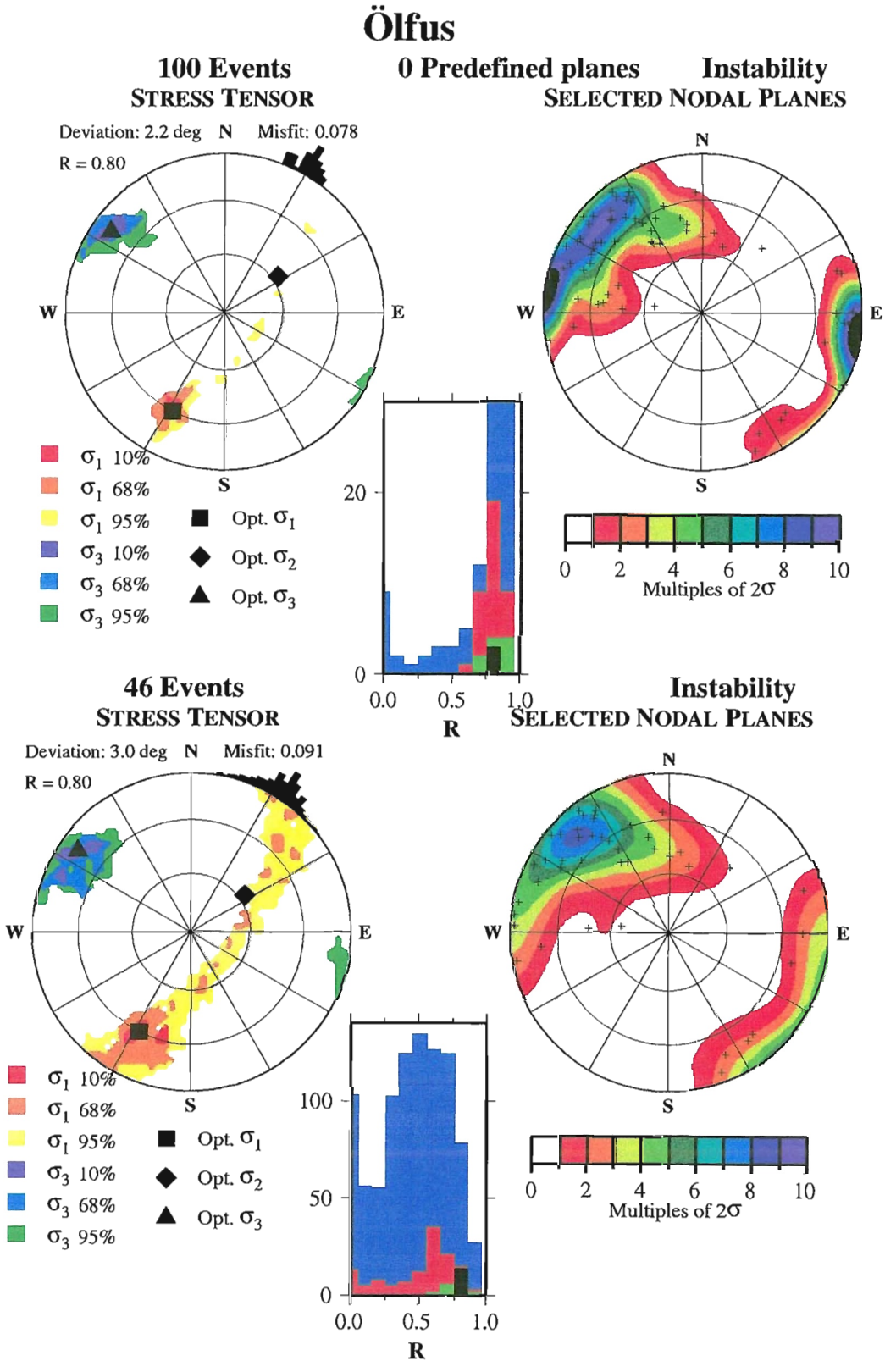
Ölfus
100 Events
0 Predefined planes
Instability
STRESS TENSOR
SELECTED NODAL PLANES
Deviation: 2.2 deg
Misfit: 0.078
R = 0.80
N
W
E
S
σ1 10%
σ1 68%
σ1 95%
σ3 10%
σ3 68%
σ3 95%
Opt. σ1
Opt. σ2
Opt. σ3
20
0
0.0
0.5
1.0
R
0
2
4
6
8
10
Multiples of 2σ
46 Events
STRESS TENSOR
Instability
SELECTED NODAL PLANES
Deviation: 3.0 deg
Misfit: 0.091
R = 0.80
100
50
0
0.0
0.5
1.0
R

Figure 23.

3.2.2.1.2 Preprocessing stress tensor inversion data

One of the purposes of the amplitude correlation method was to investigate the possibility of reducing the number of similar events in our stress tensor inversion scheme (Lund and Slunga 1999). Events having very similar focal mechanisms do not contribute any independent information to the stress tensor inversion and since the inversion is rather slow we would like to reduce the number of events in each inversion as much as possible without affecting the result. Amplitude correlation is one possible way of performing such a reduction. Figure 23 shows the inversion results using all 100 events in the Ölfus dataset in the upper section of the figure. Below is the result obtained after removing 54 events considered similar by the amplitude correlation algorithm. There were 6 groups of similar events, with a total of 60 events in the groups. We retained the event with the largest number of stations and phases as the representative for each group. We see that there are more normal faulting stress states after the reduction but that the overall stress state is rather similar to the inversion with all events. We aim toward a better match between the stress results obtained after reduction with the original, we are in the process of investigating the use of composite fault plane solutions as representatives of the groups and a more accurate calculation of the confidence limits.

3.2.3 Task 3: Investigation of variations of relative crustal velocities

The algorithm for absolute and relative location of microearthquakes is being modified for this purpose. The aim is to implement a option in the software to exclude some selected observations from the inversion for P-S velocity monitoring purpose. This modified software will then be used to analyze some earthquake swarms in a specific area at different times.

3.2.4 Task 4: Implementation of these new methods in a second EU country with high seismic risk

The established contact with the Seismological Laboratory, University of Patras in Greece has been more difficult since the main practical contact person in Patras, Dr. Nicos S. Melis, has got a new position in Athens. We have not had success in re-establishing the practical contact yet.

3.2.5 References

Slunga, R. 1981. Earthquake source mechanism determination by use of body-wave amplitudes - an application to Swedish earthquakes. *Bull. Seism. Soc. Am.* 71, 25-35.

Rögnvaldsson, S.Th. & R. Slunga 1993. Routine fault plane solutions for local and regional networks: a test with synthetic data. *Bull. Seism. Soc. Am.* 83, 1232-1247.

Rögnvaldsson, S.Th. & R. Slunga 1994. Single and joint fault plane solutions for microearthquakes in South Iceland. *Tectonophysics* 273, 73-86.

Slunga, R., S.Th. Rögnvaldsson & R. Böðvarsson 1995. Absolute and relative location of similar events with application to microearthquakes in southern Iceland. *Geophys. J. Int.* 123, 409-419.

Slunga, R., P. Norrmann & A.-C. Glans 1984. Baltic shield seismicity, the results of a regional network. *Geophys. Res. Lett.* 11, 1247-1250.

Lund, B. & R. Slunga 1999. Stress tensor inversion using detailed microearthquake information and stability constraints: application to Ölfus in Southwest Iceland. *J. Geophys. Res.* 104, 14947-14964.

3.3 Subproject 3: Shear-wave splitting to monitor in situ stress changes before earthquakes and eruptions

Contractor:

Stuart Crampin
Department of Geology and Geophysics
University of Edinburgh
Grant Institute
West Mains Road
Edinburgh EH9 3JW
United Kingdom
Tel: +44-131-650-4908
Fax: +44-131-668-3184
E-mail: scrampin@ed.ac.uk

Researcher:

Theodora Volti
Department of Geology and Geophysics
University of Edinburgh
Grant Institute
West Mains Road
Edinburgh EH9 3JW
United Kingdom
Tel: +44-131-650-8533
Fax: +44-131-668-3184
E-mail: tvolti@mail.glg.ed.ac.uk

3.3.1 Task 1: Continuous monitoring of shear-wave splitting

Continuous monitoring of shear-wave splitting is suggested for precursory changes before larger earthquakes, eruptions, and other changes of stress. The basic remit of this subproject is to respond to changes if observed and analyze data for hazard assessment.

Shear-wave splitting is sensitive to changes in stress. In anisotropic media, the two shear-waves split into two orthogonally polarized waves that propagate with different velocities. Careful examination of the seismograms can identify the polarization direction of the first (or faster) shear-wave and the time delay between the two arrivals (Figure 24a). Time-delays are particularly sensitive to changes in anisotropy.

Earthquake data provided by IMOR.DG are identified and analysed routinely. Stations with sufficient polarization measurements during the years 1997-1998 are shown in Figure 25 (Station KRO also has sufficient data but the behaviour of shear-wave splitting at KRO is highly irregular which is believed to be due to complicated ray paths near local rifting). There is a good alignment of polarizations, with average direction of the maximum horizontal stress SW-NE. During the first year, time-delay analysis was concentrated on station SAU, which had sufficient data and was closer to Vatnajökull eruption. However, during the last two years the only station with sufficient data suitable for looking for precursory changes is BJA. BJA is situated near the center of the South Iceland seismic zone (SISZ) (Figure 24b).

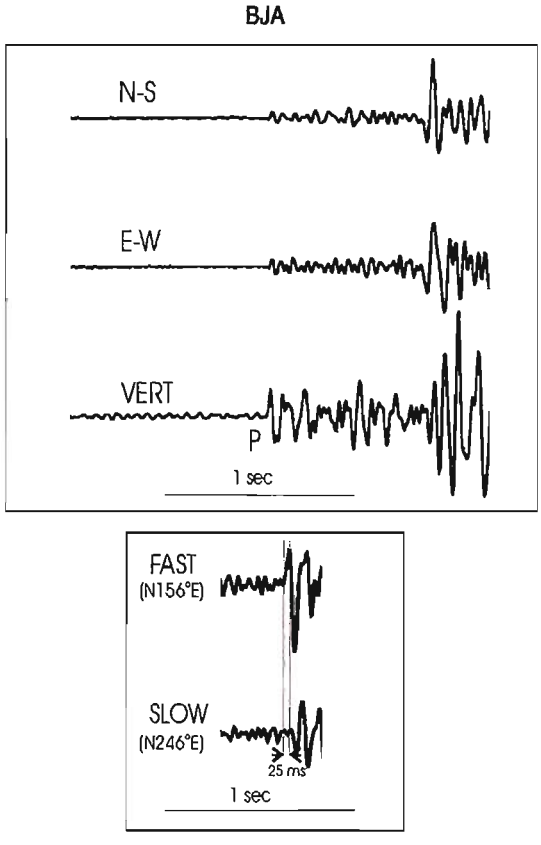

Figure 24a: Example of shear-wave splitting at station BJA. The upper diagram shows the three recorded components. On the bottom, the rotated N-S and E-W components show clearly the time-delay between the two shear-wave arrivals. (Event occurred at 21:08:7:5, September 21, 1998, at 5.6 km depth, 0.7 km from BJA).

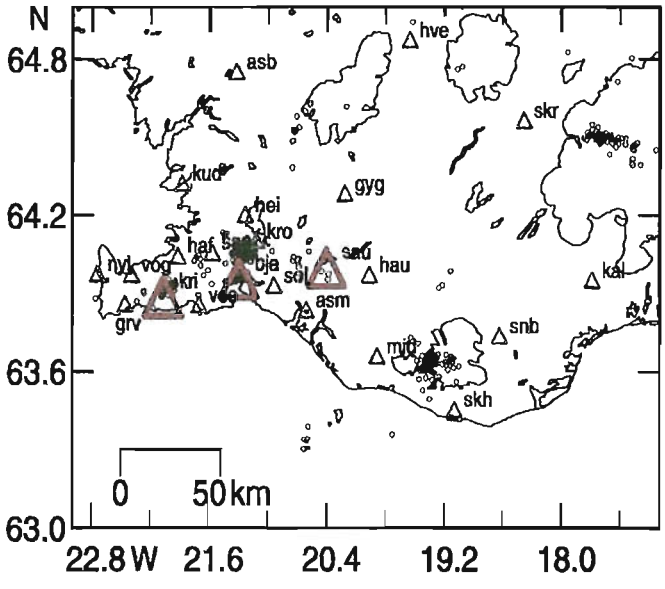

Figure 24b: Map of SW-Iceland showing all earthquakes with≥M 2, during the period January 1997 - December 1998. The small green triangles show the majority of SIL stations, wheares the three stations BJA, SAU and KRI are shown with large red triangles.

Figure 24.

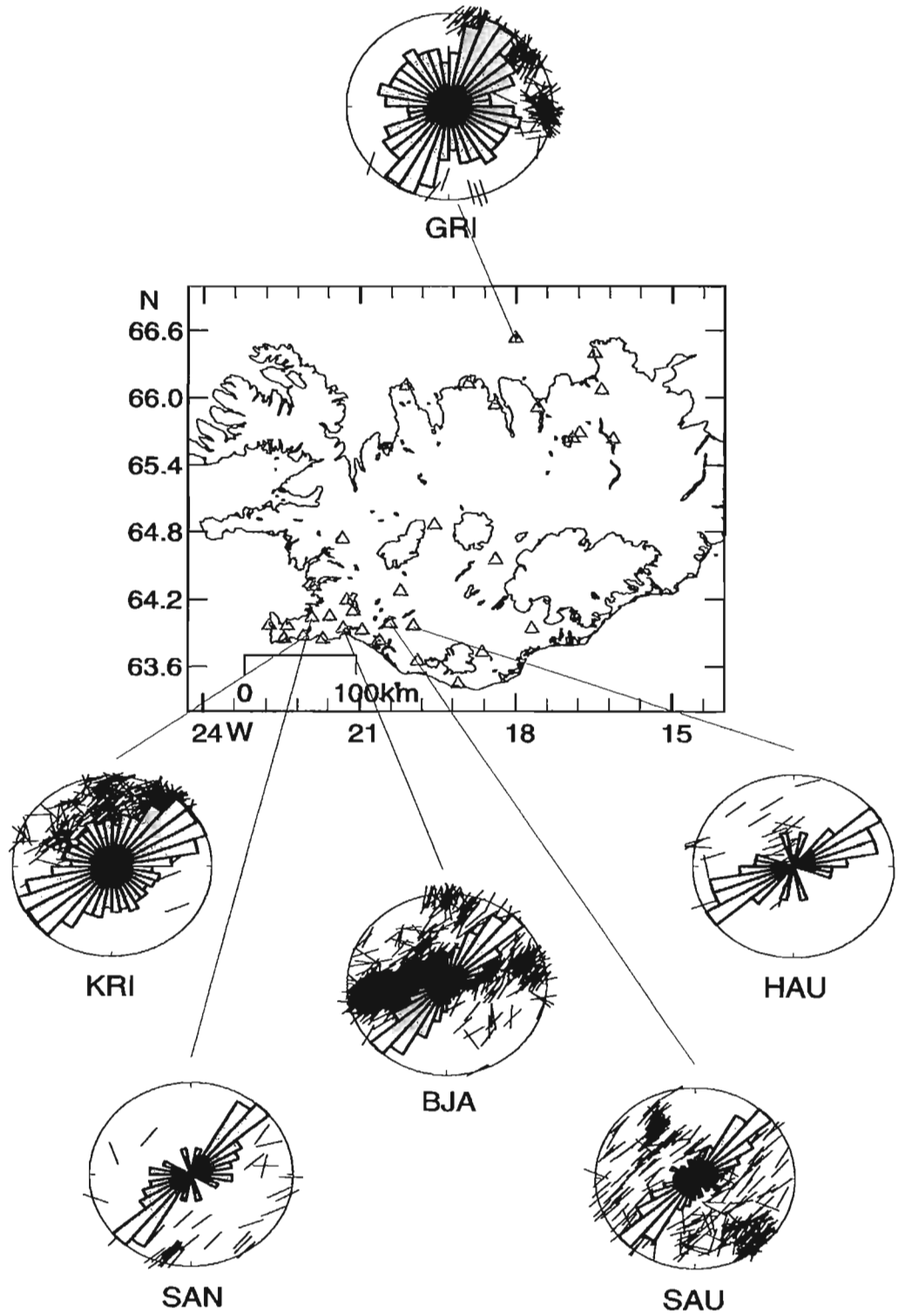

Figure 25: Shear-wave splitting polarizations at the main stations during January 1997-December 1998. All data are within the shear wave window (45°).

Figure 25.

The basic remit of this subproject is to respond to changes if observed and analyze data for hazard assessement. The bulk of our activity has been in this task as changes in shear-wave splitting are observed routinely before larger earthquakes.

3.3.1.1 Temporal variations in time-delays

Polarization directions and time-delays have been measured for all suitable data during the last two years. The suitable events (recorded with station-to-epicenter distance less than hypocentral depth) are within the shear-wave window which ensures that the shear-waves are not distorted by surface conversions. This constrains the number of events that can be used for shear-wave splitting analysis. There is also need for sufficient activity spread in time near the station. Other constrains include the focal depth, location errors and deviation from the mean polarization direction. These criteria were fulfilled mainly for station BJA and KRI. Variations in time-delays for the above two stations are shown in Figures 26a and b. At each station the mean polarization is calculated and time-delay measurements with polarizations within a standard deviation of this direction are selected (42°±30° for BJA and 51°±45° for KRI respectively). The time-delay measurements are normalized over straight-line path distance and separated into two bands. The bands are defined by incidence to the vertical plane of symmetry parallel to the mean polarization direction (the strike of aligned near-vertical cracks). Band-1 (15°-45°) is more sensitive to changes in crack aspect-ratio, the result of gradually increasing stress. Band-2 (0°-15°) is more sensitive to crack density.

In Figures 26a and b the middle cartoons show nine-point moving averages through the time delays in Band-1. The least-squares lines begin at a minima in the nine-point moving average and end when a large earthquake occurs, followed by a comparatively abrupt decrease of time-delays. The upper cartoons show nine-point moving averages through the time-delays in Band-2. They show no consistent pattern or relationship to earthquakes. The lower cartoons show the magnitudes of all $M \geq 2$ earthquakes within 20 km of the station. In Figure 26a, Band-1, the moving averages through the time-delays show a series of five minima. There is a good correlation between the five major earthquakes (which occurred within 20 km from BJA) and the increases in time-delays prior to the events. The duration and rate of increase vary with the magnitude of the eventual earthquake, and the greatest normalized time-delay varies between about 12 ms/km and 14 ms/km. Figure 26b, middle cartoon, shows time-delays variations in Band-1 in station KRI. Data are scarce and the only discernible changes are after July 1998. The largest earthquake within 20 km of KRI is only M=3.7 in February 1997 and there are no earthquakes within the shear-wave window before this event.

3.3.1.2 Stress-forecasting earthquakes

Stress-forecasting is based on the assumption that the build-up of stress before earthquakes causes progressive changes in aspect-ratios until a level of cracking, known as fracture criticality, is reached and the earthquake occurs. Therefore, changes in shear-wave splitting in Band-1 are used to monitor crack aspect-ratios and estimate the time and magnitude that crack distributions reach fracture criticality. It was recognized at the end of October 1998 that the times delays in Band-1 were increasing since July 1998 at both stations BJA and KRI (Figure 26a and b). The increase had approximately the same duration and slope as the increases before the 5.1 earthquake on June 4, and started at about the lowest level (~4 ms/km) of any of the increases associated with previous

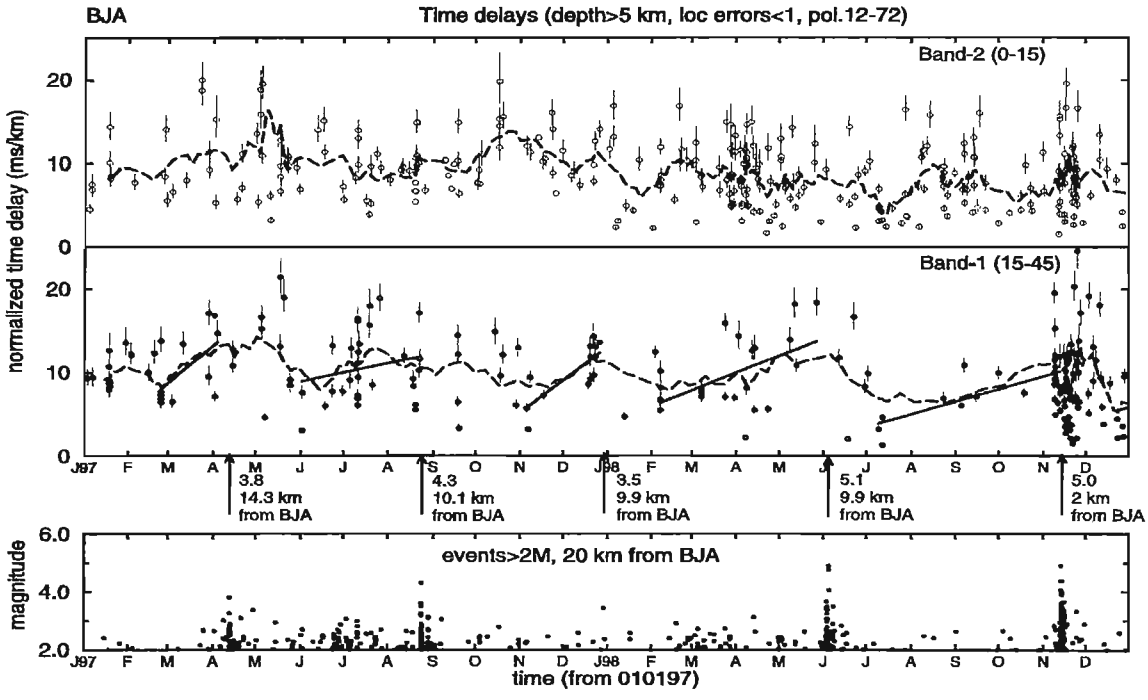

Figure 26a: Shear-wave splitting at SAU from January 1, 1997 to December 31, 1998. The upper and middle cartoons show variation of normalized time-delays with time, for ray paths in bands with incidence 0° to 15° to the crack face (Band-2) and with incidence 15° to 45° to the crack face (Band-1). There are also nine-point moving averages through the time-delays. Band-2 is sensitive to crack density whereas Band-1 is sensitive to aspect ratio. Lines are least square fits to data before a major earthquake. The lower cartoon shows the magnitudes of all $M \geq 2$ earthquakes within 20 km of BJA.

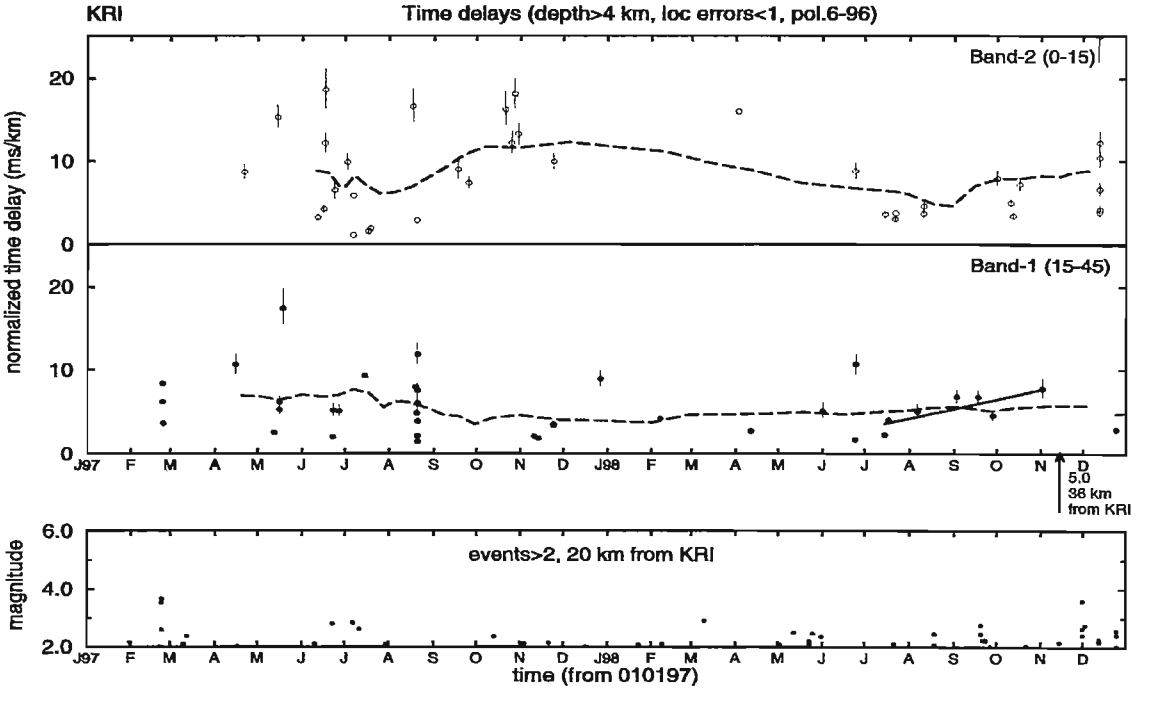

Figure 26b: Shear-wave splitting at KRI from January 1, 1997 to December 31, 1998. Diagrams as for Figure 26a.

Figure 26.

earthquakes. There appeared to be less scatter about least squares lines than for the previous earthquakes and the increase at BJA was already nearly 10 ms/km which was close to the level of fracture criticality of the previous earthquakes. Many of these features appeared simultaneously at stations BJA and KRI which are about 38 km apart. These features suggested that the crust was approaching fracture criticality before an impending larger earthquake. Consequently, an email to IMOR.DG was sent on November 10, 1998, with a specific stress-forecast that an earthquake could occur any time between now (M≥5) and end of February (M≥6) if stress kept increasing. Three days later, on November 13, 1998, IMOR.DG reported that there had been a M=5 earthquake with epicenter 2 km from BJA. We claim this was a successful forecast within a comparative narrow time-magnitude window.

3.3.2 Task 2: Analysis of shear-wave splitting measurements

Investigate reasons why observed time-delays between split shear-waves in Iceland are approximately twice those usually observed elsewhere.

The range of time-delays between split shear-waves is found to vary between different regions worldwide and sometimes between different stations in the same region. Time-delays vary with crack density, crack aspect ratio, and isotropic P- and S-wave velocities, these can be calculated. These are reasonably well-understood. They are also observed to be higher in regions with high heat flow and this is believed to be the main reason for the larger values observed in Iceland. It is interesting that since the Vatnajökull eruption in 1996, the level of time-delays has been decreasing for both Band-1 and Band-2 by approximately 2 ms/km over 1997-1998 (Figures 26a and 26b). It would appear that the crust has been slowly adjusting to the strain released by the eruption as the mid-Atlantic ridge gradually takes up the change in strain. However, there are many things we do not yet understand. In particular, the large scatter of time-delays and polarizations is difficult to explain. It is probable that the explanation for all these phenomena will take some years before they are fully understood.

3.3.3 Task 3: Establish shear-wave splitting map of Iceland

A background map will allow changes in polarizations and time-delays to be recognized before earthquakes, eruptions, and possibly strain-waves.

Figure 25 shows a map of shear-wave splitting polarizations at the stations with more than five arrivals within the shear-wave window out to 45°. Experience suggests that an overall shear-wave splitting map is not so useful as was first thought. The optimum procedure seems to require individual studies of shear-wave splitting at individual stations.

3.3.4 Task 4: Calibrate techniques and behaviour if and when changes are identified

Identify optimum areas and calibrate techniques and behaviour if and when changes are identified. This task is only carried out if changes are observed, when it has high priority (see Task 1).

The SW of Iceland was proved to be a very active seismic area during the last 3 years. More stations around SAU and BJA which show particularly good alignment of polarizations, will possibly improve the time delay patterns. If the same events are recorded at more than one stations, this will give much greater constraints on the anisotropy.

Concerning the NE part of Iceland, one or two additional SIL stations will improve the shear-wave splitting analysis near the Húsavík transform fault and Grímsey zone.

Changes have been recognized (see Task 1) where a magnitude 5 earthquake was successfully stress-forecast. It has been found difficult to separate the activities of Task 1 and Task 4 when changes in shear-wave splitting were identified. Since their activities are effectively inseparable.

3.3.5 Meetings

PRENLAB-2 workshop at Húsavík, Iceland, July 30, 1998. Attended by Stuart Crampin and Theodora Volti.

3.4 Subproject 4: Borehole monitoring of fluid–rock interaction

Contractor:

Frank Roth
Stiftung GeoForschungsZentrum Potsdam
Division: Solid Earth Physics and Disaster Research
Section: Earthquakes and Volcanism
Telegrafenberg A34
D–14473 Potsdam
Germany
Tel.: +49–331–288–1210
Fax: +49–331–288–1203
E–mail: roth@gfz-potsdam.de

Subcontractor:

Valgarður Stefánsson
National Energy Authority (Orkustofnun, OS)
Grensásvegur 9
IS–108 Reykjavík
Iceland
Tel: +354–569–6004
Fax: +354–568–8896
E–mail: vs@os.is

In the framework of the PRENLAB project, repeated loggings are carried out to obtain a time series of logs in the South Iceland seismic zone (SISZ). An 1100 m deep borehole (LL–03, "Nefsholt") inside the zone (63.92°N, 20.41°W, 7 km south of the seismic station SAU) is used and provides the unique opportunity to perform measurements much nearer to earthquake sources than usual – the hypocenter depths at that location range between 6 and 9 km. Moreover, data can be obtained for a depth interval of more than 1000 m, uninfluenced by the sedimentary cover and less disturbed by surface noise.

In the preparatory phase of an earthquake, stress accumulation is expected to be connected with the creation of borehole breakouts (BOs), changes in the number and size of cracks, a possible variation of the stress direction, etc. Therefore, the following set of geoparameters is monitored:

- P-wave travel time.
- Electrical conductivity.
- Stress information from borehole breakouts (orientation and size).
- Crack density.

This is achieved by repeated logging with tools as:

- Sonic log (BCS).
- Gamma–ray (GR).
- Spectral gamma–ray (SGR).
- Dual induction/latero log (DIL).
- Neutron–neutron log.
- 16"- and 64"-resistivity log.

- Spontaneous potential log (SP).
- Four-arm-dipmeter (FED).
- Borehole televiewer (BHTV).

The neutron-neutron log, the 16"- and 64"-resistivity log and the SP log are run with the logging equipment of OS, the rest with the Halliburton logging truck of GFZ.

Investigations on the stress field in the SISZ:

Besides the repetition of logs in borehole LL-03 Nefsholt, we performed single logging campaigns at other boreholes to check the state of the regional stress field. This is important for two reasons:

- From the San Andreas fault we know that fault zones may be in a low stress state between earthquakes, which gets visible through stress orientations perpendicular to the strike-slip fault instead of pointing at it under an angle of 30° to 45°. To determine the present state of stress in the SISZ, it is important to see if there are stress components, that are not perpendicular to existing faults and favour earthquakes on them.

- The SISZ is no typical transform zone. Looking at the orientation of opening at the adjacent rifts, one would expect a left-lateral strike-slip zone in roughly E-W direction (N103°E) to connect the Reykjanes ridge and the eastern volcanic zone of Iceland. Instead earthquakes occur on en-echelon N-S striking right-lateral faults. Assuming an angle of 45° between the maximum horizontal compressive stress and the fault (as it is done constructing fault plane solutions) both planes are equivalent. From a rock mechanics point of view, expecting an angle of about 30° between fault and maximum horizontal principal stress, the stress orientation at N-S striking faults should be N30°E, compared to N60°E at an E-W striking transform.

3.4.1 Task 1: Logging in borehole Nefsholt

Until now, 6 logging campaigns took place. The locations are shown in Figure 27. Table 1 lists the logs performed during the first three years of this project.

In 1996 three campaigns were carried out. During the first campaign, well LL-03 (Nefsholt) was chosen as the place for repeated logging after well NG-01 collapsed between two logs and was abandoned. In addition, it was measured in 4 other boreholes: HS-36 (Reykjavík), LPN-10 (Laugaland), LJ-08 (Syðra Laugaland) and TN-02 (Ytri Tjarnir). In September 1996, neutron-neutron logs, X-Y-caliper logs, SP logs and 16"- and 64"-resistivity logs were run by OS. The campaign in October 1996 only had the task of repeated logging at LL-03 (Nefsholt). In 1997 two logging campaigns were carried out, one in September, the second in December. The first was exclusively concerned with repeated logging in borehole LL-03 (Nefsholt). During the second campaign, additional logs were run with the borehole televiewer in Böðmóðsstaðir (located at the northern boundary of the SISZ, close to Laugarvatn) and in Þykkvibær (slightly south of the SISZ, near the south coast).

In 1998 since the beginning of PRENLAB-2 until now, one campaign was carried out. In addition to the repeated logging in well LL-03 (Nefsholt), BHTV-logs were run in wells BS-11 (Böðmóðsstaðir) and LJ-08 (Syðra Laugaland).

These six campaigns have contributed to the two aims of this subproject, that are:

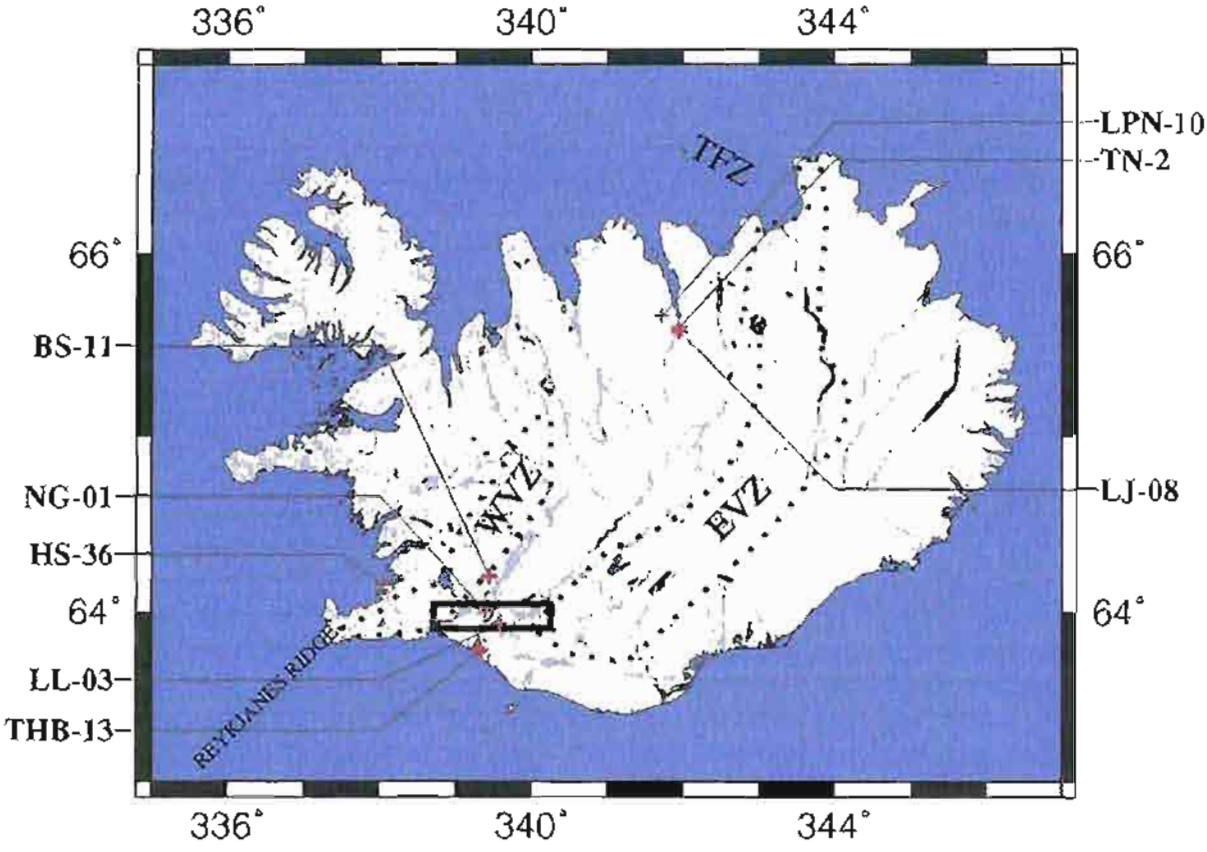

Figure 27. *Map of Iceland showing the location of the site of repeated logging (Nesjavellir) and of the other boreholes, where measurements have been performed.*

Name:	Location:	Max. depth:	Logged interval:	Tools used:	Date:
NG–01	Ólafsvellir (inside SISZ)	1070 m	180–1070 m	FED, GR	July 1996
HS–36	Reykjavík	980 m	330–980 m	BHTV, BCS-GR	July 1996
LPN-10	Laugaland near Akureyri, North Iceland	890 m	80–880 m	BHTV, BCS-DIL-GR	July 1996
LJ–08	Syðra Laugaland near Akureyri	2740 m	120–1890 m 120–1330 m 500–1980 m	FED, BHTV, BCS-DIL-GR, BHTV	July 1996 June 1998
TN–02	Ytri-Tjarnir near Akureyri	1370 m	260–1370 m	BCS, GR	July 1996
LL–03	Nefsholt (inside SISZ, site of repeated logging)	1309 m	80–1100 m	BHTV, BCS-DIL-GR SGR Logging by OS: neutron–neutron, X-Y–caliper, 16"- and 64"-resistivity, SP	July 1996 October 1996 September 1997 December 1997 June 1998 September 1997 June 1998 September 1996
THB–13	Þykkvibær SW of Hella near the south coast	1254 m	466–1225 m	BHTV	December 1997
BS–11	Böðmóðsstaðir near Laugarvatn	1193 m	703–1090 m 500–1090 m	BHTV	December 1997 June 1998

Table 1. *List of locations, were logging was performed. As borehole NG–01 partly collapsed between log runs, the hole was abandoned and well LL–03 was chosen for repeated logging. GR indicates gamma–ray log, SP stands for spontaneous potential. FED means four–arm–dipmeter, which includes an oriented four–arm–caliper. BHTV means ultrasonic borehole televiewer. BCS is borehole compensated sonic log; DIL is dual induction/latero log. The deepest parts of wells LJ–08, LL–03, THB–13 and BS–11 were not accessible anymore.*

- Observation of changes in physical parameters of the rock and of changes in degree of fracturing and orientation of principal stresses with respect to seismic activity.

- Indirect measurement of tectonic stress orientation to evaluate the tectonic stress field in the area of the SISZ. For that the borehole geometry was observed for certain structures, that allow to determinate the orientation of the horizontal principal stress, as there are borehole breakouts and vertical tensile fractures. Borehole breakouts are failures of material of the borehole wall, that result from accumulation of tangential stress at the borehole wall perpendicular to the maximum horizontal principal stress (σ_H), caused by the free surface produced by drilling. At this free surface, the tensile strength of the borehole wall can be exceeded at the azimuth of the maximum principal horizontal stress, what produces vertical fractures along σ_H. These vertical fractures extend in the direction of the maximum and open in the direction of the minimum horizontal principal stress (σ_h). The occurrence of these tensile fractures can be enhanced by thermal stress caused by cold water pumped into the well.

3.4.2 Tasks 2, 3 and 4: Cross correlation of logs of the same type of this campaign to those from earlier campaigns, to search for changes in the rock physical parameters and the physical state of the rock around the borehole; Comparison of changes in logs of different type; and Comparison of changes in logs with changes in seismicity, fault plane solutions, shear-wave splitting, gravity, borehole strainmeter readings, crustal deformation, etc., to investigate if changes found in the borehole can be related to anomalies detected with other methods and if they can be related to the preparation of seismic activity.

Repeated loggings in LL-03 - sonic velocity and latero log resistivity:

The difference in the sonic velocity of logs measured at one day varies by 3.0% around the average value (cf. Figure 28).

At some depth intervals, greater differences between repeated logs are caused by inaccurate depth matching, e.g. at 740 m in Figure 28. Depth intervals, where the amplitude of the measured signal is very low, show significant variation in the (automatically) picked travel-times, thus cannot be considered for an analysis of changes.

Greater variations between logs of different logging campaigns could not be found until now.

The latero log resistivity also shows this good repeatability, see red curves in Figure 29.

Repeated loggings in LL-03 - dual-induction-log (deep and medium penetration):

The repeated measurements with the dual induction log (deep and medium penetration) show variations in resistivity even between different logs of one day. Therefore these values can not be used for an analysis of changes. Besides that, the resistivity values of the dual induction log are much too high. They are much higher than the resistivity values of the latero log and one to even two orders of magnitude higher than values expected for Icelandic basalt.

The problem can be solved as follows: The raw data measured by the tool are values of voltage. These values show a good repeatability for logs measured at one day. They are proportional to the conductivity of the formation. Using the formula, which is used

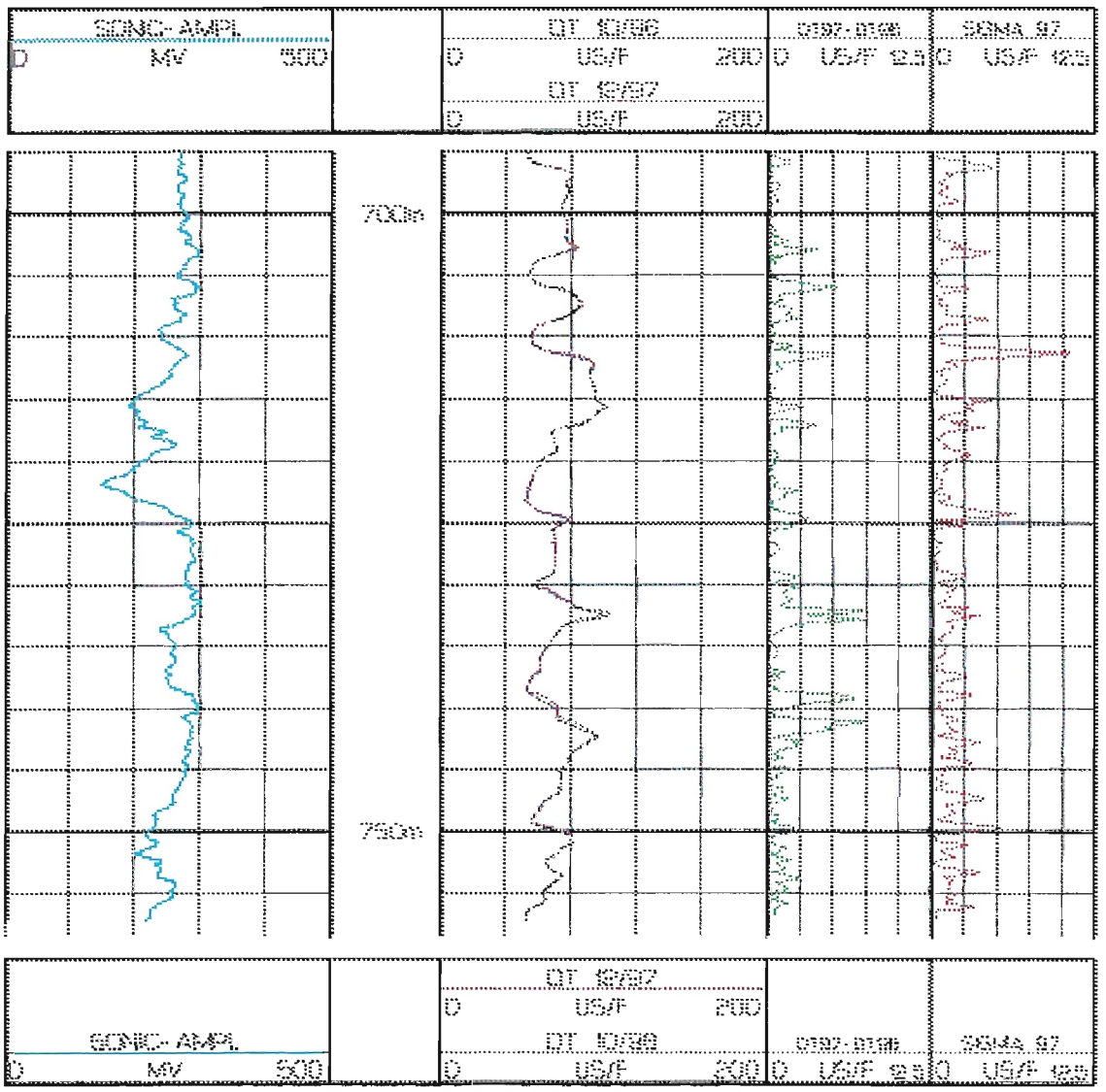

Figure 28. *Data example showing from left to right panel: an average curve of sonic amplitude, a superposition of the average compensated travel times measured in October 1996 and in December 1997 (each averaged over four runs performed immediately one after the other), the difference between these two average travel time curves (absolute value, green curve) and the standard deviation (absolute value) derived from the four runs performed in December 1997. Compensated travel times are given in microseconds per foot. The difference between the average travel times exceeds the standard deviation only in low amplitude intervals (not shown here) or at depths with inaccurate depth-matching (for example around 740 m).*

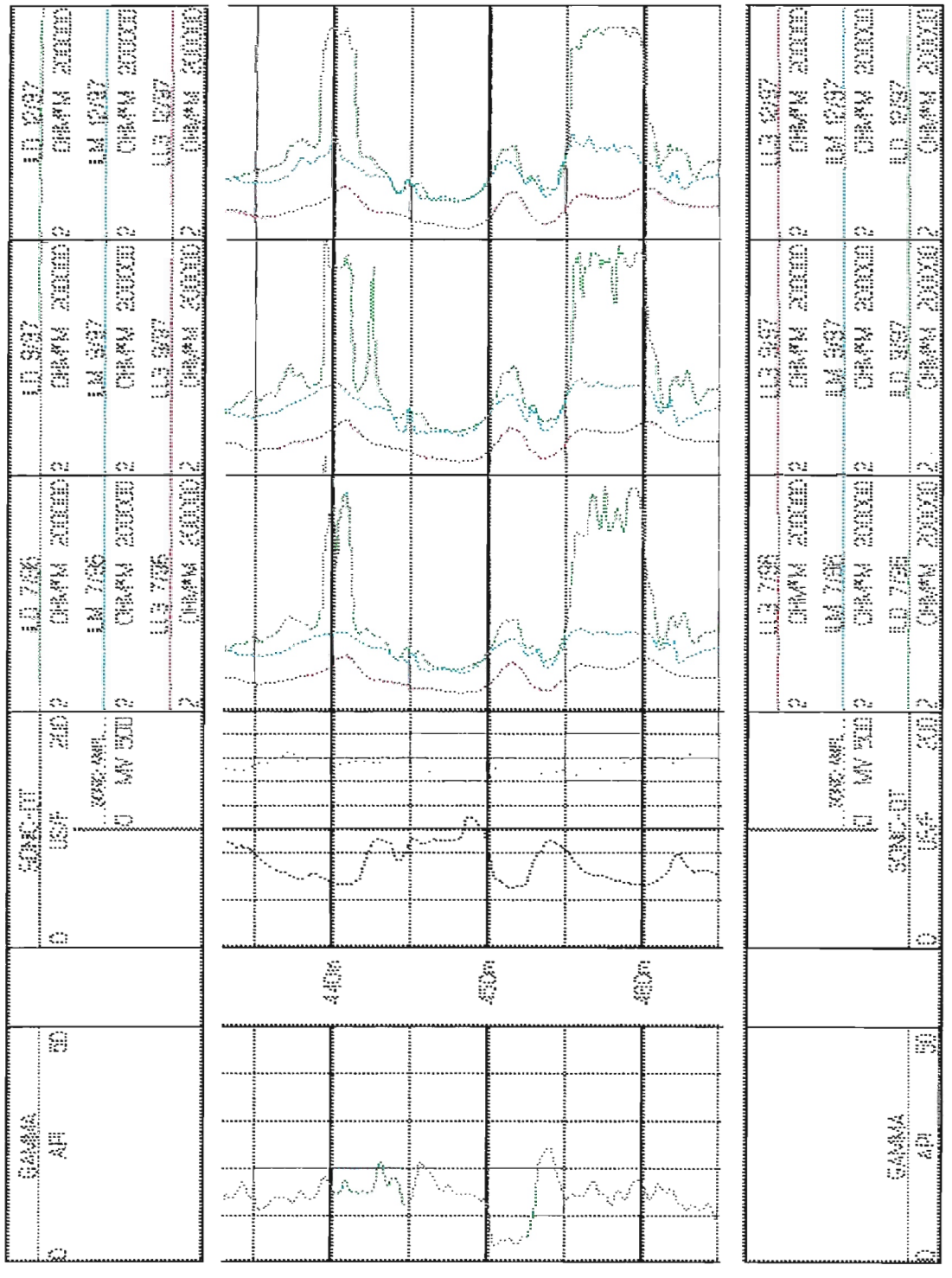

Figure 29. *Data example showing from left to right: gamma–ray log in API units, compensated travel time in microseconds per foot and the sonic amplitude, and three repeated measurements of latero log (LL3), induction log with medium penetration (ILM) and induction log with deep penetration (ILD). Month and year of campaign are given.*

for the calculation of the resistivity values by the tool, the measured resistivity values can be reproduced except in those cases where the measured values of voltage are below 0 mV. In such cases, the resistivity is set to a maximum value of 100000 Ωm by the tool. The resistivity values only show great variations in the highest values. These variations are caused by the great relative error of the values of voltage of about 0 mV, from which the highest resistivity values are calculated by the tool in calculating the reciprocal value.

Values of voltage below 0 mV can only be explained by an offset potential in the electronics, which has to be about 50 mV (the accuracy of calibration of the zero potential of the tool is 10 mV). When the values of voltage are corrected with a shift of +50 mV, the resistivity values calculated from these corrected values of voltage are in the same order than the resistivity values of the latero log. Assuming that this offset of the dual induction log (deep and medium penetration) is constant for all the campaigns, the voltage values can be used for a correlation between different loggings.

Under this assumption and correction, the values of the dual induction log (deep and medium penetration) of the campaigns since December 1997 show the same values and the logs before December 1997 show same values. However, there is a significant change in the data of the dual induction log (deep and medium penetration) between the logs since December 1997 (campaigns December 1997 and June 1998) and the logs of the campaigns before (campaigns July 1996, October 1996 and September 1997).

For the induction log with deep penetration the values of the campaigns after December 1997 are lower than the values of the campaigns before December 1997 (cf. Figure 30). The curves of the logs before December 1997 (campaign December 1997) look similar to the logs measured since December 1997, when they are multiplied with a factor of 1.2. The change of measured values unfortunately correlates with an exchange of the tool electronics of the induction log with deep penetration before the logging campaign December 1997. But a factor of 1.2 between the logs is too high to be explained by the change of the tool electronics, because the tool electronics were calibrated before each run.

Moreover, the values of voltage of the induction log with medium penetration show a behaviour inverse to the values of the induction log with deep penetration. They have decreased after the campaign September 1997 (cf. Figure 31), just when the others increased.

Investigations are made now to check whether the measuring characteristics of the tool have changed since the beginning of the project and are responsible for these offsets.

Borehole televiewer measurements:

The borehole televiewer data collected in the well at Nefsholt presented in the reports before 1998 have to be corrected for an error in orientation! To give the data the right orientation, it is necessary to change the coordinate system from clockwise to counterclockwise rotation, i.e. the azimuth has to be mirrored at magnetic north. Breakout orientations and fracture statistics from the measurements in the SISZ (including Nefsholt with the correct orientation) are shown in Table 2 and Figure 35.

Nefsholt:

The previously found orientation of the borehole breakouts of about N35°E has to be corrected to 120.5° to 126°, giving a direction of the maximum horizontal principal stress of N30.5°E to N36°E. The circular standard deviation (1σ) is of the order of 10°. The stress direction is in agreement with the expected stress direction from large scale tectonics (left–lateral strike–slip). The length of picked breakouts sums up to approximately 5.5 m.

308 fractures have been picked in the depth interval between 300 m and 1090 m.. Determination of dip–angle and –direction are presented in Figure 32. They show that

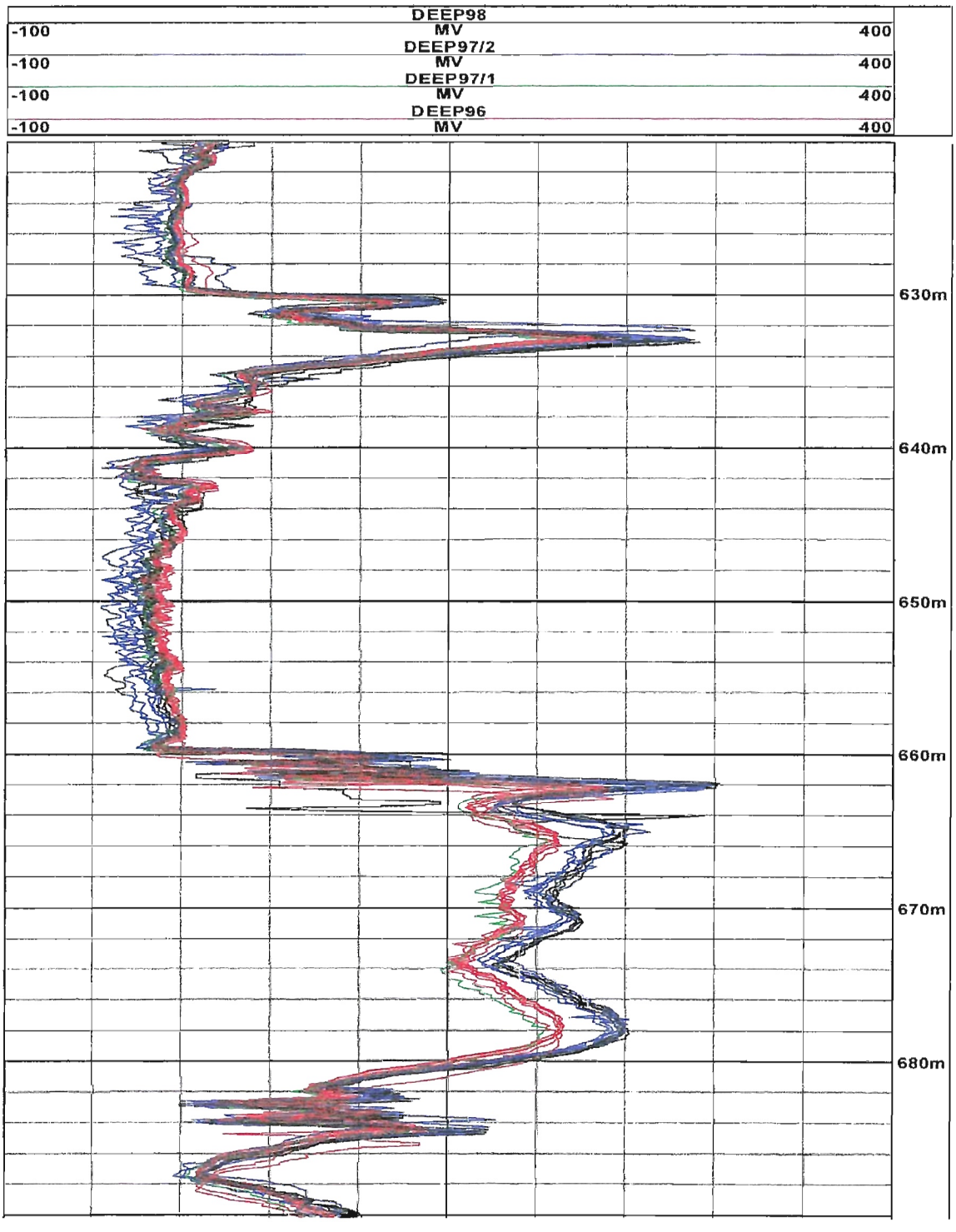

Figure 30. *Data example showing the values of voltage of the induction log with deep penetration; all four logs from June 1998 (black), all five logs from December 1997 (blue), one log from September 1997 (green) and six logs from July 1996 (red).*

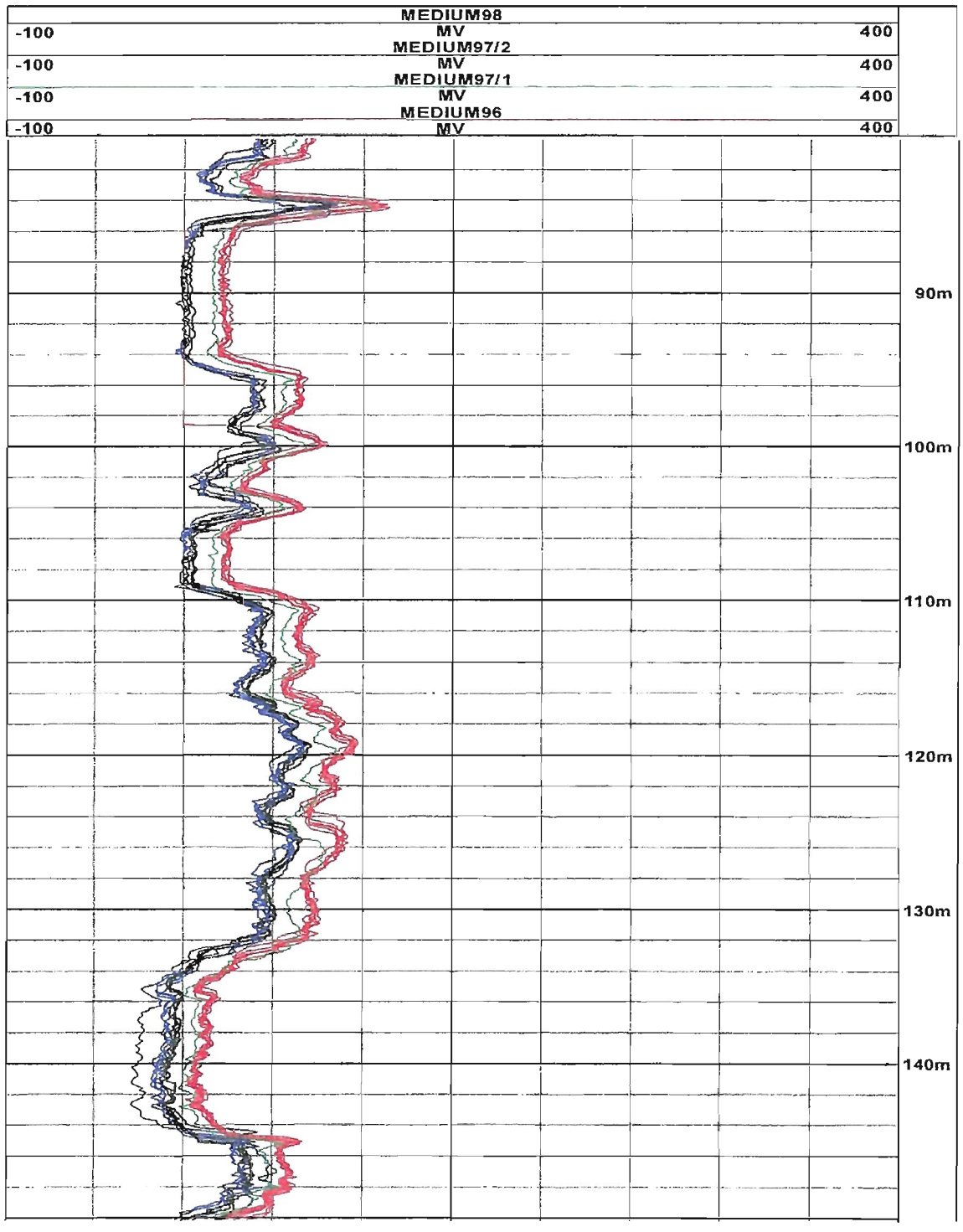

Figure 31. *Data example showing the values of voltage of the induction log with medium penetration; all four logs from June 1998 (black), all five logs from December 1997 (blue), one log from September 1997 (green) and six logs from July 1996 (red).*

most of the steep dipping fractures (dip angle greater than 60°) are dipping ESE, a slightly smaller set of steep fractures dipping WNW. Considering all fractures, this trend is much less pronounced, but there is still a preferred dip-direction of W to WNW with a smaller dataset of dip-angles ESE. The averaged strike of these fractures is thus NNE, like the strike of the fractures observable at the surface.

Þykkvibær:

Borehole breakouts have been found in the depth intervals 925 m to 927 m and 937 m to 941 m. The breakouts in these two depth intervals sum up to approximately 3.5 m. Data quality is rather poor due to weak reflection amplitudes. Figure 33 shows a data example. The average breakout azimuth is between N105°E (upper depth-interval) and N121°E (lower depth-interval). Statistic analysis over the whole depth range gives a breakout-orientation of N111°E with a circular standard deviation (1σ) of about 10°. This would mean that the larger principal horizontal stress is in average oriented N21°E. This is in agreement with the stress directions expected from the overall tectonics as well as with the results from Nefsholt.

Böðmóðsstaðir:

No breakouts have been observed in this borehole, but there are vertical fractures visible between 713 m and 934 m depth. The length of the vertical fractures sums up to 45 m. Vertical fractures are expected to occur in the direction of the maximum horizontal principal stress because of tensile failure of the borehole wall. They are supposed to be drilling induced and not of natural origin. Their orientation is the one of the larger horizontal principal stress. These fractures occur at an azimuth of N45°E to N90°E. A data example is presented in Figure 34.

Additional to the drilling induced fractures, 52 natural fractures have been picked in the depth interval between 820 m and 1060 m. The steep dipping fractures (dip angles greater 60°) show a dominant strike ENE. Regarding all natural vertical fractures, there are two datasets: one striking nearly N and the other striking ENE to E.

Well:	Logged interval:	Interval with BOs/ vert. fractures:	Total length of BOs/ vert. fractures:	Orientation of σ_H:	Std. deviation:
BS-11	703-1090 m	713-934 m	45.0 m fract.	N45°E-N90°E	—
LL-03	80-1100 m	780-983 m	5.0 m BOs	N30°E	12°
THB-13	466-1225 m	925-941 m	3.5 m BOs	N21°E	10°

Table 2. *Stress orientations found at SISZ from borehole televiewer logs.*

Results:

The results can be summarized as follows:

- The repeated measurements of sonic P-wave velocity and the latero log resistivity show good repeatability.
- The repeated resistivity measurements with the dual induction log (deep and medium penetration) show a change between the logging campaigns in September and December 1997. The values of voltage of the induction log with deep penetration generally increased and the values of the induction log with medium penetration generally decreased. No correlation to any seismic activity or other observations was found, so far. Investigations on possible reasons are still going on.

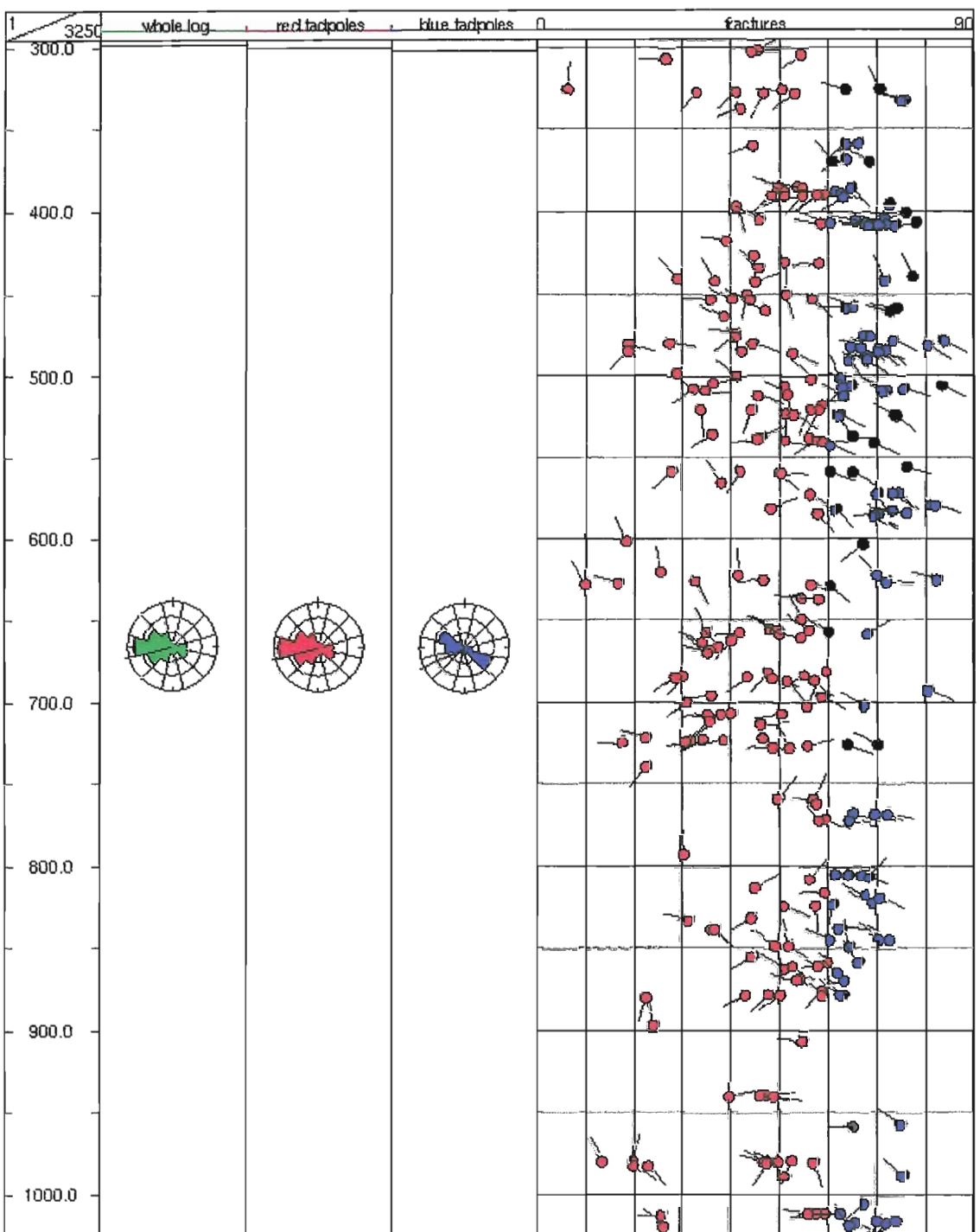

Figure 32. *Strike and dip of fractures observed in Nefsholt. Blue rose diagrams: dip–angles greater 60°; red rose diagrams: dip angles less than 60°; green rose diagrams: all fractures.*

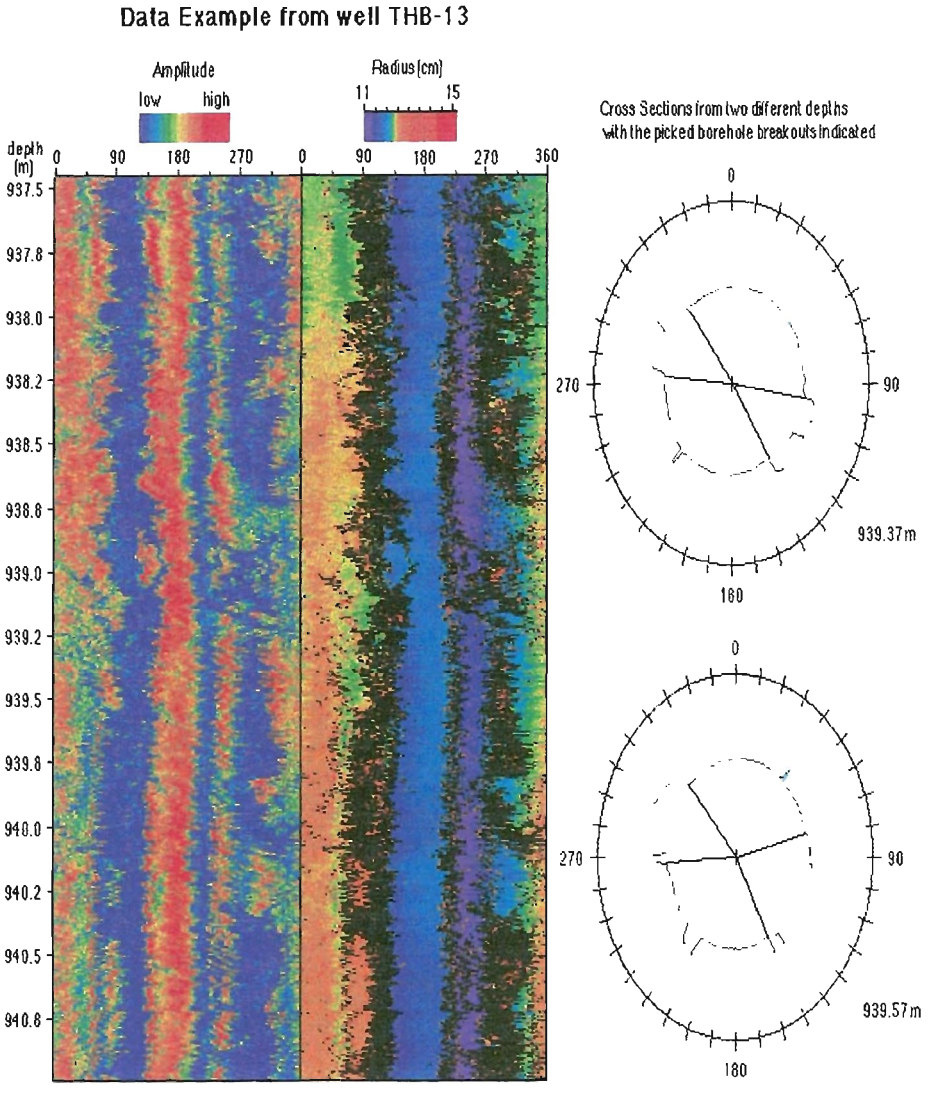

Figure 33. *Example for the borehole breakouts found in Þykkvibær with two cross sections. The two panels show the amplitude of the reflected signal (left) and the radius calculated from the travel time (right), both unwrapped from N over E, S, W to N. Vertical axis: depth in meters. Breakouts appear as vertical bands of low reflection amplitudes. Due to low reflection amplitude, the values for the radius are often missing in these parts, resulting in black bands. In the two cross sections, the black lines indicate the range in azimuth of the picked breakouts.*

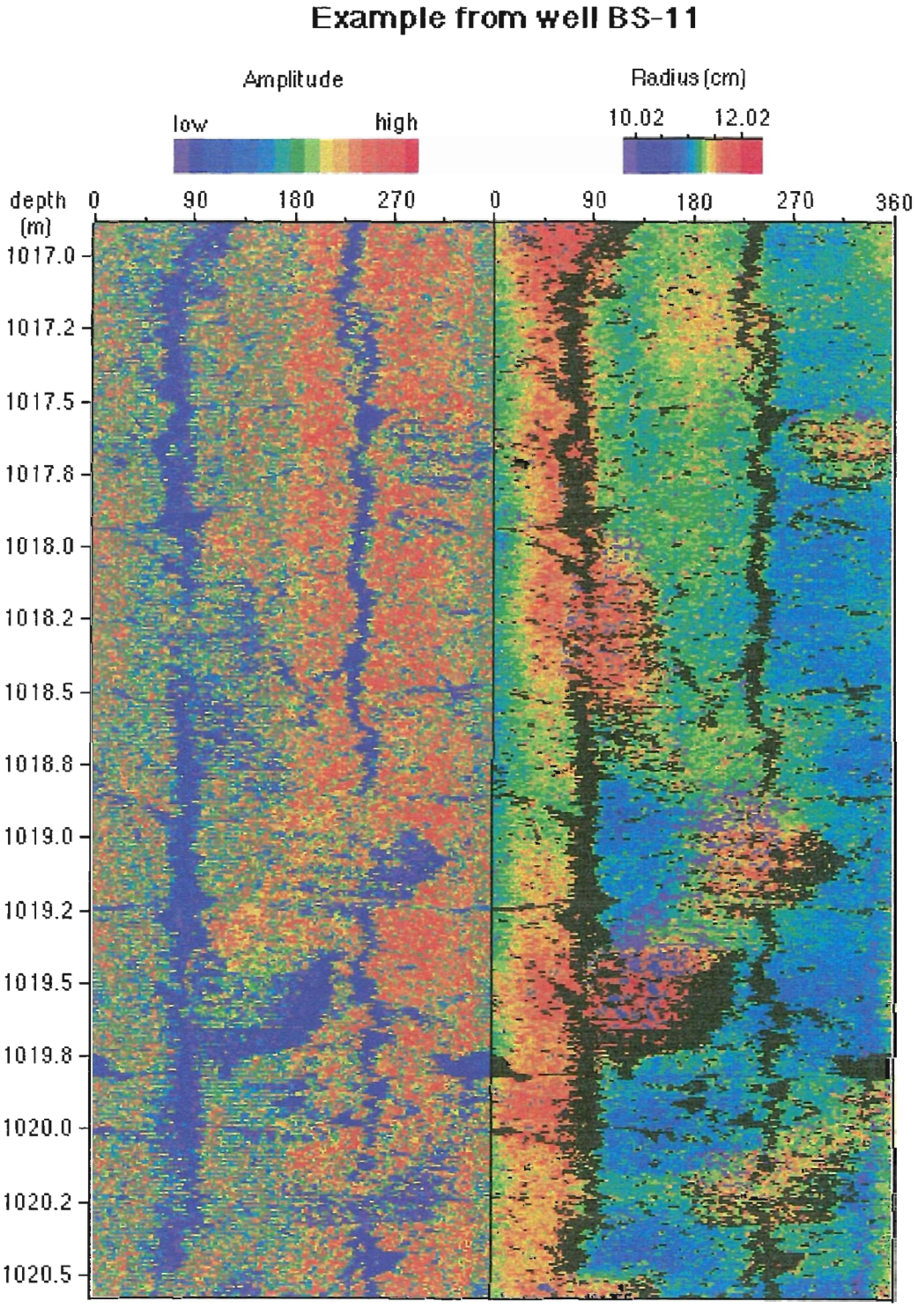

Figure 34. *Example for drilling induced vertical fractures observed in the borehole at Böðmóðsstaðir. Same principle of displaying the data as described in Figure 33. The fractures appear as narrow vertical stripes of low reflection amplitude. Values for the radius calculated from travel time are missing for these stripes due to low amplitudes.*

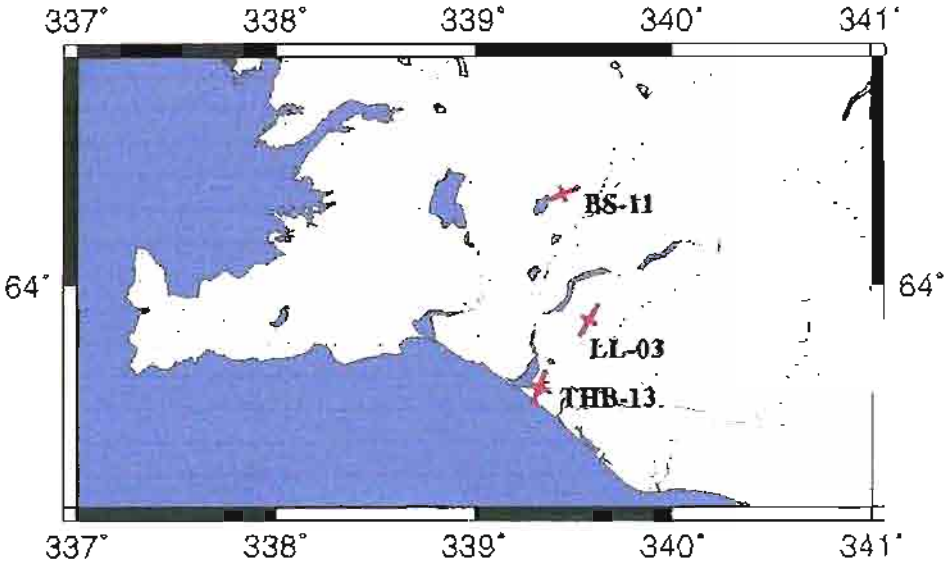

Figure 35. *Map of South Iceland showing the stress orientations found at Nefsholt, Þykkvibær and Böðmóðsstaðir.*

- The stress orientations found at all three locations are similar and agree with a left-lateral strike-slip regime. They are not perpendicular to existing ruptures found for large earthquakes in the SISZ and, therefore indicate, that the SISZ is not a weak fault, as postulated for the San Andreas fault. Borehole breakouts observed in Nefsholt and Þykkvibær show the maximum horizontal principal stress at an azimuth of approximately NNE (N21°E to N36°E), see Figure 35 and Table 2. The data obtained in Böðmóðsstaðir show an average direction of maximum principal horizontal stress ENE, see Figure 35 and Table 2. Thus, the direction of maximum principal horizontal stress, as found by the borehole televiewer data, varies from NNE (north of the SISZ, BS-11) to ENE (south of the SISZ, THB-13). This NNE variation is slightly more than the standard deviation. From a rock mechanics view, the stress directions found at Nefsholt (LL-03) and Þykkvibær (THB-13) fit to N-S striking faults, as they are found in the SISZ. On the other hand, the orientation of maximum horizontal principal stress found at Böðmóðsstaðir fits to the model of an E-W striking transform fault zone. Similar stress orientations were also found by Stefánsson et al. 1993 from fault plane solutions. This was confirmed by Angelier et al. 1999, who found a mean orientation of σ_H of N56°E derived from 1916 fault plane solutions quality selected from 4413 earthquakes in the SISZ during the years 1995 to 1997. A NE-SW orientation of σ_H was also the result of investigations of Crampin et al. 1999 on shear-wave splitting due to crustal stress anisotropy at four of six seismic stations in the SISZ.
- Fractures found down to nearly 1100 m depth show the same dominant strike as

those observed at the surface. A dependency of fracture orientation with depth or with geographical latitude could not be seen so far.

- Orkustofnun provided a lithology log of the well at Nefsholt. This log is based on cuttings (rock pieces crushed while drilling), not on cores, what strongly limits its resolution in depth and rock type. It shows a nearly continuous sequence of altered basalt, interrupted only by a few thin sedimentary layers and some thin layers of dolorite, hyaloclastites and fresh basalt. The loggings show a more detailed picture of the borehole, so that in sections of the borehole with basalt different lava flows can be distinguished. They have a core with a low porosity a high P-wave velocity and a high resistivity, while the boundaries of the layers show a higher porosity and lower resistivity and P-wave velocity. The thickness of basalt flows varies from 10 m to 20 m. For some depth intervals a good correlation between different kind of layers and characteristic sets of logs can be seen, cf. example in Figure 36 and Table 3.

Depth interval:	GR:	BCS:	Neutron-neutron:	DIL:	Lithology:
265-275m	low	low	low	high	altered basalt
275-280m	low	high	high	low	sediment
280-285m	low	low	low	high	altered basalt
285-298m	high	high	high	low	sediment
298-305m	high	low	low	high	fresh basalt

Table 3. *Characteristic set of log values for different kinds of layers, derived from Figure 36.*

Participants:

Besides the contractor and the subcontractor, the following scientists and technicians have supported the subproject in the present phase:
G. Axelsson (OS), H. Bäßler (Karlsruhe), C. Carnein (GFZ), E.T. Elíasson (OS), H.-J. Fischer (GFZ), P. Fleckenstein (GFZ), S.Þ. Guðlaugsson (OS), K. Henneberg (GFZ; now at PGS Oslo), G. Hermannsson (OS), M. Hönig (GFZ), G. Kurz (GFZ; now at NLfB-GGA Hannover), S. Mielitz (GFZ), H. Sigvaldason (OS), Ó. Sigurðsson (OS), V. Stefánsson and B. Steingrímsson (OS).

3.4.3 Acknowledgements

We are very grateful to all above named participants. We thank Orkustofnun for excellent preparation and support of the logging campaigns. We like to thank the owners of the boreholes for their permission to work in the wells. We are very grateful to GeoSys company and the Geophysical Institute of Karlsruhe University for lending us a BHTV and additional equipment for the logging campaign in June 1998. We also thank the GFZ logging team very much.

3.4.4 References

Stefánsson, R., R. Böðvarsson, R. Slunga, P. Einarsson, S. Jakobsdóttir, H. Bungum, S. Gregersen, J. Havskov, J. Hjelme & H. Korhonen 1993. Earthquake prediction

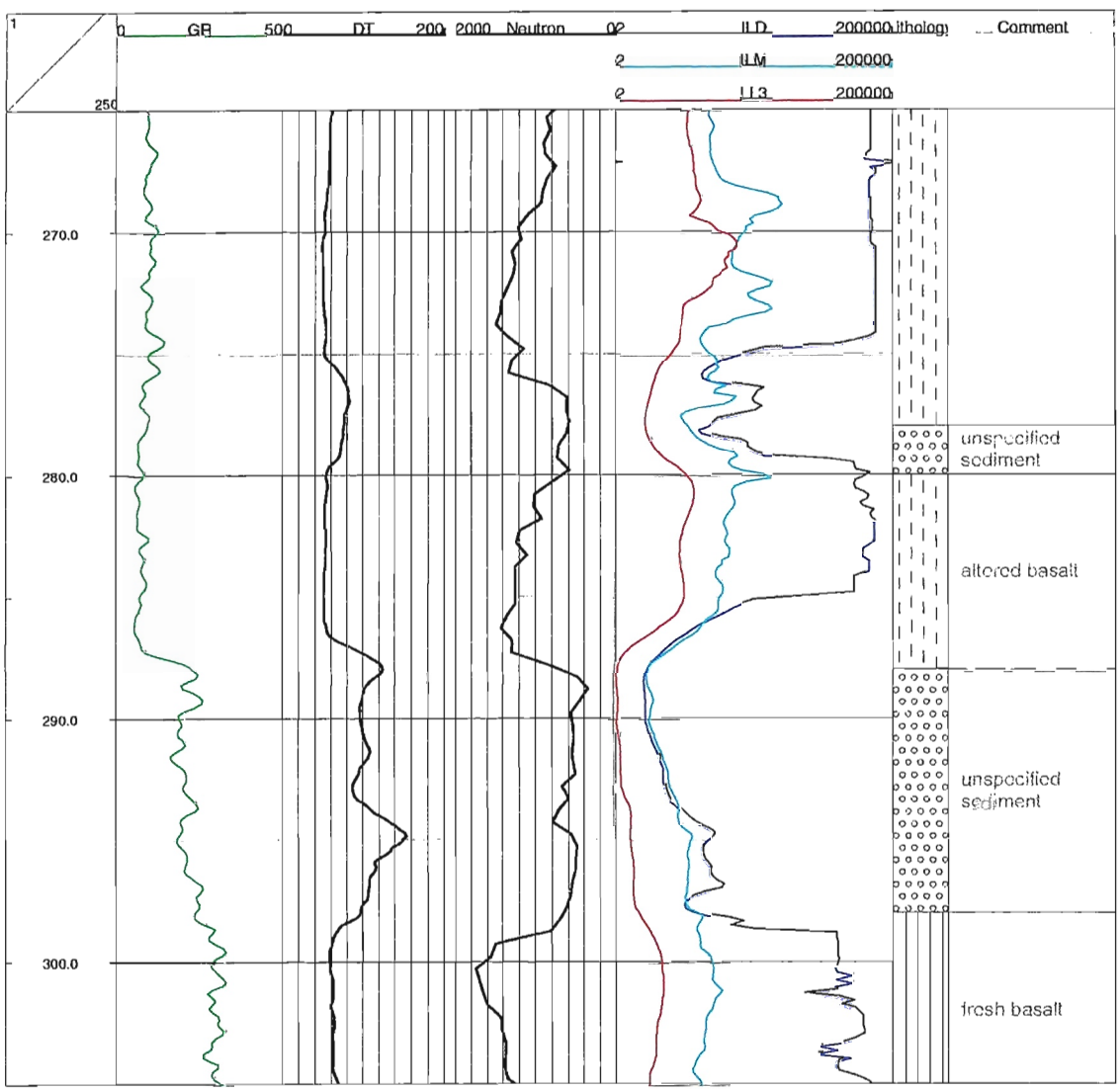

Figure 36. *Data example showing the correlation between the performed logs and the lithology based on the analysis of cuttings provided by Orkustofnun. GR = gamma-ray in API units, DT = compensated travel time in microseconds per foot, Neutron = neutron-neutron log in API units, ILD = induction log with deep penetration in Ωm, ILM = induction-log with medium penetration in Ωm, LL3 = latero log in Ωm.*

research in the South Iceland seismic zone and the SIL project. *Bull. Seism. Soc. Am.* 83, 696-716.

Angelier, J., F. Bergerat & S.Th. Rögnvaldsson 1999. Perturbation of plate-scale extension across oceanic rift and transform faults revealed by inversion of earthquake focal mechanisms in Iceland. In: *Annales Geophysicae.* Abstracts from the XXIV EGS General Asembly, The Hague, The Netherlands, April 19-23, 1999.

Crampin, S., T. Volti & R. Stefánsson 1999. A successfully stress-forecast earthquake. *Geophys. J. Int.*, in press.

3.5 Subproject 5: Active deformation determined from GPS and SAR

Contractor:

Freysteinn Sigmundsson
Nordic Volcanological Institute
Grensásvegur 50
108 Reykjavík
Iceland
Tel: +354-525-4494
Fax: +354-562-9767
E-mail: fs@norvol.hi.is

Associated contractor:

Kurt L. Feigl
Centre National de la Recherche Scientifique
UPR 0234 - Dynamique Terrestre et Planétaire
14 Avenue Edouard Belin
FR-31400 Toulouse
France
Tel: +33-5-6133-2940
Fax: +33-5-6125-3205
E-mail: kurt.feigl@cnes.fr

Subcontractor:

Páll Einarsson
Science Institute
University of Iceland
Hofsvallagata 53
107 Reykjavík
Iceland
Tel: +354-525-4816
Fax: +354-552-8801
E-mail: palli@raunvis.hi.is

3.5.1 Subpart 5A: SAR interferometry study of the South Iceland seismic zone

The Hengill triple junction, at the western end of the Southern Iceland seismic zone (SISZ), exhibits the highest level of continuous seismicity in Iceland. In July 1994, an unusually persistent swarm of earthquakes, with magnitude less than 4, continued through 1995 with intermittent activity through 1999. This seismicity appears to be mechanically coupled to the ongoing volcanic activity. To study this coupling, we measure crustal deformation using interferometric analysis of synthetic aperture radar (INSAR) images acquired by the Earth Resources Satellites ERS-1 and ERS-2 of the European Space Agency. This technique provides dense ($\sim$100 pixels/km^2) spatial coverage and monthly sampling in the summer months between 1993 and 1998. The resulting interference patterns show clear fringes, even after four years, on the barren ground cover near the Hengill central volcano. The radar coherence breaks down, however, in less than a month in the coastal lowlands containing most of the active faults of the SISZ. The principal signal in the interferograms

is a concentric pattern with radius of approximately 10 km, centered on Hrómundartindur volcano. These fringes indicate a relative shortening of the radar line-of-sight distance (range) of approximately 1.5 cm/year. We intepret this signature as mostly vertical uplift due to increasing pressure in a magma chamber at depth. To explain it, we employ a simple "Mogi" model of a point source in an elastic half space. After estimating the four parameters of this model for each of the 10 observed interferograms, we find that the rate of uplift is constant, with an average value of 19±2 mm/year from 1993 through 1998. The best fitting models locate the point source at a depth of 7±2 km depth at 64.032/*circ*N and 21.213/*circ*W. The constant rate of volcanic deformation contrasts markedly with the episodic moment release by swarms or "crises" of earthquakes. To explain this contrast, we propose that the ongoing volcanic activity increases the stress in the brittle country rock. When the stress reaches the Coulomb failure threshold, the rock breaks, rupturing a fault and releasing the stress (Figure 37).

3.5.2 Subpart 5B

3.5.2.1 Subpart 5B(1): GPS measurements of absolute displacements

The work planned in this subproject changed significantly in response to the enhanced earthquake activity at Hengill at the western end of the SISZ. Rather than operating one semi-continous GPS station, we participated in the installation of 4 continously recording GPS stations in the Hengill area as described in Subproject 1. The equipment for these stations was bought from funding external to the PRENLAB-2 project, but PRENLAB-2 funding was used for the installation.

The planned static GPS measurements were also concentrated on the Hengill area. The static measurements have been conducted at regular intervals of few months since the beginning of the PRENLAB-2 project, and these show the continued expansion and uplift of the area of the enhanced earthquake activity (Hreinsdóttir et al. 1999a).

PRENLAB-2 related work includes also static GPS measurements on the Reykjanes peninsula in 1998, that shows how left-lateral shear is continuously accumulating across the plate boundary in South Iceland (Hreinsdóttir et al. 1999b). A study has also been conducted on how to relate crustal uplift, to the volume of magma/gas accumulation at depth in the crust (Johnson et al. 1999). This is considerable of interest for the activity at Hengill, as one must understand how to relate the observed crustal deformation to changes that take place at deeper level in the crust, e.g. magma accumulation.

3.5.2.2 Subpart 5B(2): Digitized fault map (subcontract)

A digitized fault map of the South Iceland seismic zone is a prerequisite for a meaningful interpretation of deformations measured by SAR and GPS technology. Surface expressions of seismogenic faults of the area have been mapped in varying detail during the last two decades, most extensively by students in the Department of Geology and Geography of the University of Iceland. It was decided to gather this information and assemble a homogeneous map of the faults in digital form. This task was approached in two steps:

- Field work to fill in the largest gap in the area, the Holt district. This part of the seismic zone is covered with loose material such as glacial moraines and moors as opposed to postglacial lavas in most other parts. Surface faults and fractures are therefore poorly preserved. The structures found were mapped with differential GPS instruments at a scale of 1:1000.

Hengill Area

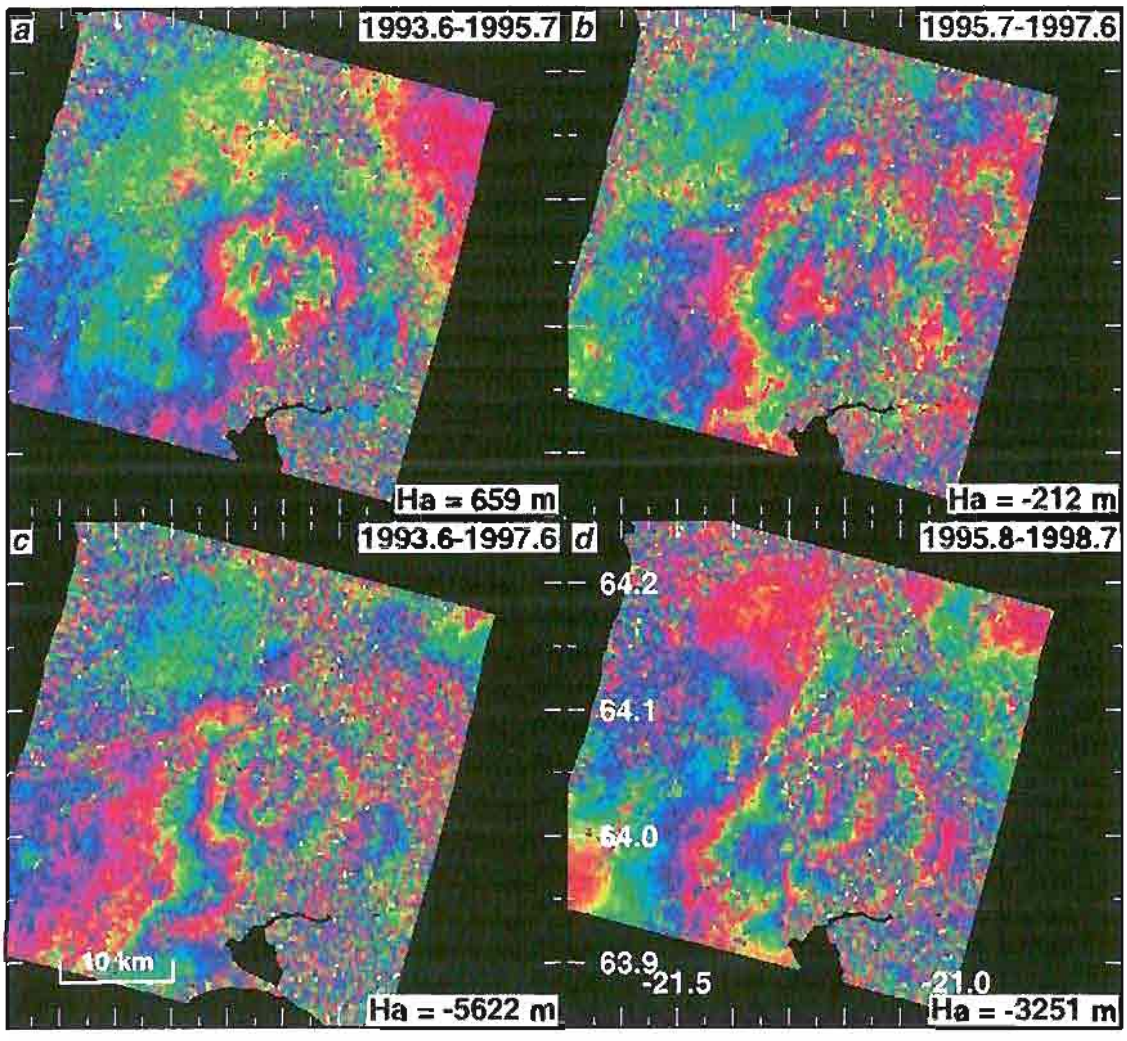

28 mm per fringe

Figure 37 *Four interferograms of the Hengill area. Radar images were acquired by the ERS-1 and ERS-2 satellites from ESA. a) Orbit numbers 10761 and 1953 from August 1993 and September 1995. b) Orbit numbers 1953 and 11973 from September 1995 and August 1997. c) Orbit numbers 10761 and 11973 from August 1993 and August 1997. d) Orbit numbers 2454 and 17985 from October 1995 and September 1998. One fringe in the interferogram represents 28 mm of range change. The main signal is a 10 km circular fringe pattern interpreted as an uplift of the area due to a pressure increase in a magmatic source at depth. The uplift rate is constant with time with a value of $h_o/\Delta t$ = 1.9 cm/year. In the four-year interferogram (c), up to 2 fringes are visible. The inferred uplift estimated from a Mogi model during this internal is 7.5 cm.*

- Systematic mapping of faults of the whole zone from aerial photographs at a scale of 1:50000 and digitizing of the maps.

3.5.3 Achievements

- Structure of the active faults and fault systems. The active faults of the seismic zone are expressed at the surface by arrays of en-echelon fractures. The fractures themselves have a NNE to NE orientation. Most of the arrays, on the other hand, have a N to NNE orientation. The en-echelon arrangement is therefore left-stepping reflecting a large component of right-lateral horizontal shear movement along the arrays. Evidence for faulting along the conjugate direction, i.e. left-lateral slip on ENE striking faults, exists but is very rare. Individual fractures are either purely extensional or have a component of right-lateral movement. Push-up structures are frequently observed between the tips of adjacent fractures. These are hillocks of different size, ranging between a few centimeters in height to a few meters. They reflect horizontal compression in the direction of maximum compressive stress. The en-echelon arrangement of fractures can be seen on many scales within the same fracture system. Individual fractures ranging in length between 1 and 50 m may thus form an array 100-200 m long. The arrays may then be arranged en-echelon within a system on the scale of a kilometer. The kilometer sized systems may then again be arranged en-echelon to form a super-system of 10 km length. Description and maps of these structural relationships have been published in a series of papers, e.g. Einarsson et al. (1981), Einarsson and Eiríksson (1982), Bjarnason et al. (1993), Erlendsson and Einarsson (1996), Einarsson et al. (1998, 1999 in preparation).

- Surface ruptures of the earthquakes of 1630 and 1784 identified. Contemporary accounts of a large earthquake in the year 1630 mention ".. that large fissures were formed where there had been none before, in particular near the farm Minnivellir". These fractures have been mapped and found to belong to an extensive fracture system with the typical structures of the strike-slip faults of South Iceland. The system is more than 7 km long and has a N-S orientation.

  The earthquake of August 14, 1784, is considered to be the largest historical earthquake in Iceland (M=7.1). Its causative fault has been unknown except for the general area. Contemporary accounts mention that large fissures were formed in the northern part of the Holt district. The largest fractures found in this part of the seismic zone can be traced as a faint N-S system for a distance of 8 m. We assume that this is the expression of the 1784 causative fault.

  Maps of the 1630 and 1784 faults are presented at the spring meeting of the Geoscience Society of Iceland (Jónsdóttir et al. 1999) and will be published in a paper shortly.

- Digitized fault map. The compilation of fault data is in progress. About 3/4 of the area of the zone has been covered. Only the easternmost part is still to be done. This work has led to some new projects, including detailed mapping of faults around the towns of Selfoss and Hveragerði. The fault map of the South Iceland seismic zone will be published shortly with an accompanying paper.

3.5.4 References

Hreinsdóttir, S., P. Einarsson, F. Sigmundsson & Þ. Árnadóttir 1999a. Measurements of continued uplift and expansion at the Hrómundartindur volcanic system. In: Abstracts from the spring meeting of the Geoscience Society of Iceland, Reykjavík, Iceland, April 20, 1999. In Icelandic.

Hreinsdóttir, S., P. Einarsson & F. Sigmundsson 1999b. Crustal deformation at the oblique Reykjanes peninsula plate boundary, SW Iceland, 1993-1998, observed with GPS geodetic measurements. In: Abstracts from the AGU spring meeting, Boston, Massachusetts, May 28 - June 4, 1999.

Johnsson, D.J., F. Sigmundsson & P. T. Delaney 1999. Comment on "Volume of magma accumulation or withdrawal estimated from surface uplift or subsidence, with application to the 1960 collapse of Kilauea volcano" by P.T. Delaney and D.F. McTigue. *Bull. Volc.*, in review.

Einarsson. P., S. Björnsson, G. Foulger, R. Stefánsson & Þ. Skaftadóttir 1981. Seismicity pattern in the South Iceland seismic zone. In: D. Simpson and P. Richards (editors), Earthquake prediction - an international review. *Maurice Ewing Series* 4. American Geophysical Union, 141-151.

Einarsson, P. & J. Eiríksson 1982. Earthquake fractures in the districts Land and Rangárvellir in the South Iceland seismic zone. *Jökull* 32, 113-120.

Bjarnason, I.Þ., P. Cowie, M.H. Anders, L. Seeber & C.H. Scholz 1993. The 1912 Iceland earthquake rupture: growth and development of a nascent transform system. *Bull. Seismol. Soc. Am.* 83, 416-435.

Erlendsson, P. & Páll Einarsson. The Hvalhnúkur fault, a strike-slip fault mapped within the Reykjanes peninsula oblique rift, Iceland 1996. In: B. Þorkelsson (editor), *Seismology in Europe.* Papers presented at the XXV ESC General Assembly, Reykjavík, Iceland, September 9-14, 1996. Reykjavík, 498-504.

Einarsson, P., P. Imsland, A.K. Ingimarsson, E.R. Guðmundsdóttir, H. Hallsteinsson, H. Sigurjónsson, J. Guðbjartsson, J. Hendriks, K. Jónsdóttir, K. Ísleifsson, Ó. Hilmarsson, R.H. Sigurðardóttir, S. Hreinsdóttir & V. Roth 1998. Strike-slip faults near Geitafell in the eastern Reykjanes peninsula. In: Abstracts from the spring meeting of the Geoscience Society of Iceland, Reykjavík, Iceland, April 21, 1998. In Icelandic. Paper in preparation 1999.

Jónsdóttir, K., P. Einarsson & V. Hjörleifsdóttir 1999. Fracture systems active in the earthquakes of 1630 and 1784. In: Abstracts from the spring meeting of the Geoscience Society of Iceland, Reykjavík, Iceland, April 20, 1999. In Icelandic.

3.6 Subproject 6: Effects of stress fields and crustal fluids on the development and sealing of seismogenic faults

Contractor:

Françoise Bergerat
Département de Géotectonique, Boite 129
Université Pierre et Marie Curie
4, place Jussieu
FR-75252 Paris Cedex 05
France
Tel: 33-1-4427-3443
Fax: 33-1-4427-5085
E-mail: bergerat@lgs.jussieu.fr

Subcontractors:

Jacques Angelier
Département de Géotectonique, Boite 129
Université Pierre et Marie Curie
4, place Jussieu
FR-75252 Paris Cedex 05
France
Tel: 33-1-4427-5857
Fax: 33-1-4427-5085
E-mail: jacques.angelier@lgs.jussieu.fr

Ágúst Guðmundsson
University of Bergen
Norway

Philip Meredith
University College London
London
United Kingdom

Thierry Villemin
Université de Savoie
France

3.6.1 Task 1: Determine the paleostress fields associated with the test areas from fault-slip data

The analysis of the South Iceland seismic zone already carried out during the PRENLAB-1 project by F. Bergerat, J. Angelier, S. Verrier and Á. Guðmundsson has been completed and published or accepted for publication.

Since 1998, we focussed the analysis of fault slip data and the reconstruction of paleostress tensors on the Tjörnes fracture zone.

Detailed field observations carried out by Á. Guðmundsson in the Tjörnes fracture zone and elsewhere show that major fault zones consist of two main structural units: a fault core and a fault damage zone. The core, where most of the fault displacement is accommodated, consists mostly of breccia and cataclastite; for major zones, it is commonly up to a few tens of metres thick. On either side of the core is a damage zone, as much as several hundred meter thick. The damage zone includes numerous faults and fractures,

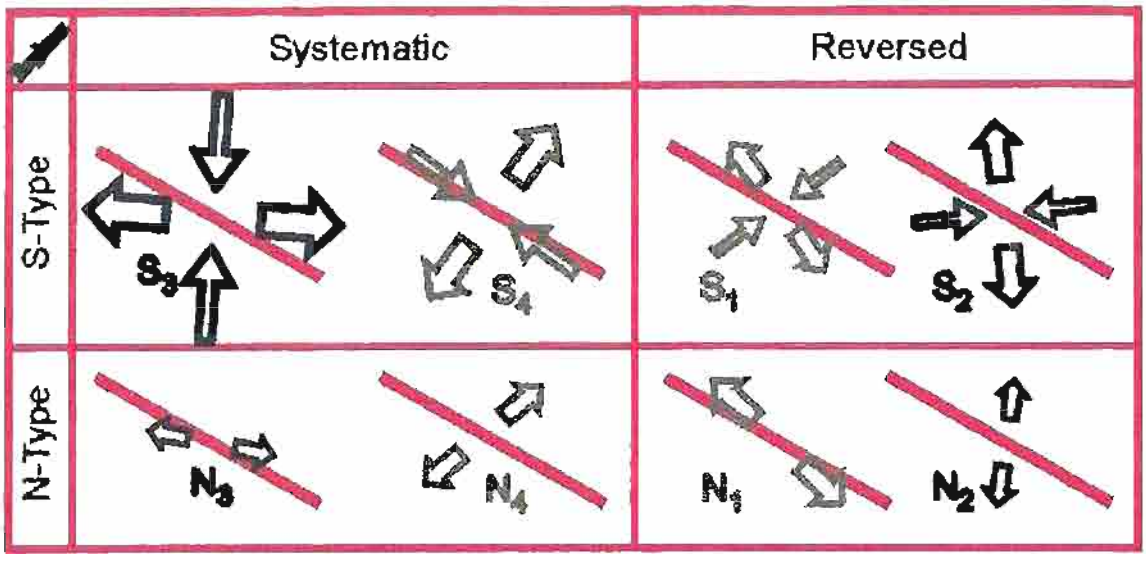

Figure 38. *Synthesis of results in terms of natures and orientations of the eight main tectonic regimes identified in Flateyjarskagi. Divergent arrows: average trends of extension (s3 axes), for S- and N-type regimes. Convergent arrows: average trends of compression (s1 axes), for S-type regimes. Thick line: N120° E trend of right-lateral transform fault zone.*

many of which are filled with secondary minerals, but lacks large volumes of cataclastic rocks and breccia. A model is being developed where during the interseismic period of an active fault zone, the fault core normally behaves as a porous medium with a very low hydraulic conductivity whereas the damage zone behaves as a parallel-fractured medium with a normal hydraulic conductivity many orders of a magnitude higher than that of the interseismic core (see Task 3).

A field work has been carried out by F. Bergerat, J. Angelier, C. Homberg and S. Garcia in the Flateyjarskagi peninsula. This peninsula has been chosen because the main fault of the Tjörnes fracture zone: the Húsavík-Flatey fault, is well expressed along the northern coast of this peninsula by a large zone of crushed rocks. Collection of more than 1300 fault slip data in 20 sites and determination of paleostress tensors in Flateyjarskagi allowed us to identify eight major brittle tectonic regimes arbitrarily named S1, S2, S3 and S4 (strike slip in type) and N1, N2, N3 and N4 (normal in type). Frequent contradictions in this relative chronology data suggest that these tectonic states alternated in a complex manner. These eight regimes can be arranged two by two (normal and strike-slip regimes with a same direction of S3) They have not the same importance in terms of numbers of sites and data. The tectonic regimes S3, S4, N3 and N4 are widespread. The main couple, S3-N3, indicates a N95°E trending extension on average. The second couple, S4-N4, indicates a N35°E trending extension on average. The two other couples, less important, S1-N1 and S2-N2 are related to N130°E and N175°E trending extensions on average, respectively. For each couple, the relationships Si-Ni involves simple permutation s1/s2 (Figure 38).

Considering the geometrical relationships between the directions of two major groups. Each group countains dominating S-type and N-type regimes, consistent with right-lateral transform motion, but also minor S-type and N-type compatible with left-lateral motion. One group is constituted by S3-N3 and S2-N2, the other one by S4-N4 and S1-N1. The

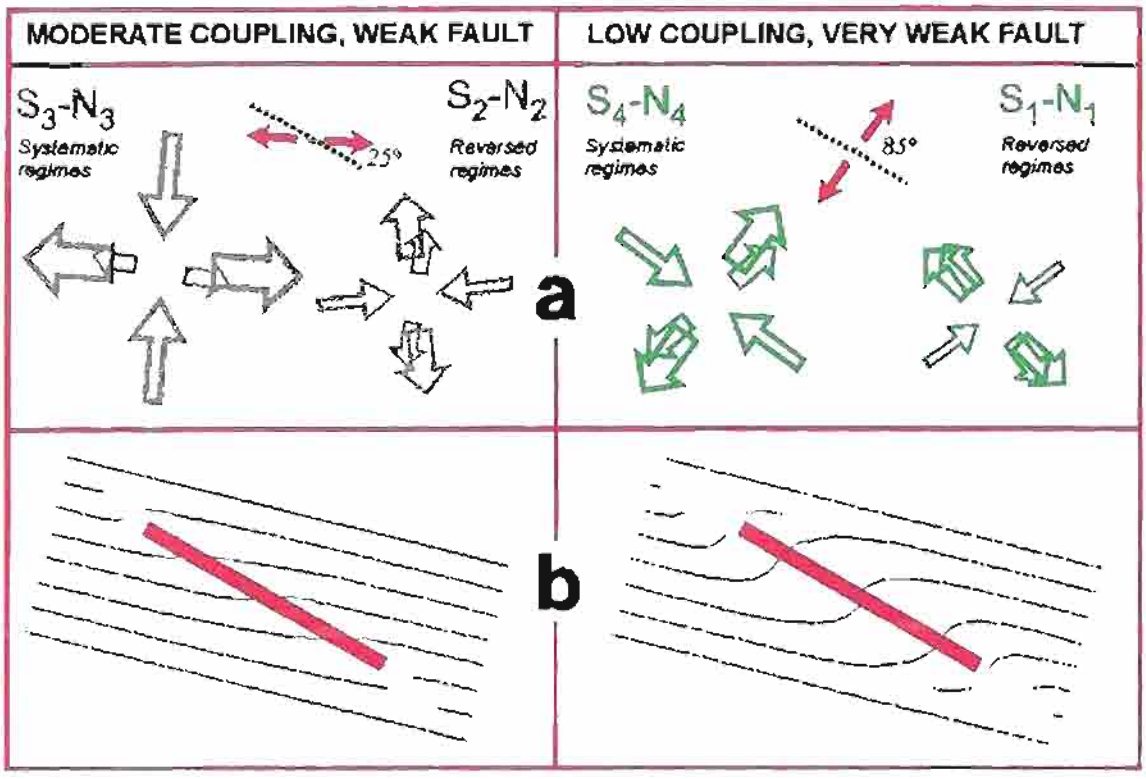

Figure 39. *Interpretation of the Flateyjarskagi results, in terms of variable coupling near a transform zone. Moderate coupling on left, very low coupling on right. (a) groups of tectonic regimes. (b) schematic pattern of minimum stress trajectories (thin lines) around oblique transform fault zone (thick line).*

dominating couple S3-N3 shows an angle of 25° between the trend of extension (s3) and of the Flatey segment of the transform zone. This behaviour of the transform zone reflects moderate mechanical coupling. In contrast, the couple S4-N4 shows an angle of 85° between extension and the transform direction (Figure 39).

This behaviour of the transform zone indicates very low mechanical coupling. The reversed regimes (S1-N1 and S2-N2) have little expression except near the transform, where large deformation occured. The drastic reversal s1/s3 relative to the dominating stress regimes S3 and S4 and the minor ones S2 and S1, respectively, probably results from elastic rebound, fault block accommodation and magmatic injection phenomena. Variations in mechanical coupling accross the Tjörnes fracture zone are the major source of the variations in the nature and orientation of tectonic regimes. Evidences for intermediate situations are few, suggesting that changes in coupling were abrupt rather than progressive.

3.6.2 Task 2: Reconstruct the current stress fields associated with the test areas using: a) inversion of large sets of focal mechanisms of earthquakes, b) seismotectonic analysis of individual faults, c) geodetic analysis of present-day crustal displacements

For the first part of this task we used inversion of large population of earthquake focal mechanisms to derive the regional seismotectonic field. We studied a population of 48669 double-couple focal mechanisms of earthquakes, from 67717 events recorded in and around

Iceland by IMOR.DG during the years 1995 to 1997. Magnitudes range between -1.8 and 4.8. The propose of this study was to determine whether such a large mass of data has the potential to indicate the general tectonic field. Many reasons suggested that this may be not the case: uncertainties of determinations, perturbations in tectonic regimes, and so on.

We considered two zones surrounding the major transform-rift zones north and south of Iceland: the Tjörnes quadrangle (66°-67°N, 16.5°-19.75°W) and the South Iceland seismic zone (SISZ) quadrangle (63.7°-64.25°N, 19.8°-21.1°W). Inversion was carried out based on a new direct method established by one of us during the PRENLAB-1 project (J. Angelier), using 10547 and 4413 double-couple focal mechanisms in these two quadrangles respectively.

In both cases, the reconstructed s2 axes plunge 78° or steeper, indicating dominating strike-slip mode. The average direction of extension (s3 trend) is N66°E for the Tjörnes quadrangle and N143°E for the SISZ one. Selecting only the data fit significant quality requirements results in no or little change, with N66°E and N146°E trend respectively: 9831 and 1916 mechanisms are thus retained (respectively). This stability of the inversion indicates that the resuls are significant. The ratio F between principal stress differences average 0.6-0.7, indicating that in terms of magnitudes, s2 is closer to s1 than to s3. This is consistent with the association of normal and strike-slip faulting modes.

Considering the general trend of plate separation and related extension in Iceland, that is, N104°E, these results in the main zones where transform faulting occurs north and south of the Icelandic rift (right-lateral and left-lateral respectively) are of particular interest. To the north, the trend of average extension is deviated counterclockwise of 38°. To the south, it is deviated clockwise of 42°. These deviations are in perfect agreement with the pattern of transform motions between the segments of the North-Atlantic oceanic spreading axis.

Another part of Task 2 concerns the geodetic survey of the Tjörnes fracture zone. The Tjörnes GPS Network (TGN, Figure 40) established by T. Villemin consists of about 45 sites distributed in the northern Iceland seismic zone.

It completes the geodetic networks already installed over the whole Iceland at a smaller scale. The TGN has been designed to measure the surface displacement field on each side of the Húsavík-Flatey fault (HFF). It has been done in order to estimate if there are locked fault segments in the area and who these segments can contribute to increase the seismic risk. 32 points have been measured both in 1995 and 1997 by T. Villemin, F. Jouanne and O. Henriot. The whole network will be remeasured during the summer 1999. The 1995 and 1997 data were analyzed with the Bernese V4.0 software.

The 1995-1997 velocities (Figure 41) have been computed by reference to a point located in the southern part of the network. All vectors are significant at a 95% confidence level. Two tendencies can be distinguished on the Tjörnes peninsula: eastward velocities reaching 13 mm/year for the most northern points of the peninsula and NNE velocities up to 15 mm/year for the points located on both sides of the HFF. Displacements to the east have been computed for the points located in the fissure swarms. Points on Flateyjardalur move to the north. The point on the Flatey island reveals a large displacement to the NE that could be due to a local instability. The assumption of an interseismic strain has been tested by using a simple dislocation model. This model assumes that a set of buried planar fault surfaces are locked above a given depth and affected by uniform aseismic creep below this depth. In order to determine this brittle/ductile transition we used the microseismicity recorded by the SIL network from 1995 to 1997. We assume that most earthquakes are localized in the brittle crust. Thus gives us a limit at a 10 km depth

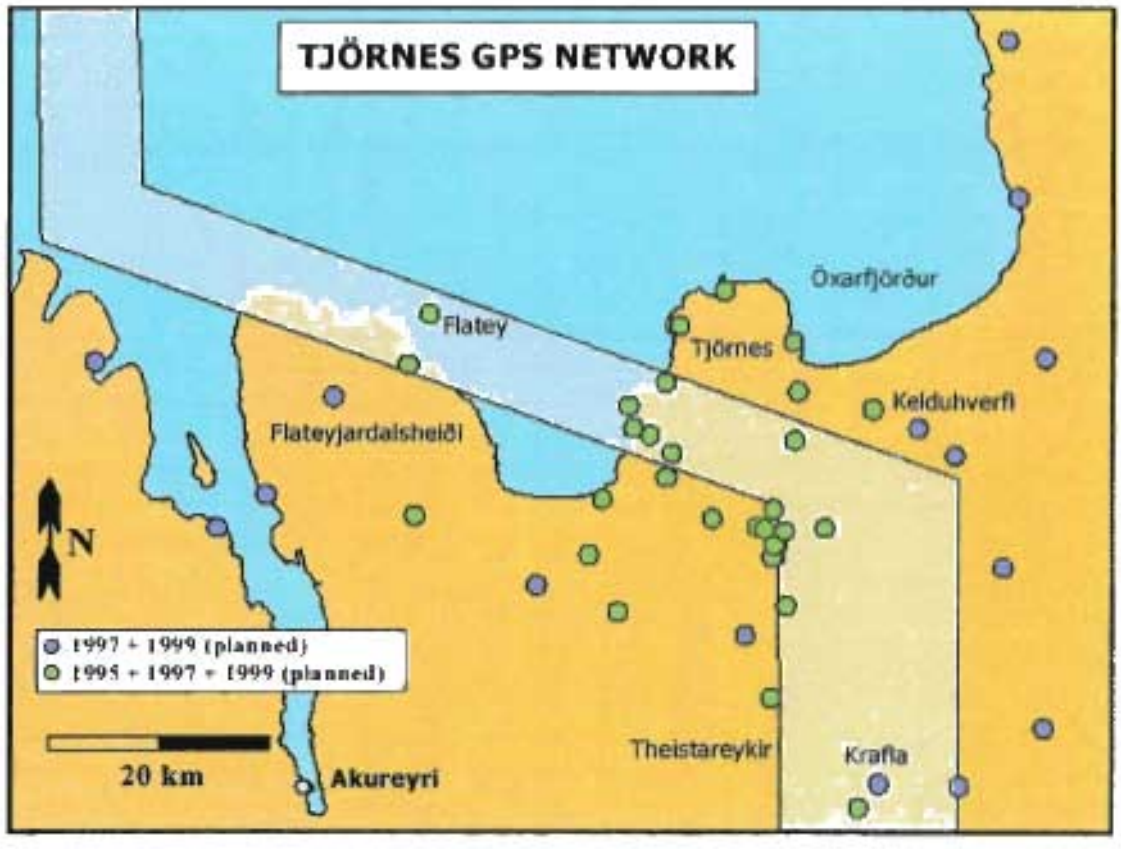

Figure 40. *The Tjörnes GPS network in northern Iceland.*

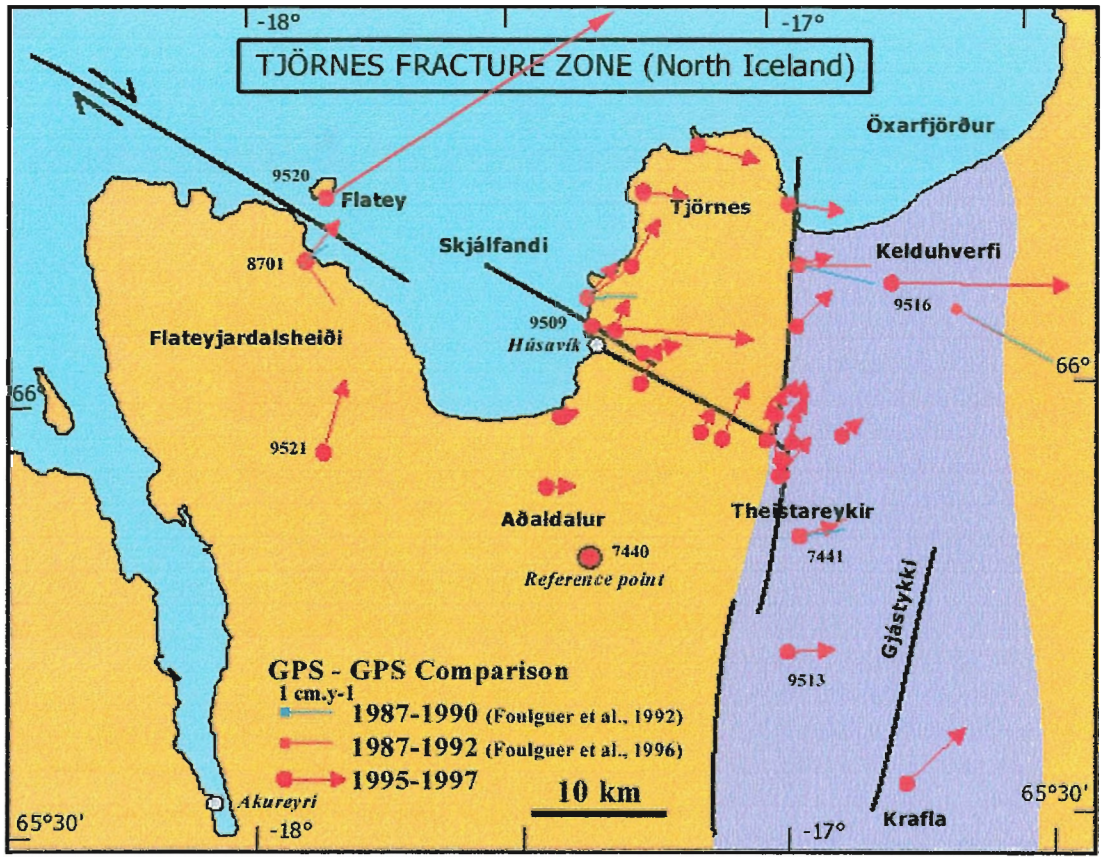

Figure 41. *1995-1997 displacements computed from GPS observations on the TGN network.*

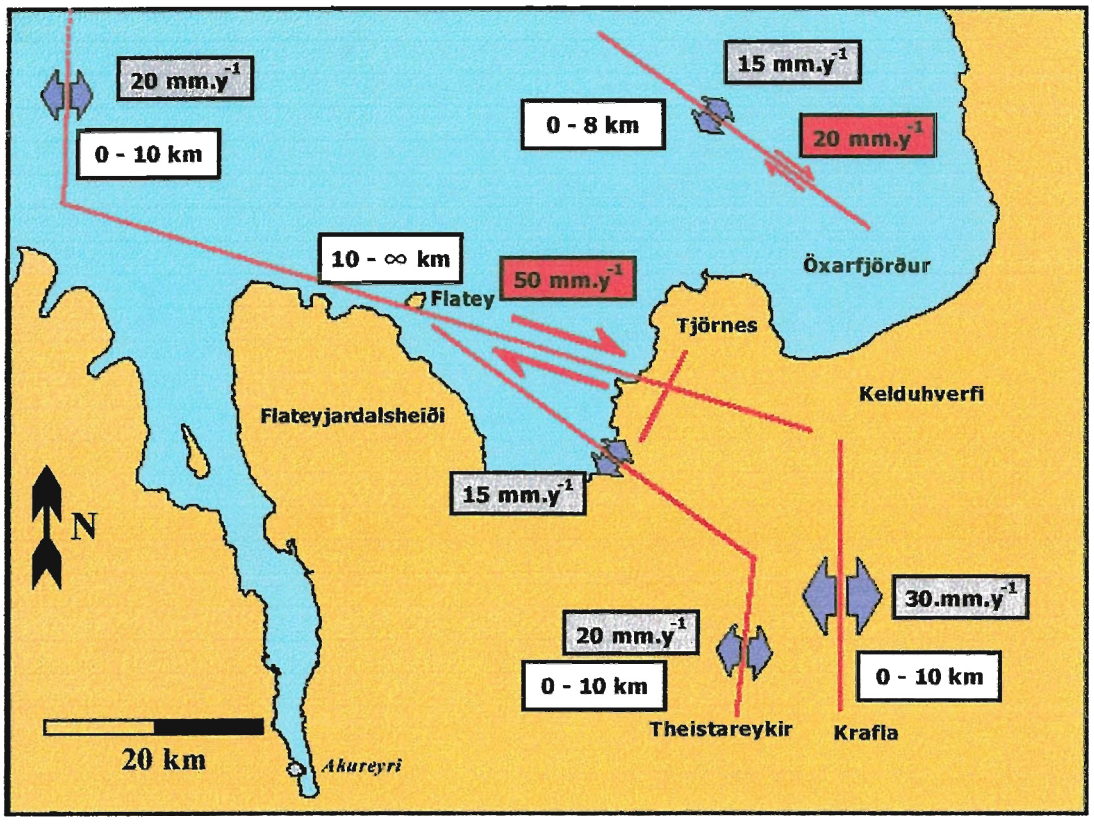

Figure 42. *Model of fault pattern and present day activity for the transform zone in North Iceland. White boxes indicates the limit of the faults at depth; red boxes give the strike-slip velocity and pink boxes indicate the opening velocity for each fault.*

in average. We founded a solution that minimizes the differences between simulated and observed velocities.

The model (Figure 42) assumes: (1) a dyke opening of 20 mm/year affecting all the brittle crust along the Kolbeinsey ridge; (2) two dyke openings of 30 mm/year and 20 mm/year respectively along the Krafla and Þeistareykir fissure swarms; (3) a dextral strike slip fault striking N100°E between the two previous rift segments with a velocity of 50 mm/year below a depth of 10 km and completely locked above the brittle/ductile transition; (4) a 15 mm/year opening zone striking N140°E south of the HFF; (5) a fault along the Grímsey lineament with both a 15 mm/year opening and 20 mm/year dextral strike-slip movements. In addition small wavelength tendencies has been adjusted by superficial faults. This model based on our 1995-1997 TGN comparison revealed extension and strike slip movements 3 to 4 times larger than the average velocity. The transform motion is locked on a large (150x10 km) fault surface and this represents the main risk for destructive earthquakes in the near future. From a mechanical point of view, the lockage could be due to the increase of normal stress on this surface following the double opening north and south of the fault zone.

3.6.3 Task 3: Investigate the potential effects of fluid pressure on the probability of faulting

Studies of the aspect ratios of nearly 400 mineral-filled veins in the on-land parts of the Húsavík-Flatey fault on the Flateyjarskagi peninsula have been carried out by Á. Guðmundsson. They indicate that the average fluid overpressure with reference to the minimum compressive principal stress, at the time of vein emplacement, was around 20 MPa. In the current model on fluid transport along fault zones, it is proposed that during transport of overpressured fluids, such as are commonly associated with seismogenic faulting, the hydraulic conductivity of the damage zone can greatly increase. An overpressured fluid increases the apertures of the fractures constituting the network of the damage zone, and as a consequence the volumetric flow rate can, temporarily, be several hundred times greater than during fluid flow under hydrostatic pressure. Similarly, during periods of seismogenic faulting along the core, its hydraulic conductivity, and the associated transmissivity (conductivity times core thickness), may increase by many orders of a magnitude. As an example, a single fault plane along the core with an aperture of only 0.1-1 mm can transmit many hundred to many hundred thousand times more water than a porous fault core, tens of meter thick and with high values of hydraulic conductivity. This model may partly account for the great volumes of water that are commonly inferred or observed to be transported during seismic activity in large-scale fault zones. This work has been published in 1999 (see Chapter 4).

3.6.4 Task 4: Make analytical and numerical studies of the nucleation and development of the seismogenic faults and fault populations

As regards the results of Tasks 1 and 2, some of the principal new conclusions are presented in paper in 1999 (see Chapter 4) and may be briefly summarized as follows: Measurements show that stress magnitudes in the crust are normally limited by the frictional equilibrium on pre-existing, optimally oriented faults. Fault zones where these limitations are frequently reached are referred to as seismic zones. Fault zones in the crust concentrate stresses because their material properties are different from those of the host rock. Most fault zones are spatially relatively stable structures, but the associated seismicity in these zones is very variable in space and time. It is proposed that this variability is attributable to stress-concentration zones that migrate and expand through the fault zone. We suggest that following a large earthquake and the associated stress relaxation, shear stresses of a magnitude sufficient to produce earthquakes occur only in those small parts of the seismic zone that, because of material properties and boundary conditions, encourage concentration of shear stress. During the earthquake cycle, the condition for seismogenic fault slip migrate from these stress-concentration regions throughout the whole seismic zone. Thus, while the stress-concentration regions continue to produce small slips and small earthquakes throughout the seismic cycle, the condition for slip and earthquakes are gradually reached in larger parts of, and eventually the whole, seismogenic layer of the seismic zone. Prior to the propagation of an earthquake fracture that gives rise to a large earthquake, the stress conditions in the zone along the whole potential rupture plane must be essentially similar. This follows because if they were not, then, on entering crustal parts where the state of stress was unfavourable to this type of faulting, the fault propagation would be arrested. The proposed necessary homogenization of the stress field in a seismic zones as a precursor to large earthquakes implies that by monitoring the state of stress in a seismic zones, its large earthquakes may possibly be forecasted. We have

made numerical models of the evolution of the stress field as appropriate for a seismic zone located between two ocean-ridge segments and test them on data from the South Iceland seismic zone. The proposed model broadly explains the historical, as well as the current, patterns of seismogenic faulting in the South Iceland seismic zone and, even more easily, those of the Húsavík-Flatey fault of the Tjörnes fracture zone.

3.6.5 Task 5: Make a detailed analysis of the Tjörnes fracture zone test site and its vicinity

The Krafla fissure swarm (KFS) has been very active during the last rifting episode (1975-1984). This 80 km long and 10 km wide swarm includes numerous tension fractures and normal faults. Most of them has been reactivated during the last volcano-tectonic episode. Part of them elongated and we noticed the creation of new fissures. A complete mapping of the swarm before and after the rifting episode has been made from aerial photos by T. Villemin and V. Ferber. If we assume that the deformation along a transverse section increases with the number of fractures encountered through the section we observe an evolution of the dilation along the swarm strike. This could be related to an unique dyke present at a small depth which controlled the surface fracturing. A comparison between the two mapped states (1960 and 1990) permits us to distinguish between reactivated and new fractures. If we assume that the growth process has not changed since the swarm creation a limited number (<10) of tectonic episodes occurred on the KFS. This implies that the volcanic episodes are not necessary associated with dilation along the whole swarm.

The Þeistareykir swarm (TFS) lies 20 km west of the Krafla fissure swarm and is connected with the transform zone in its northern end. A complete mapping of the fissure swarm has also been made from aerial photos by T. Villemin and O. Henriot. The western boundary faults consist in high scarps where both active normal and strike slip faulting has been characterized during the 1998 field trip. In addition displacement profiles has been measured by kinematic GPS on a set of 8 en-echelon normal faults just where the Húsavík fault meets the TFS. No clear evidence for a continuation at depth of the Húsavík lineament can be found on these profiles.

3.6.6 Task 6: Analyze the fracture properties of Icelandic rock in the laboratory and to make theoretical, observational and experimental studies on the sealing of seismogenic faults with application to the test areas in Iceland

Our main overall objective was to determine the range of temperature, pressure and damage conditions in the crust under which rocks will fracture in a brittle-elastic manner. In order to achieve that objective, we have designed and constructed an apparatus for the measurement of rock fracture properties at high temperatures and pressures, and performed a series of experiments to measure rock fracture and fluid transport properties. This work has been carried out by P. Meredith.

We have designed and manufactured an environmental cell for the measurement of fracture mechanics parameters under high-temperature/high-pressure conditions. The design conditions are: (i) confining pressure up to 70MPa, (ii) temperature up to 450°C, and (iii) water as the confining/pore fluid. Due to the highly corrosive nature water under these conditions, it was necessary to manufacture the cell and all its internal components from Hastalloy C (a high-strength nickel alloy developed by the US Navy). The cell,

which has an outside diameter of 170 mm and an internal bore of 100 mm, is shown in Figure 43.

The cell is designed to take 60 mm diameter "short-rod" fracture mechanics specimens, manufactured to the standard ISRM geometry. Sample are heated by a fixed internal element, and are loaded to failure in tension by means of a small internal hydraulic actuator.

Starting material:

Most of the measurements reported here were made on samples of a macroscopically isotropic basalt collected from a roadstone quarry located south-east of Reykjavík, Iceland. Microscopically it has an aphyric texture, comprising euhedral laths of unaltered plagioclase averaging 0.2 mm in length, and anhedral augite microphenocrysts averaging 0.1 mm in diameter, with accessory anhedral oxides up to 0.1 mm in diameter. No free quartz was visible under either optical or SEM microscopy.

Changes and evolution of rock physical properties with temperature:

In order to better interpret results from experiments conducted at high temperatures, we have first made measurements at room temperature on samples that have previously been heat-treated to temperatures up to a maximum of 900°C in order to induce thermal crack damage. Thermal cracking can occur due both to thermal expansion mismatch between different mineral phases, and to thermal expansion anisotropy within a single mineral phase. In a shallow crustal environment where the geothermal gradient is anomalously high, such as in Iceland, thermal stresses may well be large enough to induce such fracturing. Furthermore, where enough fractures propagate and link up to provide an interconnected network, they can provide permeable pathways for fluid flow which can in turn lead to embrittlement and weakening of the rock.

All samples were heated in a tube furnace to the desired temperature at a controlled rate of 1°C/min, then held at that temperature for one hour, before cooling to ambient temperature at the same rate. This rate results in a temperature gradient across the sample of less than 1°C/cm, which is too low to cause any cracking due to thermal gradient stresses.

Thermal cracking in the basalt was monitored by measuring the compressional (P) and shear (S) wave velocities through the samples both prior to and following heat-treatment, and the results are shown in Figure 44.

Note that both P-wave and S-wave velocities remain essentially constant up to 400°C, with values of about 5.3 km/s and 3.0 km/s respectively. For higher temperatures the velocities decrease rapidly, so that by 800°C they have decreased to about 3.4 km/s and 2.2 km/s repectively.

Fracture toughness of heat-treated Icelandic basalt:

We have also performed a series of fracture toughness measurements on heat-treated 60 mm diameter short-rod specimens of Icelandic basalt using the ISRM recommended methodology. The results are presented in Figure 45.

The fracture toughness value of 2.71 $MPa/m^{\frac{1}{2}}$ for the samples that were not heat-treated compares well with previously published data for very similar materials (Meredith 1989). The fracture toughness remains essentially constant up to 400°C, but there is then a very rapid decrease in fracture resistance between 400°C and 600°C, with relatively little change between 600°C and the highest heat-treatment temperature of 900°C. This pattern of behaviour is entirely consistent with the wave velocity data. These experiments were conducted in air with rapid loading, so that environmentally-assisted subcritical crack

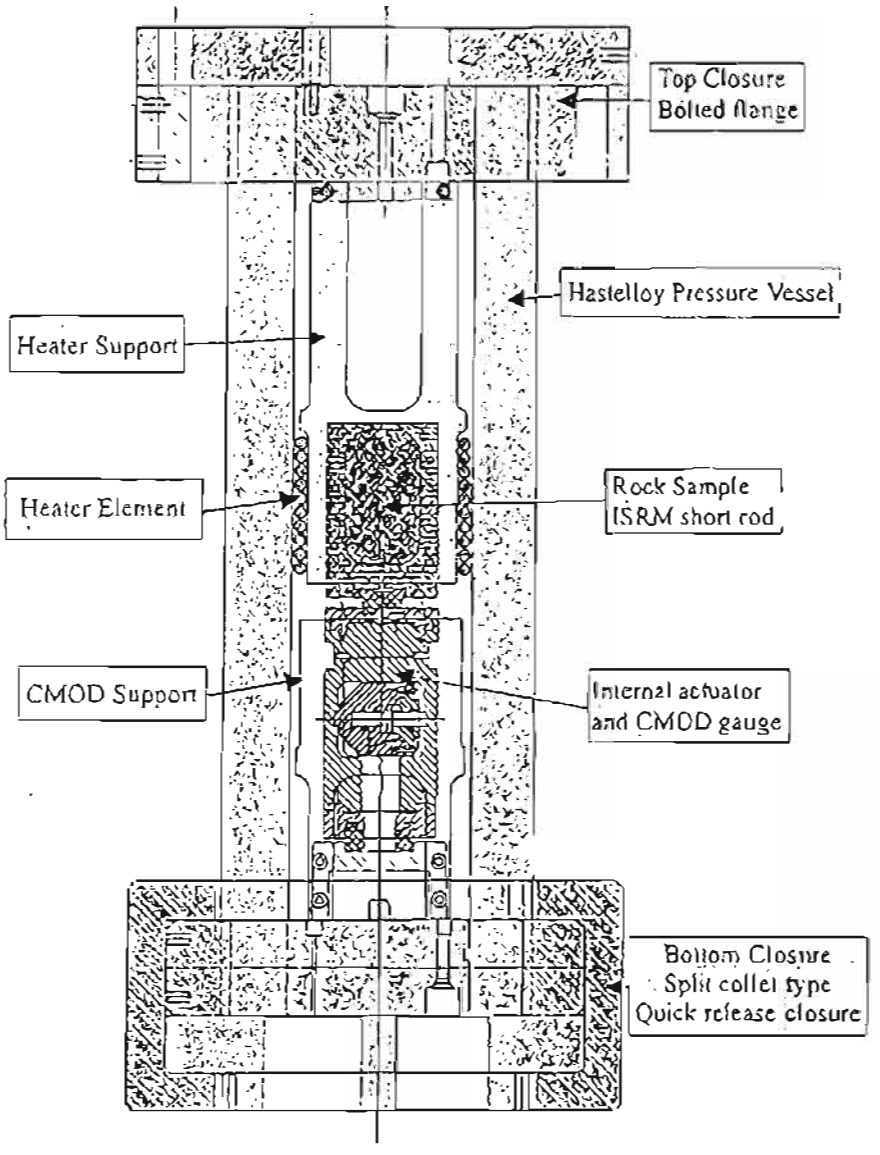

Figure 43. *Environmental cell for high-T/high-P fracture mechanics measurements.*

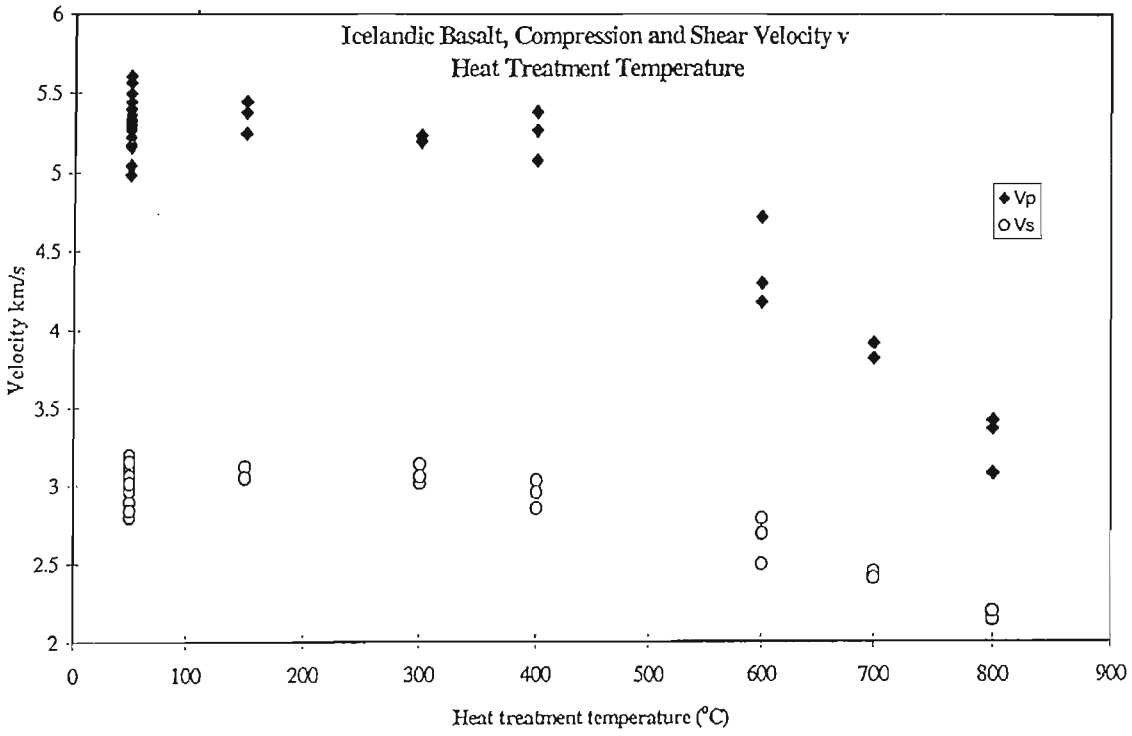

Figure 44. *Variation in acoustic wave velocity with heat-treatment temperature.*

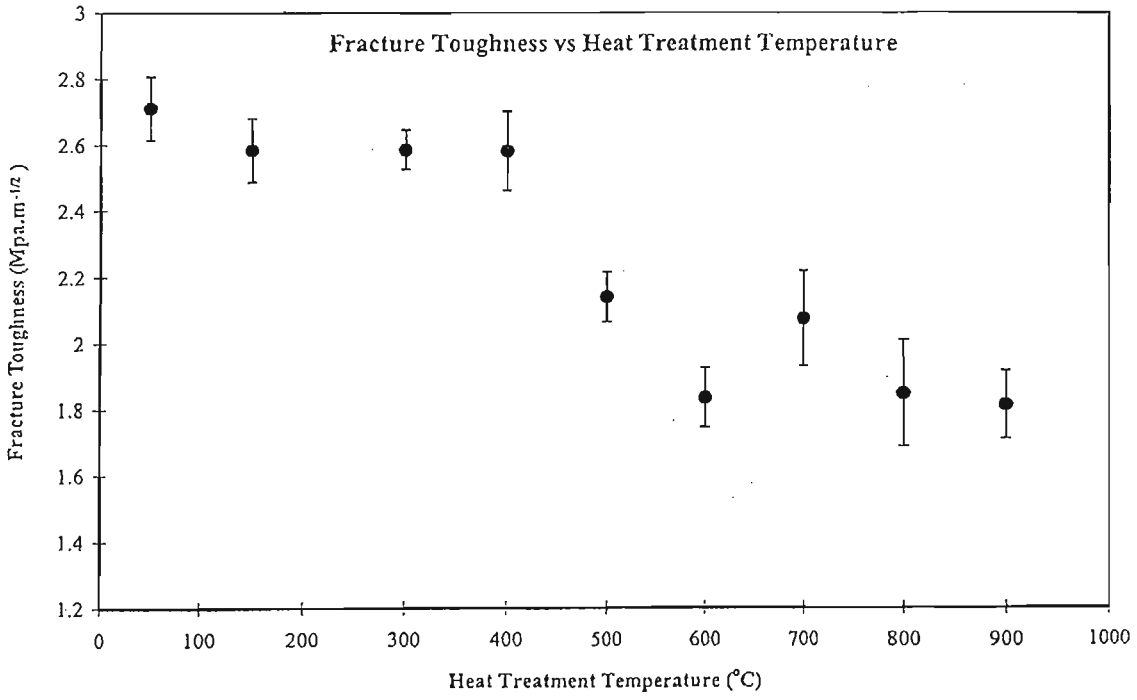

Figure 45. *Variation in tensile fracture toughness for Icelandic basalt.*

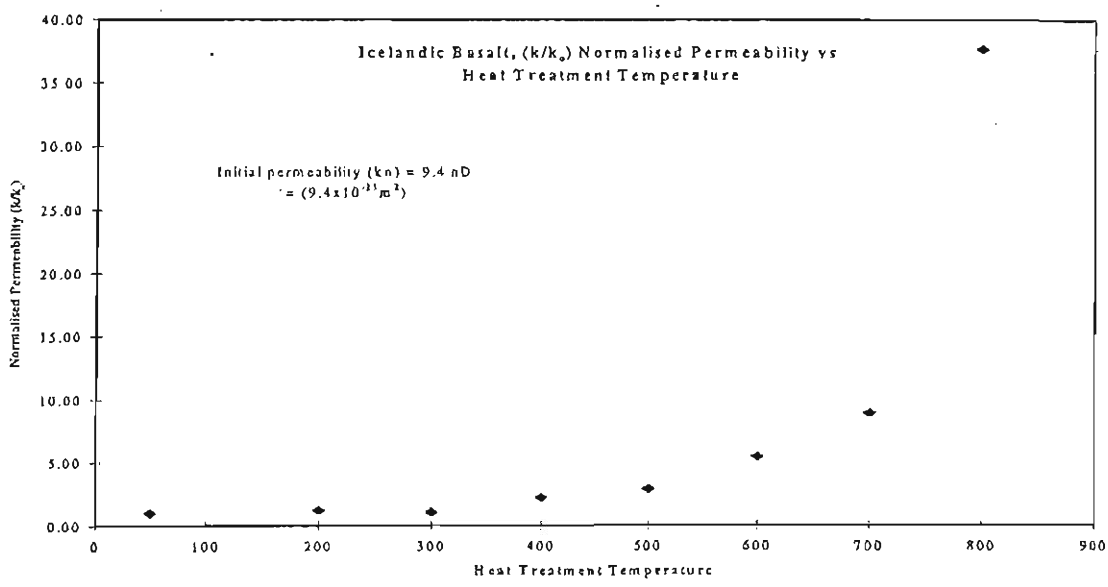

Figure 46. *Increase in basalt permeability as a function of heat-treatment temperature.*

growth was not a significant factor. Any reduction of fracture resistance must, therefore, be due to changes in the microstructure of the rock due to thermal cracking.

We have observed very similar trends in measurements of the indirect Brazilian tensile strength and Young's modulus for heat-treated basalt samples. These other results are not reported here due to space constraints.

Crack linkage and enhanced fluid permeability in heat-treated Icelandic basalt:

In these experiments, the fluid permeability of basalt samples 40 mm in diameter by 40 mm in length were measured both prior to and following heat-treatment. All permeability measurements were carried out using a new wide-range permeameter system that makes use of two servo-controlled fluid pressure intensifiers to enable permeabilities from 1 darcy to lower than 1 nanodarcy to be measured, using water as the pore fluid. The mean permeability of the basalt prior to heat-treatment (k0) was 9.4 nanodarcy ($9.4 \cdot 10^{-21} m^2$), and the change in normalized permeability (k/k0) as a function of heat-treatment temperature is plotted on Figure 46.

Similar to the previous results, the normalized permeability remained essentially constant after heat treatment to temperatures up to 300°C, and showed only a slight increase after treatment to 400°C. At higher temperatures, however, the normalized permeability changed dramatically, increasing by an order of magnitude at 700°C and by a factor of 40 by 800°C.

It is clear that such a large increase in permeability is unlikely to result merely from the increase in the number or size of thermally-induced cracks. Note, for example that over the same temperature interval the rock strength (as measured by fracture toughness and Brazilian tensile strength) decreased by only about 30%. We believe, therefore, that these permeability results show the profound effect of crack linkage processes above some percolation threshold to form extensive sample-spanning permeable pathways for fluid flow.

Due to the high temperature gradient and low lithostatic stress, thermal cracking may be an important process in controlling fracture in Icelandic crust. In the absence

of confining stress, such cracking starts in the temperature range 300°C to 400°C in fresh basalt. This leads to significant decrease in mechanical strength and resistance to crack propagation at higher temperatures. Thermal cracking also leads to increased fluid permeability above about 300°C, with the permeability increasing very non-linearly with temperature. The decrease observed in rock strength is likely to be considerably enhanced by the presence of a chemically active pore fluid (e.g. water), especially when its activity is increased by elevated temperatures.

In the next phase of the project, we will measure the same key parameters under elevated temperature and pressure, and modify our experimental apparatus for the measurement of compressional and extensional strength.

3.6.7 Meetings

Some members of the subproject participated to the half yearly PRENLAB-2 workshops in Húsavík, Iceland, July 30, 1999 (J. Angelier, F. Bergerat, S. Garcia, Á. Guðmundsson, O. Henriot, C. Homberg) and in Strasbourg, France, March 31, 1999 (J. Angelier, F. Bergerat, Á. Guðmundsson, O. Henriot, F. Jouanne, T. Villemin).

On the other hand, the results of the first year PRENLAB-2 work have been presented at the tenth biennial EUG meeting in Strasbourg, France, March 28 - April 1, 1999, and at the XXIV EGS General Assembly in The Hague, The Netherlands, April 19-23, 1999 (see Chapter 4).

3.6.8 Reference

Meredith, P.G. 1989. Comparative fracture toughness testing of rocks. In: *Fracture toughness and fracture energy.* Balkema, Rotterdam, 265-277.

3.7 Subproject 7: Theoretical analysis of faulting and earthquake processes

Contractor:

Maurizio Bonafede
Section of Geophysics
Department of Physics
University of Bologna
Viale Berti–Pichat 8
I-40127 Bologna
Italy
Tel: +39–51–630–5001
Fax: +39–51–630–5058
E–mail: bonafede@ibogfs.df.unibo.it

Associated contractor:

Frank Roth
GeoForschungsZentrum Potsdam
Division: Solid Earth Physics and Disaster Research
Section: Earthquakes and Volcanism
Telegrafenberg A34
D–14473 Potsdam
Germany
Tel: +49–331–288–1210
Fax: +49–331–288–1203
E–mail: roth@gfz-potsdam.de

3.7.1 Subpart 7A: Ridge-fault interaction in Iceland employing crack models in heterogeneous media

Researchers:

Maurizio Bonafede

Eleonora Rivalta
Department of Physics
University of Bologna
Viale Berti-Pichat 8
I-40127 Bologna
Italy
Tel: +39-051-630-5001
Fax: +39-051-630-5058
E-mail: rivalta@ibogfs.df.unibo.it

Andrea Neri
Department of Physics
University of Bologna
Viale Berti-Pichat 8
I-40127 Bologna
Italy
Tel: +39-051-630-5001

Fax: +39-051-630-5058

Beatrice Parenti
Department of Physics
University of Bologna
Viale Berti-Pichat 8
I-40127 Bologna
Italy
Tel: +39-051-630-5001
Fax: +39-051-630-5058

Contractor Maurizio Bonafede has been working 75% of his research time on the project since April 1998 until now. Eleonora Rivalta and Andrea Neri were supported with fellowships under contract ENV4-CT97-0536 until December 1998. Andrea Neri is presently serving in the Army. Beatrice Parenti has been working on the project as a voluntary research assistant until December 1998, when she left our institute. Since January 1999 Eleonora Rivalta is being supported with a post-graduate fellowship within the Ph.D program in physics. Eleonora Rivalta has been working on the project 100% of her time since July 1998 until present. Beatrice Parenti and Andrea Neri have been working 100% of their time on the project since July 1998 until December 1998.

3.7.1.1 Task 1: Magma upwelling as driving mechanism for the stress build-up in the elastic lithosphere

Tensile cracks are often employed to model magma migration in rift zones or within volcanic edifices, through lateral or feeding dykes. In a crack model, the overpressure of magma Δp with respect to the horizontal stress in the host rock, is assumed to be responsible for dyke opening and propagation. Most crack models of dykes have been developed so far in homogeneous media. The most simple heterogeneous medium has been considered, made up of two welded half-spaces, characterized by different elastic parameters. The analytical solutions available for the elementary dislocation problem in such a medium (Bonafede and Rivalta 1999) has been employed to set up an integral equation with generalized Cauchy kernel, representing the condition for static equilibrium. The unknown in such a problem is the dislocation density distribution, whose singular behaviour has been studied near the crack tips and near the intersection with the interface between the two media. When the crack is in half-space 1 but touches the interface, the order of singularity of the dislocation density distribution at the interface changes from the classical behaviour $\sim r^{-1/2}$ to $\sim r^{-b}$ (where r is the distance from the interface) and the order of infinity b is obtained solving a trascendental compatibility equation; some results are shown in Table 4.

$m = \mu_1/\mu_2$	∞	10	5	2	1	0.5	0.2	10^{-1}
b	0.255	0.312	0.352	0.430	0.500	0.576	0.678	0.752

Table 4. *Crack touching the interface.*

A crack crossing the interface $z = 0$ between the two half-spaces with rigidities μ_1 (in $z > 0$) and μ_2 (in $z < 0$) has been considered in detail. A system of generalized Cauchy equations is obtained, which is solved for the dislocation density distributions of

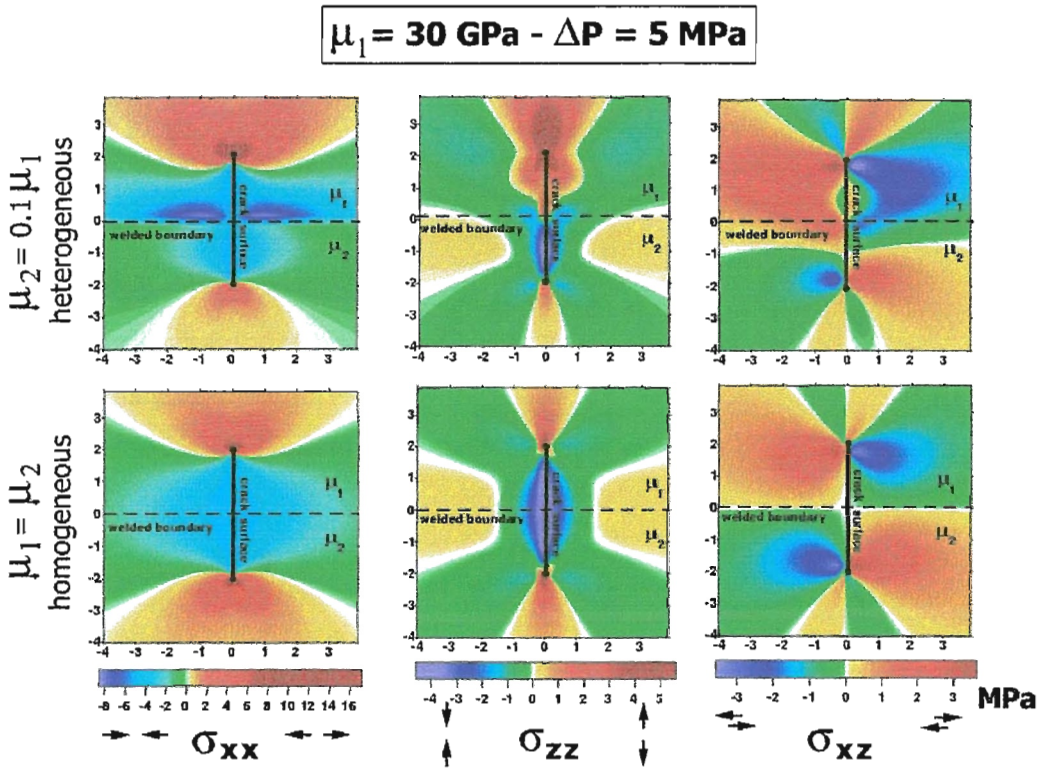

Figure 47. *Stress components induced by rifting in proximity of a structural discontinuity.*

each crack section. An internal singularity in the dislocation density distribution appears at the intersection between the crack plane and the interface. This singularity is again of the type is r^{-b} on both sides of the interface and its order b depends only upon the elastic parameters of the media in welded contact and the ratio between the crack lengths in the two half-spaces (see Table 5). More specifically, the order b does not depend on the stress drop.

$m = \mu_2/\mu_1$	1	0.5	0.1	0.05	0.001
b	0	0.030	0.170	0.208	0.245

Table 5. *Crack crossing the interface.*

Crack induced stress components are plotted in Figure 47, assuming a 5 MPa overpressure within the crack. From a comparison with solutions pertinent to a homogeneous medium, it appears that layering can be responsible of stress changes, localized along the the interface, which may be considerably higher than the overpressure within the dyke. These results provide useful hints for the interpretation of induced seismicity in rift zones and in volcanic areas. A paper is in press on Geophys. J. Int.

3.7.1.2 Task 2: Space-time evolution of the stress field following earthquakes and episodes of magma upwelling

Mechanical effects left by an earthquake on its fault plane, in the post-seismic phase, are investigated employing the "displacement discontinuity method" and imposing the

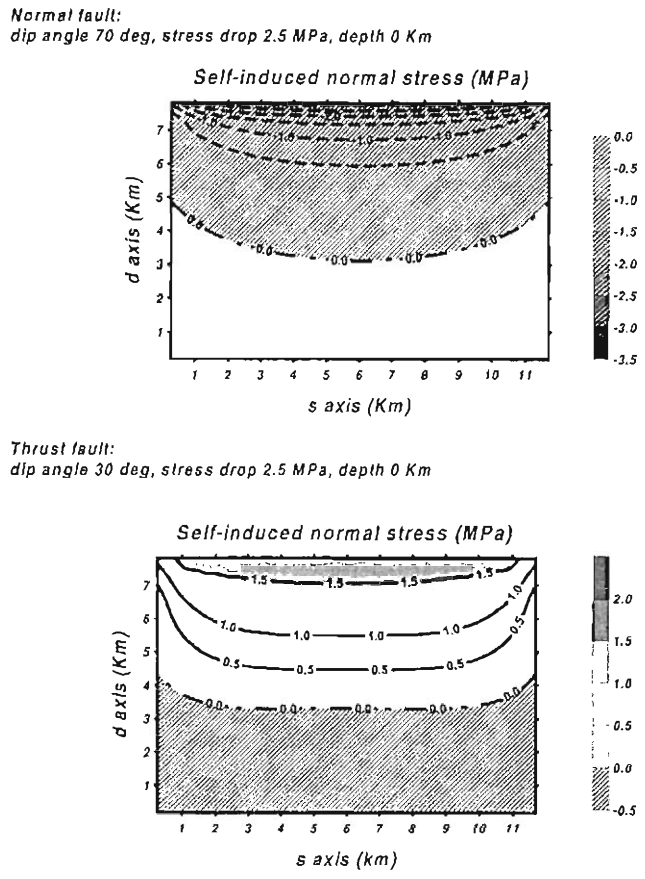

Figure 48. *Normal stress induced by uniform stress drop over a high-dip normal fault and a low-dip thrust fault.*

release of a constant, uni-directional shear traction. Due to unsymmetric interaction between the fault plane and the free surface, significant normal stress components are left over the shallow portion of the fault surface after the earthquake (Figure 48) these are compressive for normal faults, tensile for thrust faults, and are typically comparable to the stress drop.

In Figure 48 the s-axis is along the strike of the fault, the d-axis is along the dip (positive upwards). Several observations can be explained from the present model: low-dip thrust faults and high-dip normal faults are found to be favoured, according to the Coulomb failure criterion, in repetitive earthquake cycles; the shape of dip-slip faults near the surface is predicted to be upward-concave; the shallow aftershock activity commonly observed in the hanging block of a thrust event is easily explained. A paper has been submitted for publication.

Effects of structural inhomogeneities on the stress and displacement fields induced by strike-slip faults in layered media is presently under study. An elastic medium is considered, made up of an upper layer bounded by a free surface and welded to a lower half-space characterized by different elastic parameters. The case of a strike-slip fault crossing the interface between two elastic media is particularly interesting. The dislocation density distribution is found to be affected by a jump discontinuity at the interface, which is responsible for inducing high concentrations of deviatoric stress, not only in proximity of

fault edges, but also along the interface where it may be even higher than the stress drop on the fault plane. The displacement field observable over the ground surface (Figure 49) is found to be strongly affected by the presence of a soft sedimentary layer (with rigidity $\mu_2 \ll \mu_1$).

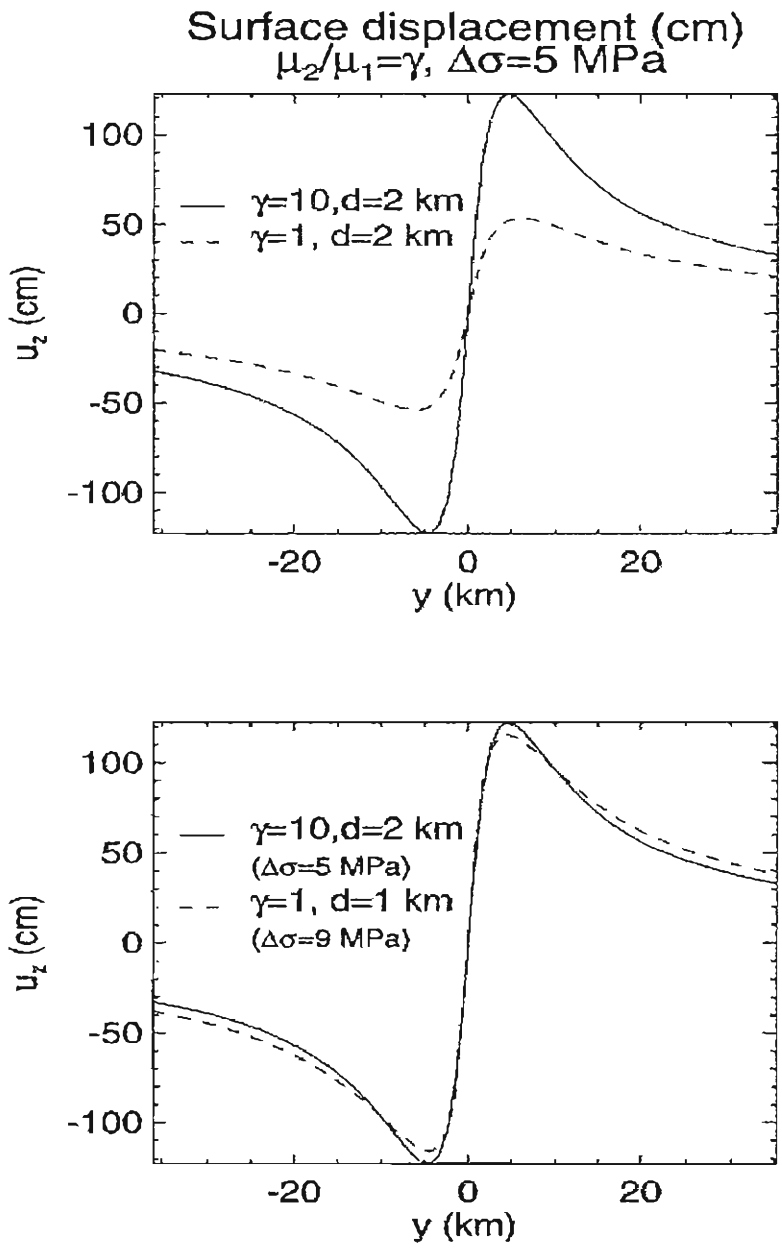

Figure 49. *Displacement at the free surface after a strike-slip event with uniform stress drop: layered half-space solutions are shown as solid lines, homogeneous half-space solutions as dashed lines.*

In Figure 49 the solid line shows the surface displacement induced by strike-slip faulting at depth greater than $d = 2$ km, computed in the heterogeneous medium, the dashed

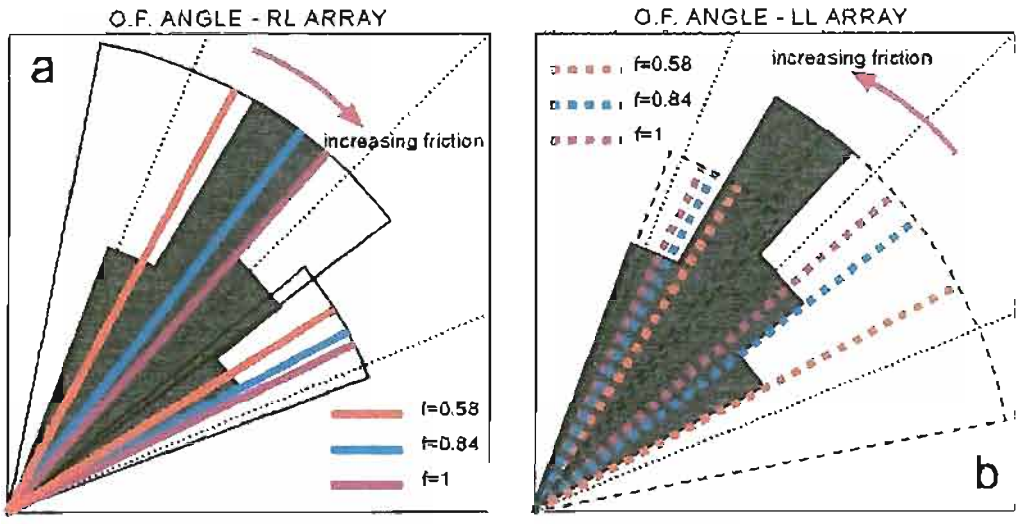

Figure 50. *Open fractures (O.F.) angles predicted from the combined effect of the main fault rupture and secondary fault (S.F.) rupture along the strike direction. The observed range and relative frequency of O.F. angles is shown shaded (from Bjarnason et al. 1993). If the friction coefficient f varies between 0.2 and 1.5 predicted O.F. angles vary within the circular sectors contoured in black. Solid lines in panel (a) represent the angle expected for O.F. belonging to dextral arrays. Dashed lines in panel (b) represents the angle expected for O.F. belonging to sinistral arrays. In both panels, longer lines indicate the predicted mixed-mode O.F. trends, while shorter lines indicate pure tensile trends. Mixed-mode O.F. are assumed to share the same style of faulting (sinistral or dextral) with the array to which they belong. The dotted lines indicate 22.5°, 45°, 67.5° directions (for reference). Coloured lines refer to particular friction values (indicated). Friction increases as indicated by the red arrow.*

line show computation in a homogeneous half-space. It appears from panel (b) that estimates of d and $\Delta\sigma$ derived from geodetic observations can be severely biased if structural heterogeneities are not taken into account. A paper is in preparation.

3.7.1.3 Task 3: Secondary earthquake fractures generated by a strike-slip fault in the South Iceland seismic zone

This task was included in the PRENLAB-1 workprogramme and was not originally included within the PRENLAB-2 workprogramme. The latest developments of this topic, however, lead us to include the main results in the present report. Most earthquakes in the South Iceland seismic zone occur on N-S trending dextral strike-slip faults. The resulting rupture zones display complex en-echelon patterns of secondary structures including NNE-trending arrays of (mostly) NE-trending open fractures (O.F.) and hillocks.

Three spatial scales characterize the surface faulting pattern: the length of the main fault (M.F. ~104 m), the arrays here interpreted as surface evidence of secondary faults (~102 m) and the individual O.F.(~10 m). In order to improve our understanding of the genetic relationship between the O.F. and the M.F. we computed the stress field induced by slip on a buried M.F. using a dislocation model in a layered half-space: the fault surface

is assumed to be embedded in the basement rock, topped by a softer near-surface layer. The O.F. were preliminarily considered as pure mode-I cracks opening in the near surface layer in the direction of the maximum (tensile) principal stress. Alternatively, secondary fractures were interpreted, as mixed-mode cracks, slipping at depth as shear cracks and opening near the surface due to low confining pressure. The Coulomb failure function after the earthquake (obtained summing the M.F. stress change and the lithostatic stress) suggests that secondary faulting (S.F.) can be expected to occur in response to the main rupture below the upper soft layer down to few hundreds of meter depth. The total stress change induced by the M.F. and the S.F. (of smaller scale) is shown to yield quantitative explanations of the complex geometry observed in the fault region in terms of simple frictional laws and friction coefficients very close to those measured in the lab (Figure 50).

3.7.1.4 Meetings and Conferences

XXIII EGS General Assembly, Nice, France, April 20-24, 1998. LXXXIV Congresso Nazionale Società Italiana di Fisica, Salerno Italy, September 28 - October 2, 1998. PRENLAB-2 workshop, Strasbourg, France, March 31, 1999. XXIV EGS General Assembly, The Hague, The Netherlands, April 19-23, 1999.

3.7.1.5 References

Bonafede, M. & E. Rivalta 1999. The tensile dislocation problem in a layered elastic medium. *Geophys. J. Int.* 136, 341-356.

Bjarnason, I.Þ., P. Cowie, M.H. Anders, L. Seeber & C.H. Scholz 1993. The 1912 Iceland earthquake rupture: growth and development of a nascent transform system. *Bull. Seism. Soc. Am.* 83, 416-435.

3.7.2 Subpart 7B: Modelling of the earthquake related space–time behaviour of the stress field in the fault system of southern Iceland

Associated contractor:
Frank Roth

In the framework of PRENLAB-1, a model study was continued to obtain forward models of the stress field and stress changes in the South Iceland seismic zone (SISZ).

This proposal has the target to model the space–time development of the stress field using data on strain and stress changes from the other experiments and from databases.

Two models were prepared during PRENLAB-1:

- A model of the South Iceland seismic zone and the adjacent part of the eastern volcanic zone.
- A scheme comprising the main ridge parts on Iceland and the North Atlantic ridge to the north and to the south of the island, including both faults and the load due to Katla and Hekla volcanoes.

It was modelled:

- The changes in crustal strain and stress due to earthquakes and aseismic movement in the fault system of the South Iceland seismic zone.

- The interaction of faults.
- The mutual influence between volcanic and earthquake activity, e.g. magmatic upwelling and shearing at fault zones.

3.7.2.1 The model for the earthquake sequence at the SISZ

The main features of this model are given again to ease comparison with the new results:

The method:

The forward modelling of stress fields is done by applying static dislocation theory to geodetic data and data obtained through the seismic moments from seismograms. It allows to calculate displacements, strain and stresses due to double-couple and extensional sources in layered elastic and inelastic earth structures. Besides the change in displacement during the event, the changes caused by the movement of plates is included (for further details see e.g. Roth 1989).

Usually, for earthquake hazard estimation, the location, magnitude and statistically estimated recurrence period of former events is used. To improve this, here the rupture length and width as well as the tectonic setting and the crustal deformation rates are considered while calculating the space-time development of the stress field.

The targets:

In general, with these models, the subproject aims:

- To achieve a better understanding of the distribution of seismicity in space and time, its clustering and migration in Iceland.
- To provide models for the joint interpretation of the data gathered in the whole research programme, of which this is one part.
- To compare models of stress fields at SISZ to those for stress fields in other regions, e.g. the North Anatolian fault zone.
- To make a contribution to the intermediate-term earthquake prediction in this populated and economically important region of Iceland.

The tectonic setting:

The SISZ is situated between two sections of the mid-Atlantic ridge, the Reykjanes ridge (RR) and the eastern volcanic zone (EVZ). Even though the angle between the SISZ and the neighbouring ridges is far from 90°, it is considered as a transform fault. Following the transform fault hypothesis, left-lateral shear stress is expected along the E-W striking zone. This is equivalent to right-lateral shear stress with N-S orientation. In fact, earthquakes seem to occur on N-S trending en-echelon faults (cf. Einarsson et al. 1981; Hackman et al. 1990 and further references there). They are located side by side between the Hengill triple junction, where the RR meets the low activity western volcanic zone (WVZ) and Hekla volcano, a part of the EVZ (cf. Einarsson et al. 1981 and Figure 51). As we further know from Subprojects 4 and 5, the orientation of the larger horizontal principal stress is NE–SW, i.e. fits to an active N-S or E-W trending fault, which is not a weak fault like the San Andreas fault, and the stress orientation seems to be constant since Pliocene time.

In detail, the questions to be solved are:

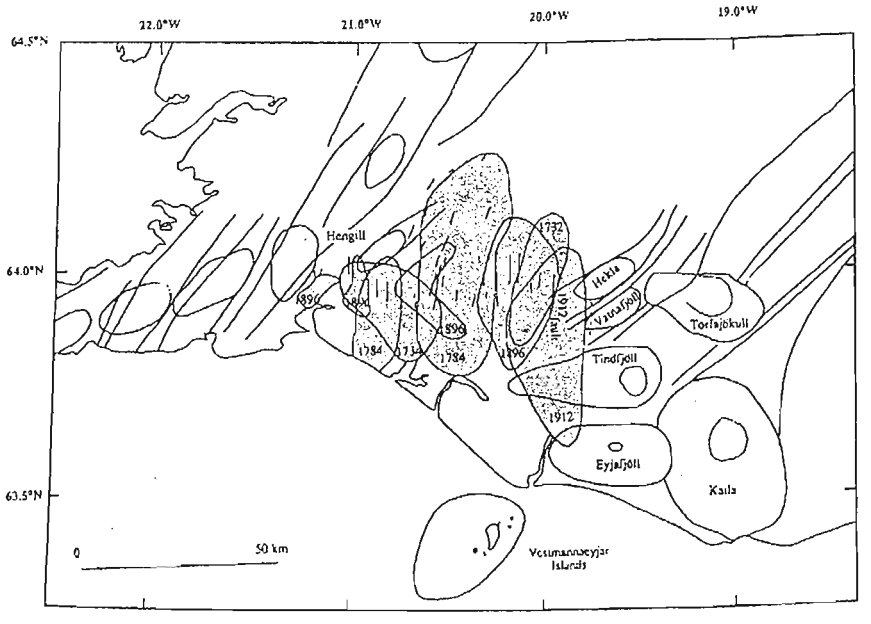

Figure 51. *The South Iceland seismic zone showing mapped surface breaks and regions in which over half of the buildings were destroyed in historic seismic events (after Einarsson et al. 1981). The N-S dashed line near Vatnafjöll indicates the estimated location of the fault on which the May 25, 1987, earthquake occurred (after Bjarnason and Einarsson 1991). The structural features and the coastline are after Einarsson and Sœmundsson (1987).*

- Do these events, placed on parallel faults, release all the energy stored in the 3-D volume of the SISZ?
- Do the earthquakes always take place in areas of high stress?
- What is the critical stress level? How large is its variability?
- Where are the highest stresses nowadays?

The area investigated extends from 18 to 24°W and from 63 to 65°N. The origin is set to 24°W, 64°N (cf. Figure 52) it includes the SISZ, ±1° north and south of 64°N, the SW edge of the EVZ, and the north eastern most part of RR.

The initial stress field:

The initial stress field is determined as follows: A tensional stress acting N103°E (nearly parallel to the SISZ; cf. DeMets et al. 1990) is assumed, due to ridge push or basal drag of the adjacent plates. This rifting induces shear stresses in the region of the transform fault. The stress magnitude, which is unknown, is set to a value that produces left-lateral shear stresses in E-W direction as large as the stress drop determined for the largest event (M=7.1) in the studied earthquake sequence.

Tensional stresses at both ridges are modelled as constantly being released to have zero values at the rifts. These are the major disturbances of the unknown background stresses.

On this initial field, the stress changes due to earthquakes are iteratively superposed as well as the stress changes due to further spreading at the ridge segments based on an opening of 2 cm/year. This value is taken from DeMets et al. (1990). As the simplest assumption, lacking other data, the spreading rate is taken to be constant during the modelled time period, even though this can be questioned as for instance the present debate on the stress increase in the New Madrid seismic zone shows.

The stress field before every event is thus the sum of the initial field, the stress drop of all preceding events, and the plate tectonic stress build-up since the starting time of the model, which is set to 1706, when the first event in the series occurred.

Results were calculated for 56x44 test-points covering 280 km in E-W direction and 220 km in N-S direction. Stresses were computed for a homogeneous half-space, as a starting model. Although surface stress changes are calculated, these should be representative for crustal stresses using values for the moduli, that are typical for oceanic crust (see Dziewonski et al. 1975) and not for sedimentary layers at the surface.

The earthquake data:

All events with $M \geq 6$ since 1706 were used (listed in Table 6, following Halldórsson et al. 1984; after Hackman et al. 1990, Stefánsson and Halldórsson 1988, and Stefánsson et al. 1993). The catalogue is supposed to be complete from 1706 for these earthquakes.

All ruptures were set to be oriented N-S, according to the isolines of damage intensity and surface ruptures shown in Figure 51. As only the 1912 event was instrumentally recorded, the source parameters are not very accurate – a problem to be discussed further below.

The results from PRENLAB-1:

The stress fields at 18 dates were calculated: the pre- and post-seismic situation for all 11 events and the stresses in 1998. The time before 5 events was too short to accumulate

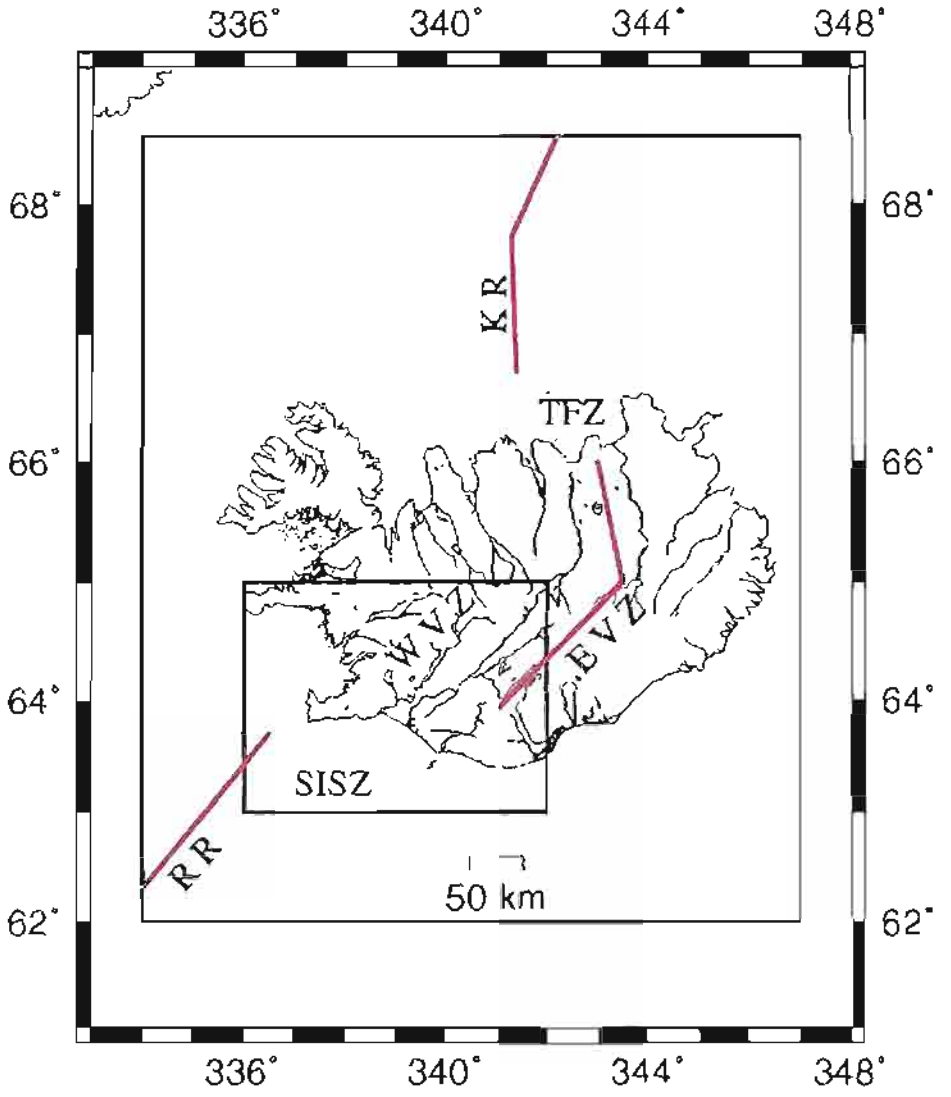

Figure 52. *Map of Iceland and surrounding area. Thick red lines indicate mid-Atlantic ridge segments, as used in the modelling. The smaller box shows the region of the model on the South Iceland seismic zone. The SISZ extends here approximately between 336.5° E, 63.9° N to 341.2° E, 64° N. The large box gives the region for the Iceland rift model.*

Date[1]	Magnitude[1]	Epicenter[1]		South end of rupture[2]		Co-seismic slip[3]	Rupture length[4]
		Lat. °N	Long. °W	x [km]	y [km]	U_0 [m]	L [km]
1706	6.0	64.0	21.2	131	-5	0.30	10
1732	6.7	64.0	20.1	183	-11	0.77	22
1734	6.8	63.9	20.8	150	-23	0.96	25
14.08.1784	7.1	64.0	20.5	164	-18	1.9	35
16.08.1784	6.7	63.9	20.9	145	-22	0.77	22
26.08.1896	6.9	64.0	20.2	178	-14	1.2	28
27.08.1896	6.7	64.0	20.1	183	-11	0.77	22
05.09.1896	6.0	63.9	21.0	140	-16	0.30	10
05.09.1896	6.5	64.0	20.6	159	-9	0.48	18
06.09.1896	6.0	63.9	21.2	131	-16	0.30	10
06.05.1912	7.0	63.9	20.0	187	-27	1.5	32

Table 6. *Earthquakes $M \geq 6$ since 1706 in the South Iceland seismic zone. 1) Data taken from Stefánsson et al. 1993. 2) Position in the model coordinate system with origin at 64° N, 24° W. 3) Calculated via the magnitude moment relationship* $\log M_0$ *[dyne cm]* $= 1.5 M_S - (11.8 - \log(\sigma_a/\mu))$ *with the apparent stress* $\sigma_a = 150$ *MPa and the shear modulus* $\mu = 0.39 \cdot 10^{11}$ *Pa (Kanamori and Anderson 1975), followed by using the values of* μ *above, the rupture length as given in the table as well as a vertical fault width of 14 km east of 21° W and 7 km between 21° W and 21.2° W. Finally, the values were reduced by a factor of 2, following the discussion in Hackman et al. 1990. 4) Calculated using* $\log L$ *[km]*$= 0.5M - 2$ *(after Qian 1986) which results in slightly lower values compared to e.g. Schick 1968.*

appreciable plate tectonic stresses since the preceding event. In these cases, the post-seismic stress field of the preceding event was set equal to the pre-seismic stress field of these earthquakes.

Figure 53 gives the initial stress field in 1706. The rift segments, lower left and upper right, with about zero tensile stresses, also show low shear stresses. The area between the tips of the rifts shows increased left-lateral E-W shear stresses (equivalent to right-lateral N-S shear stresses). The SISZ as a strike-slip fault zone extends here approximately from 23.5°W, 63.9°N or ((60 km, -10 km) in model coordinates) to 18.8°W, 64°N or (250, 0) (cf. also Figure 52).

Figure 54 gives the initial stress field again with the dark red areas subject to the highest shear stress.

Figure 55 shows the stress field after the 1912 event.

As a simple assumption, one might expect, that earthquakes in a certain fault zone usually occur at about the same critical shear stress level. We examine here, if such an expectation matches the known facts about the earthquakes, given above, and the stress field in the SISZ from knowledge about plate motion and the modelling here. Figure 56 summarizes the mean shear stress level before each of the earthquakes at the area of the impending event. The stress level for the 1706, 1732, 1734, the first 1784, the first and last 1896, and the 1912 events are rather high ($\geq$2.0 MPa). The second 1784 earthquake (two days after the first, 0.4 in magnitude smaller, 19 km away) might have been an aftershock and therefore situated in a lower stress area (1.2 MPa). The same might apply to the second and forth of the 1896 events, whereas the last 1896 shock hit a high stress area (2.5 MPa) – the place of the 1706 earthquake, where the stress had recovered since then.

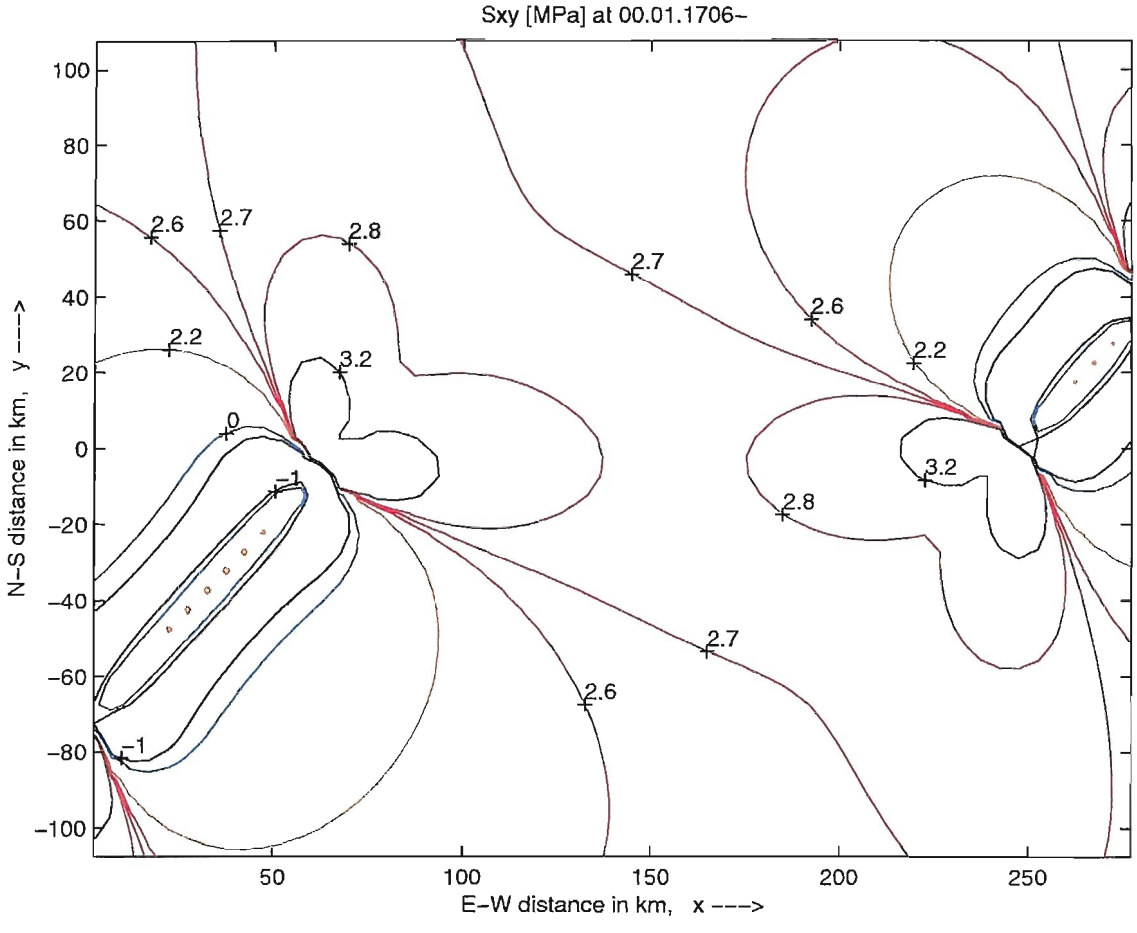

Figure 53. *Shear stress field in the South Iceland seismic zone and its surroundings as assumed in 1706 – the starting field for the model calculations in PRENLAB-1. The background stress is between 2.6 and 2.7 MPa. It is increased between the rift tips which are at (60, -10) and (250, 0).*

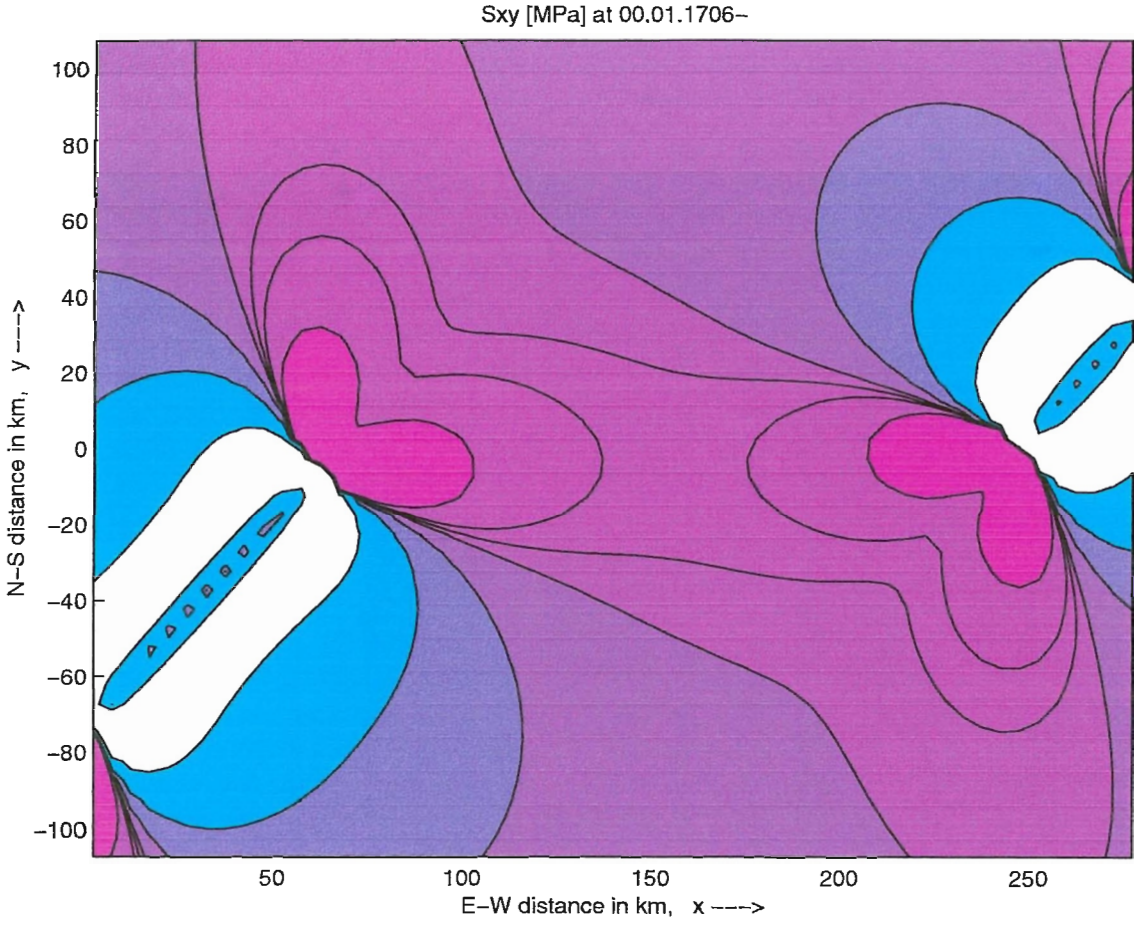

Figure 54. *Shear stress field in the South Iceland seismic zone and its surroundings as assumed in 1706. — The same as Figure 53 with coloured areas between isolines.*

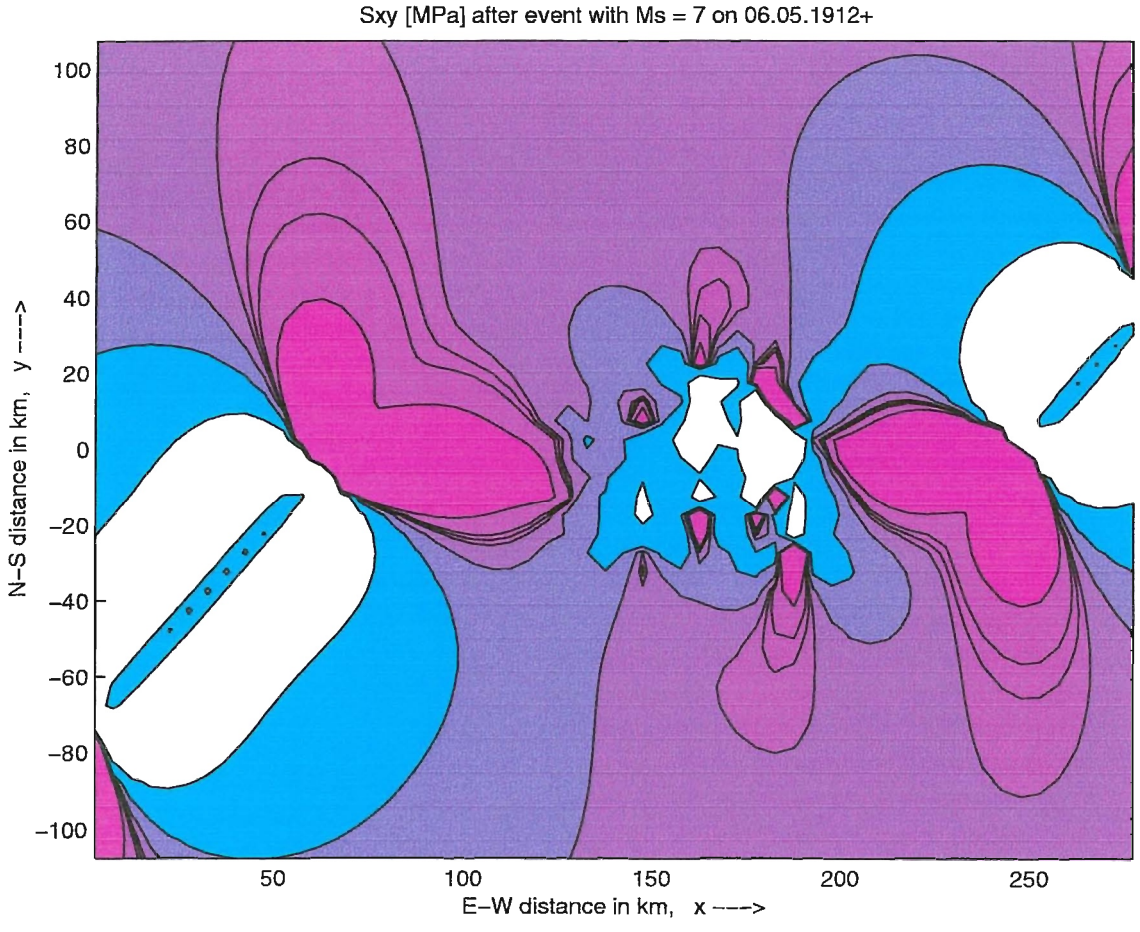

Figure 55. *The stress field after the May 6, 1912, M=7.0 earthquake occurred at (187, -11).*

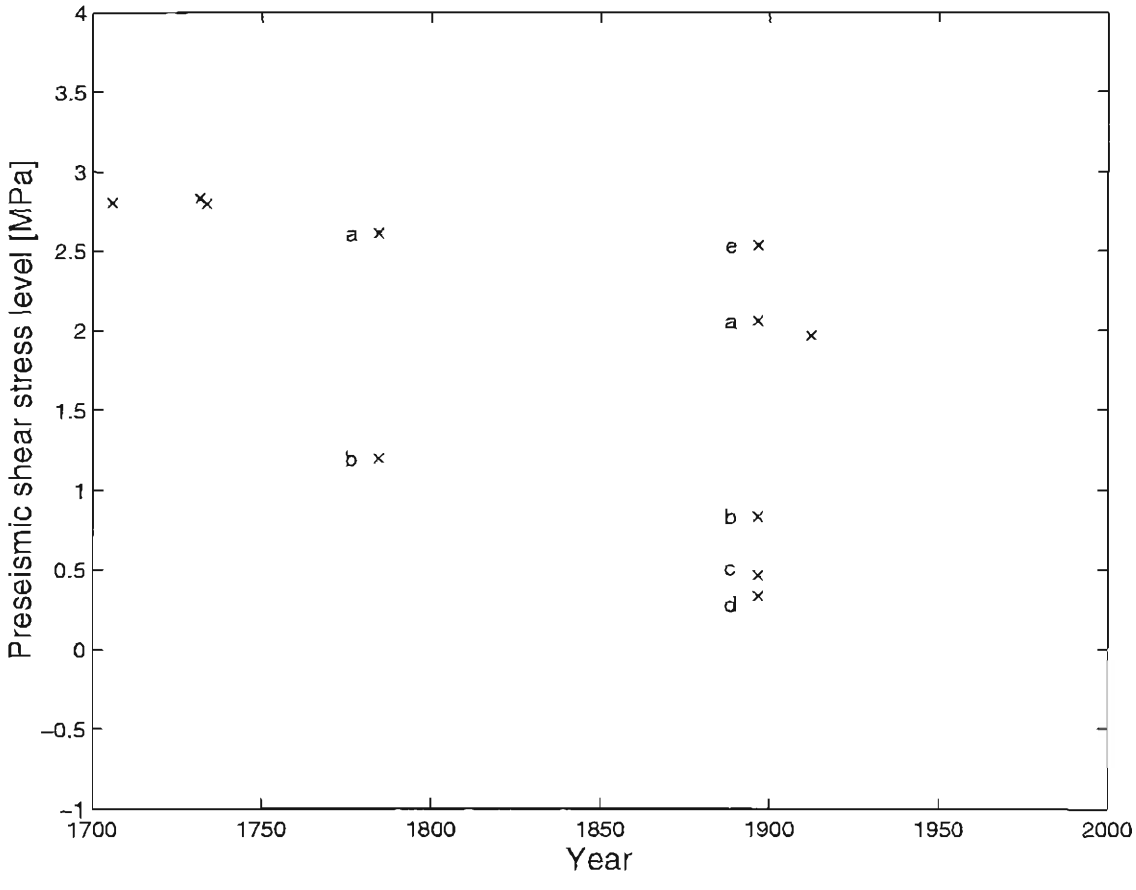

Figure 56. *Cross plot of the pre-seismic shear stress level at the site of the impending earthquakes vs. occurrence time. The stress values at 2 to 14 test-points near the surface trace of the rupture plane were averaged. — Letters "a" through "e" denote the events in one year in temporal sequence.*

3.7.2.2 Changes and improvements in PRENLAB-2

In the first phase of PRENLAB-2, the models developed in PRENLAB-1 were improved:

A At the western end of the SISZ, segments with aseismic oblique slip (mainly normal faulting with a smaller component of left-lateral strike-slip) were introduced, to better fit the Reykjanes ridge (RR) between the SW tip of the Reykjanes peninsula to Hengill triple junction (Figure 57).

B The test-point density was increased from 56x44 (5 km distance) to 280x220 (1 km distance) to get more details of the stress field and to reduce interpolation errors.

C A layered model, including an inelastic asthenosphere below a brittle seismogenic upper layer, is in preparation.

D To investigate the model resolution a set of different models is produced: Besides the main model, several extreme cases are assumed and the variation of the main results under these assumptions is observed.

E The stress field at 1912, the end of the series of strong events with $M \geq 6$, is extrapolated to April 1999.

Concerning item A, the RR on Iceland is treated now completely as a zone of aseismic rifting, consisting of 2 sections with changing rifting and strike-slip components to model the bend of the ridge from SW towards the Hengill triple junction, as displayed in Figure 57. Doing so, not only the geometry of the rift is better fitted, but also stress build-up by plate motion is concentrated in the west near the Hengill triple junction instead of farther west in the RR. Now, seismic slip is confined to the SISZ ((125, -5) — (250, 0)), where the series of strong earthquakes simulated here, took place.

This model was calculated with a test-point spacing of only 1 km (item B). It will be named "improved model" below.

A selection of the results obtained by this model is given in Figures 58, 59, and 60. Figure 58 gives the initial stress field again with the dark red areas subject to the highest shear stress, now at the rift tip east of Hengill.

The pre-seismic stress level is expected to be smoother than before with the wider spacing of the test-points. As – at the same change, however – the high stress tip of the SISZ was shifted to Hengill, the westernmost events (1706, 1784b, 1896c and e) got into a higher stress region. This produces a larger scatter of the pre-event stress level, cf. Figure 60. However, the stress level for the main events remains in a similar range as before (between 2.0 and 2.8, now between 1.7 and 2.9 MPa).

Two problems were addressed next:

1. To see how sensitive the results depend on the model parameters, it was begun to check extreme cases and their outcome.

2. The average stress level before some events is only slightly above and even below the background stress of about 2.65 MPa (see the main shocks 1706 and 1784a, and 1896a and 1912, respectively). This is, among other reasons, due to the fact that the rupture planes, used until now, extend rather far to the north and south of the SISZ.

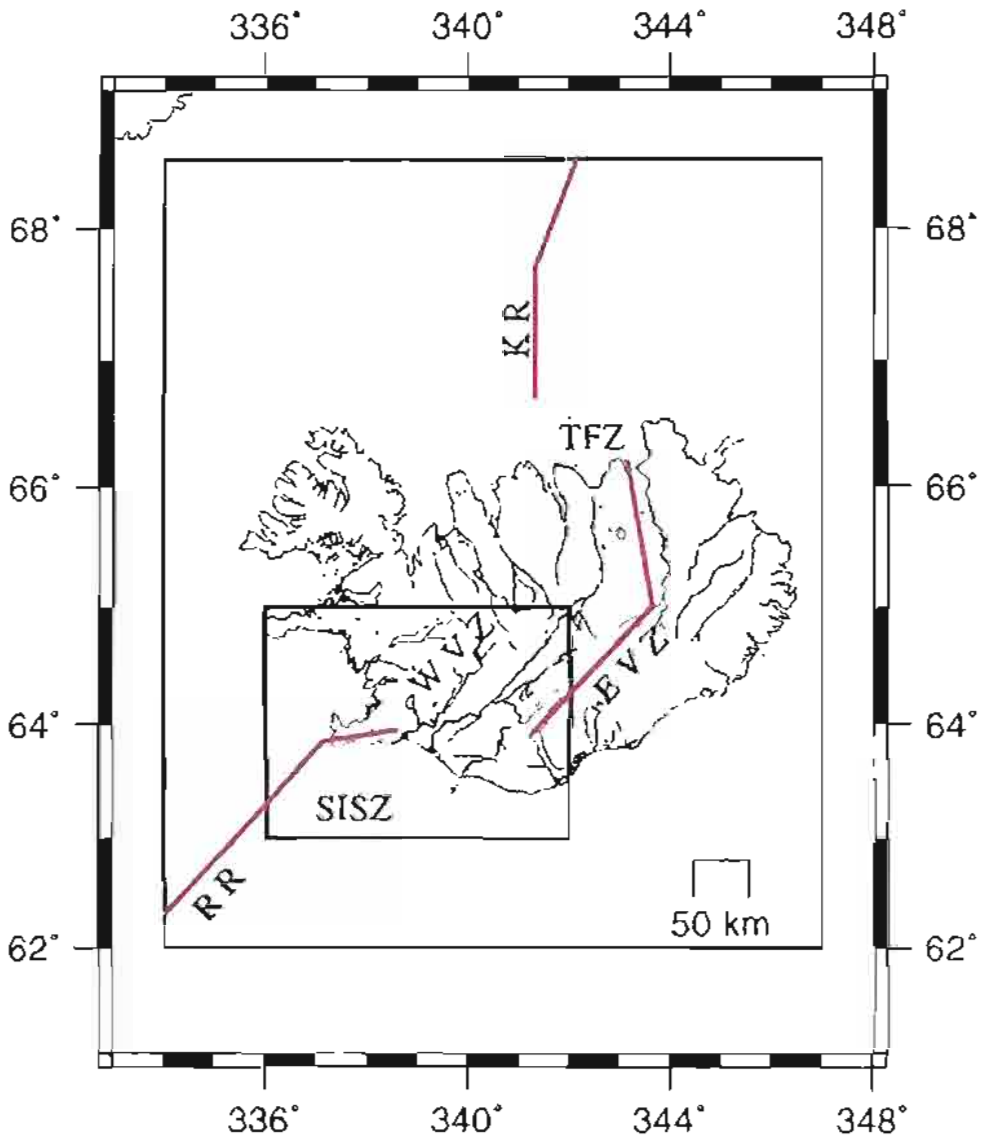

Figure 57. *Map of Iceland and surrounding area. Thick red lines indicate mid-Atlantic ridge segments, as used in the "improved model" and further. The smaller box shows the region of the model on the South Iceland seismic zone. The SISZ extends approximately between (338.6° E, 63.95° N) to (341.2° E, 64° N). The large box gives the region for the Iceland rift model.*

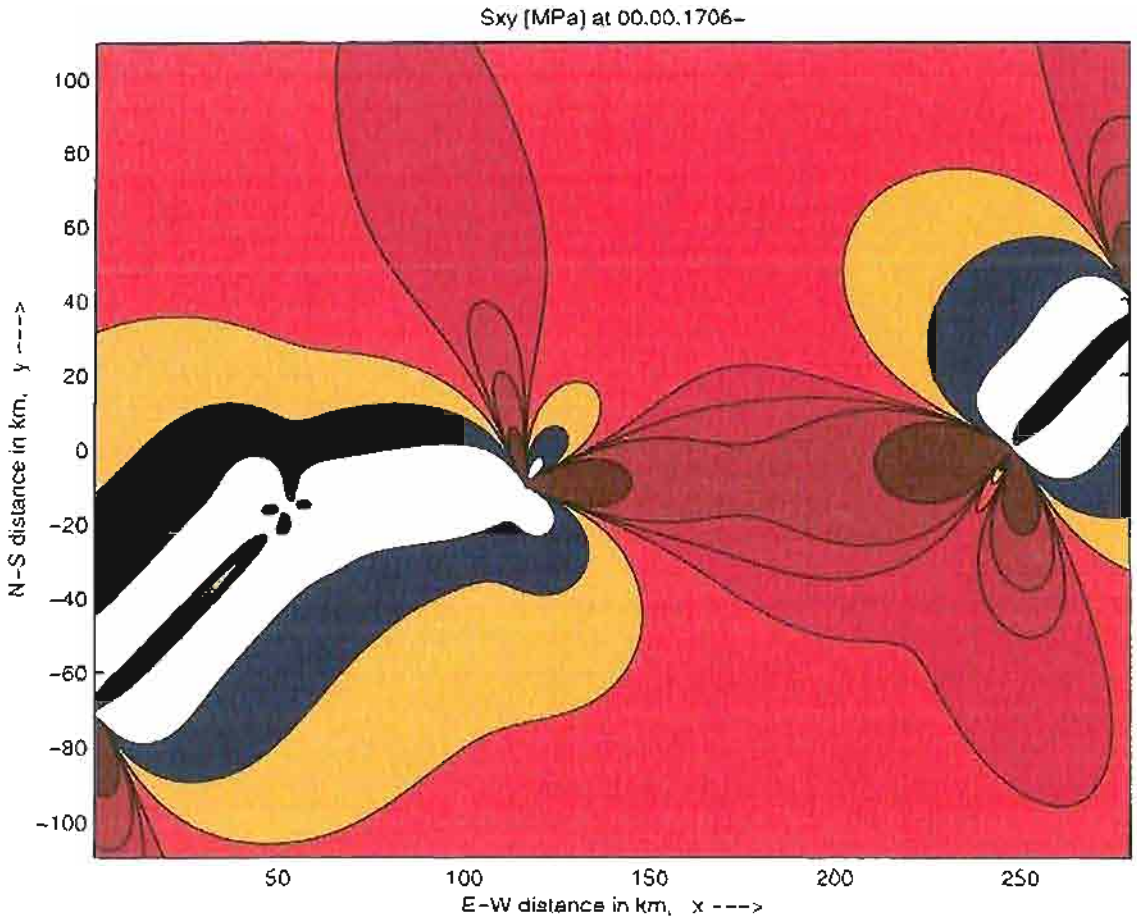

Figure 58. *Shear stress field in the South Iceland seismic zone and its surroundings as assumed in 1706 ("improved model"). — The same values of the isolines apply as in Figure 53.*

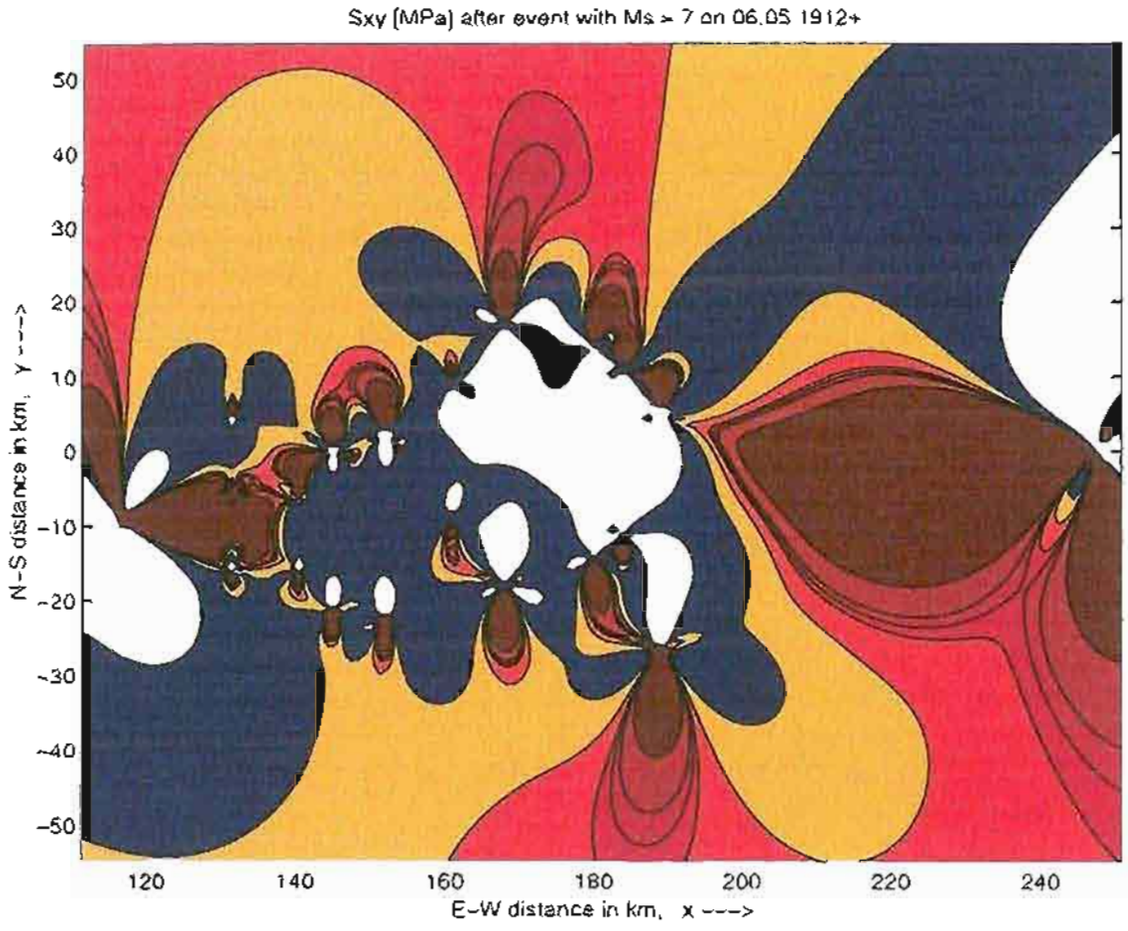

Figure 59. *The stress field after the last strong event May 6, 1912, M=7.0 earthquake occurred at (187, -11) in the "improved model". Here, only the central region of the modelled area is displayed, so that the details inside the SISZ are clearly visible.*

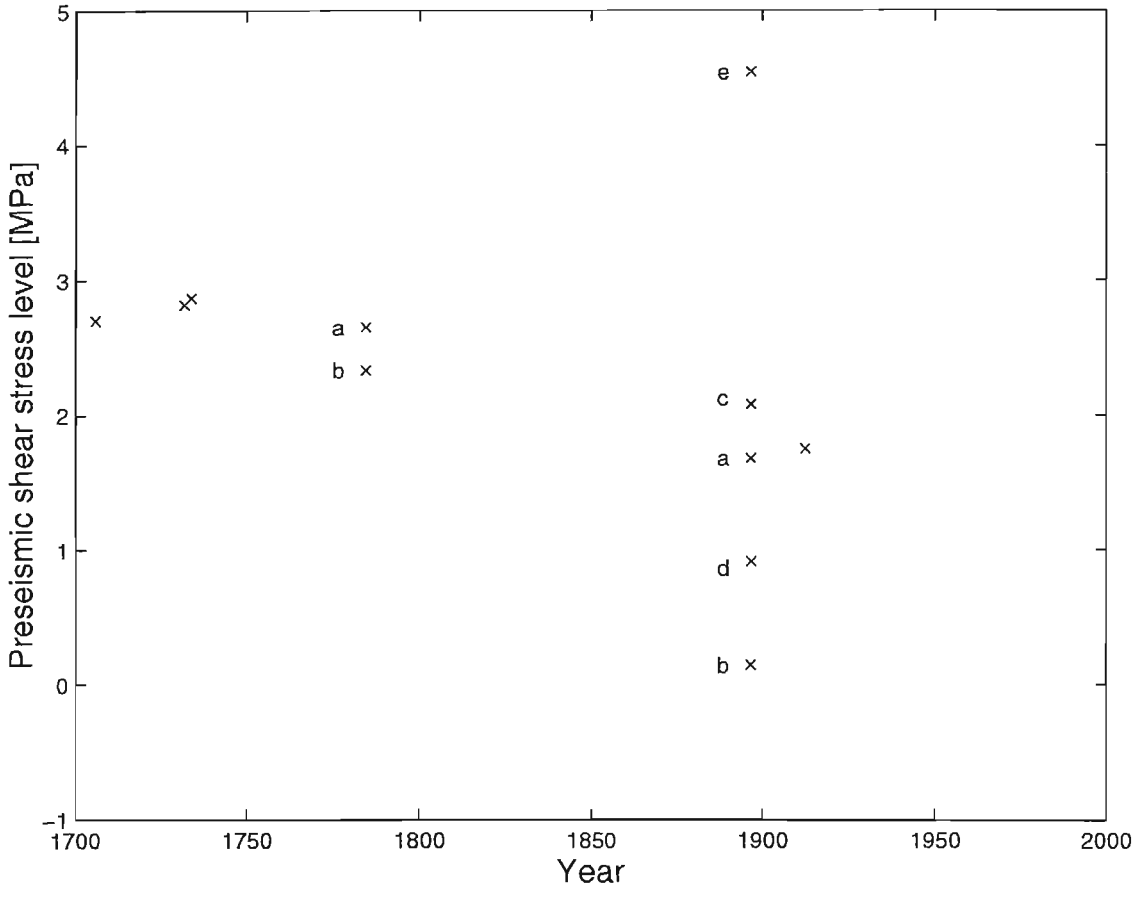

Figure 60. *Cross plot of the pre-seismic shear stress level at the site of the impending earthquakes vs. occurrence time. Here in the "improved model", the stress values at 10 to 70 test-points near the surface trace of the rupture plane were averaged. — Letters "a" through "e" denote the events in one year in temporal sequence.*

The damage areas from historical records are not gathered by scientists and are usually biased by uneven population density. So the magnitudes and locations are not very accurate, as stated earlier. As mentioned in the footnotes of Table 6, there are doubts on the correct rupture size from global relations between magnitude and rupture length.

From both reasons, given here, a model was calculated that uses the same seismic moment of the events, but cuts the fault length to 50% while doubling the co-seismic displacement. It will be termed "short rupture model". One side-effect of this change is an increase of the stress level by a factor 2.5, as the moment release is concentrated to a smaller area. The background stress field amplitude was increased accordingly, because - as described above - this field is adjusted to the average stress change of the strongest event. It is important to note that the increase in stress level does not change the stress pattern of the initial stress field; as we are not looking for specific stress amplitudes but for stress concentrations, the change in level is not important.

The resulting pre-seismic stress level is expected to be smoother than before due to the concentration of stress release to high stress areas.

For comparison with the models above, some results obtained in the "short rupture model" are given in Figures 61 through 64.

Figure 62 gives the initial stress field again with the dark red areas subject to the highest shear stress. The shape is identical to Figure 58, as only the amplitude of the shear stress has increased (differences are due to the selection of isoline values).

The pre-event stress level now varies between 6.5 and 7.4 MPa for the main shocks (for more details cf. Figure 64). It is more stable than the level in the previous models, if relative values are compared. For most events, the initial stress level is considerably higher than the background. Only for two main shocks it is near the background (1706 and 1896a) and only for two strong aftershocks it is below (1896b and d). The differences to the previous model are not very large, but a further improvement of the "improved model" could be achieved in using shorter rupture planes. Concerning the extension to a layered crustal structure with an inelastic substratum to include post-seismic relaxation processes, these models will be addressed as soon as the elastic ones are finished. A new code has been prepared for this, much faster, more accurate, and capable of including even more layers than the existing code. The extension of the computer programme for the superposition of stress fields with the new code has already begun. The results will not only be compared to those from the purely elastic models, but also to continuous GPS crustal deformation data, as soon as these are available.

3.7.2.3 Task 1: Extrapolation of the stress field calculated within PRENLAB for the next years

The stress field for the new models was extrapolated to spring 1999, with the additional stresses due to plate motion since 1912. In the "improved model", shear stress inside the SISZ (Figure 65) are only high at small places like (150, 5) and at some places at the northern and southern margins of the seismically active zone (y-values larger than +10 km or lower than -10 km). This is similar in the "short rupture model" (Figure 66), even though there are high stresses around x-values of 155 to 160 km, too. In general, in the west and in the east, where the SISZ meets the ridge segments, stresses are concentrated. Is this a weakness of the models or is it the real situation?

An argument against high stress there is, that there was no large event ($M \geq 6$) since 1706. The origin of the stress concentrations at the end of the SISZ, i.e. at the tips of the adjoining ridges, is the fact that the ridges do not extend to infinite depth, but are

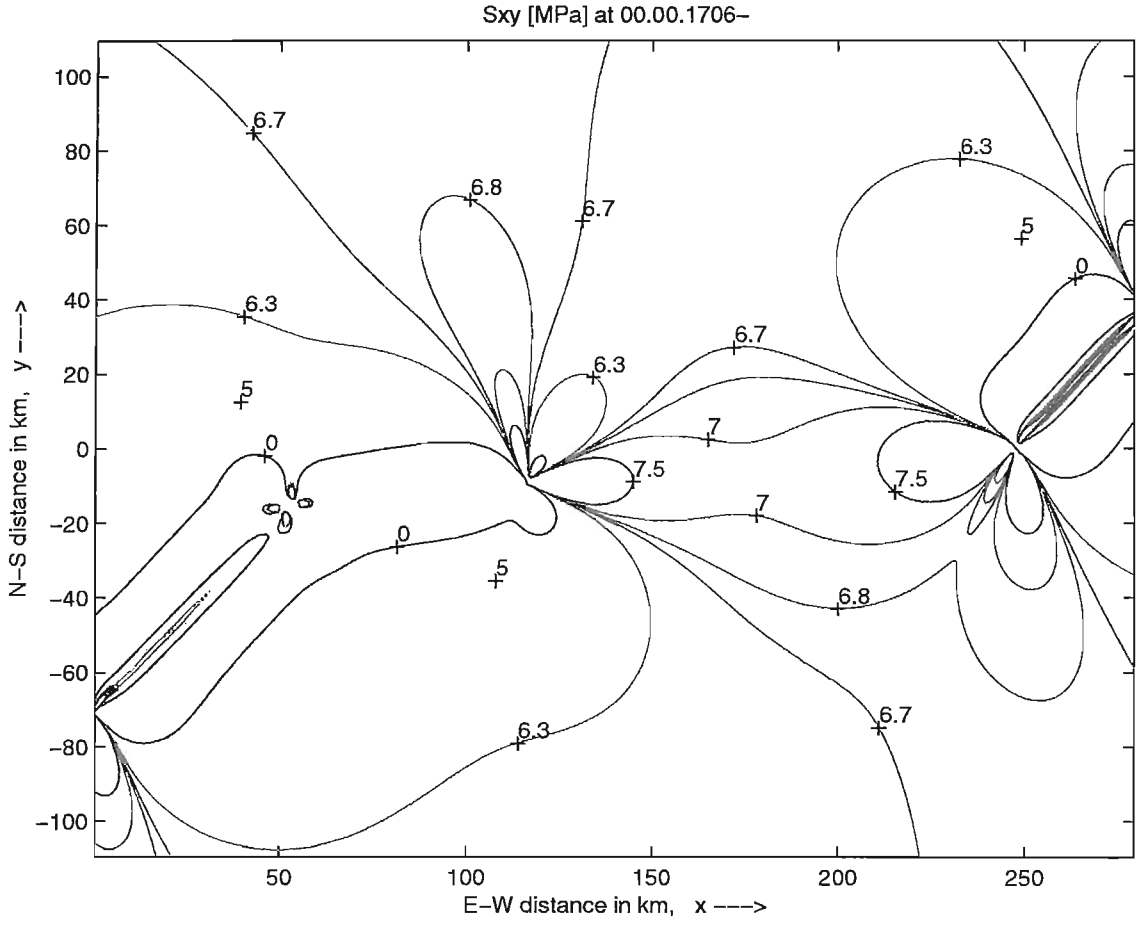

Figure 61. *Shear stress field in the South Iceland seismic zone and its surroundings as assumed in 1706 – the starting field for the model calculations in the "short rupture model". The background stress is about 6.5 MPa. It is increased between the rift tips which are at (125, -5) and (250, 0).*

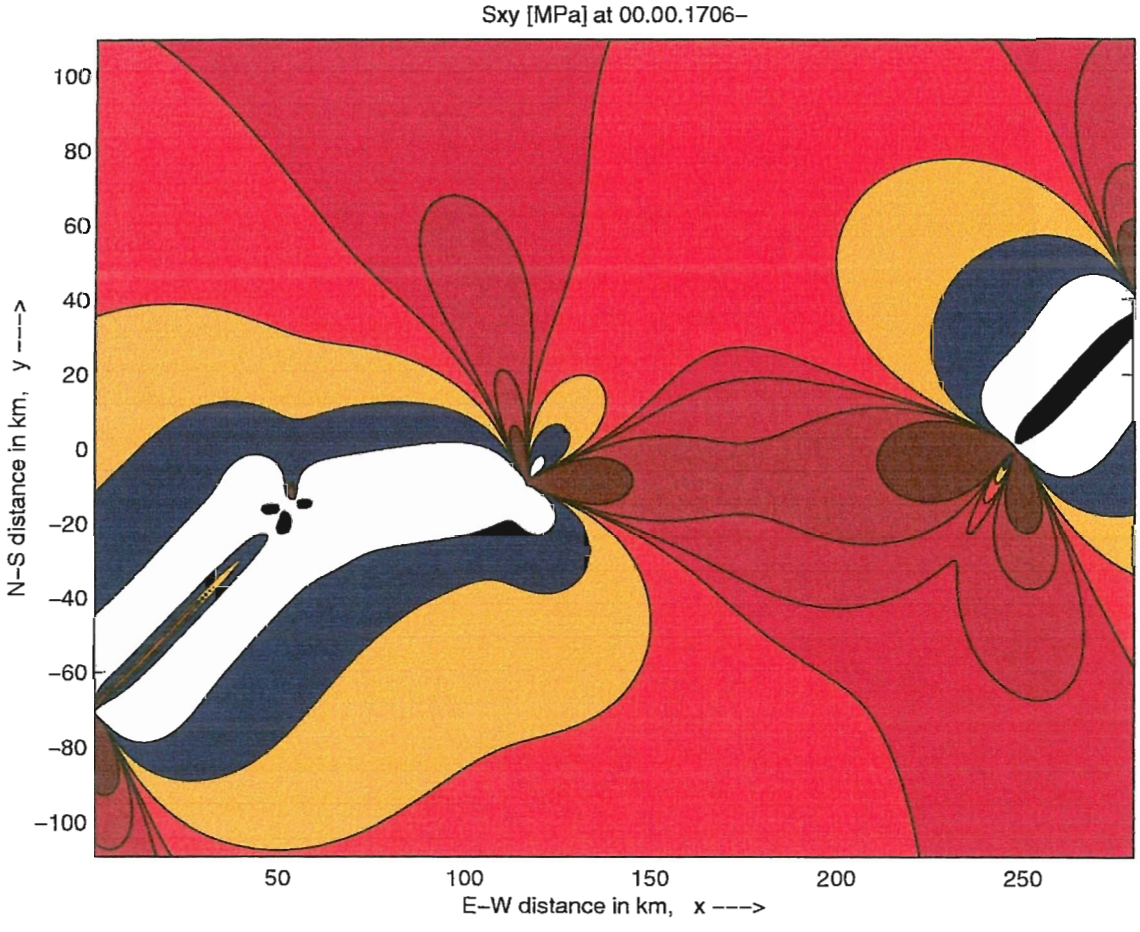

Figure 62. *Shear stress field in the South Iceland seismic zone and its surroundings as assumed in 1706 ("short rupture model"). — The values of the isolines as in Figure 61 apply.*

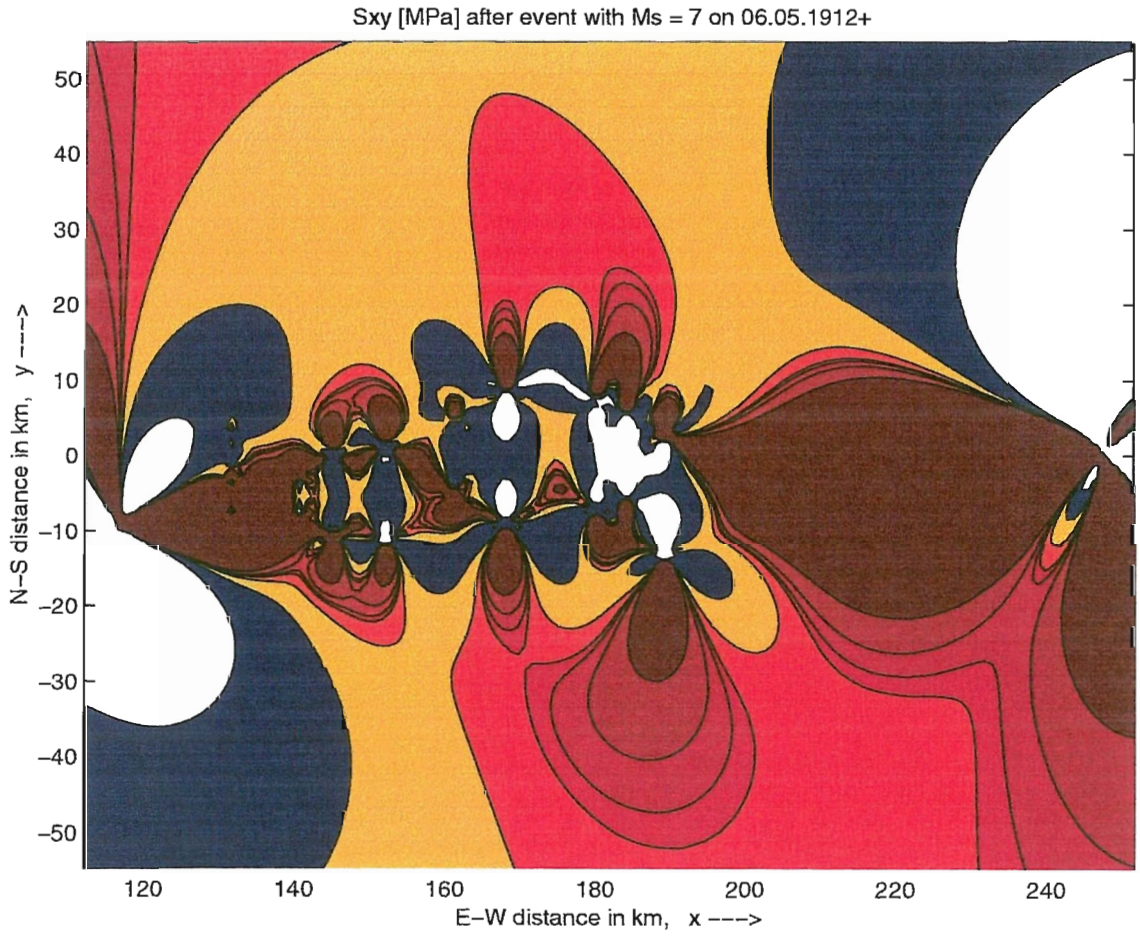

Figure 63. *The stress field after the last strong event May 6, 1912, M=7.0 earthquake occurred at (187, -6) ("short rupture model"). The values of the isolines as in Figure 61 apply.*

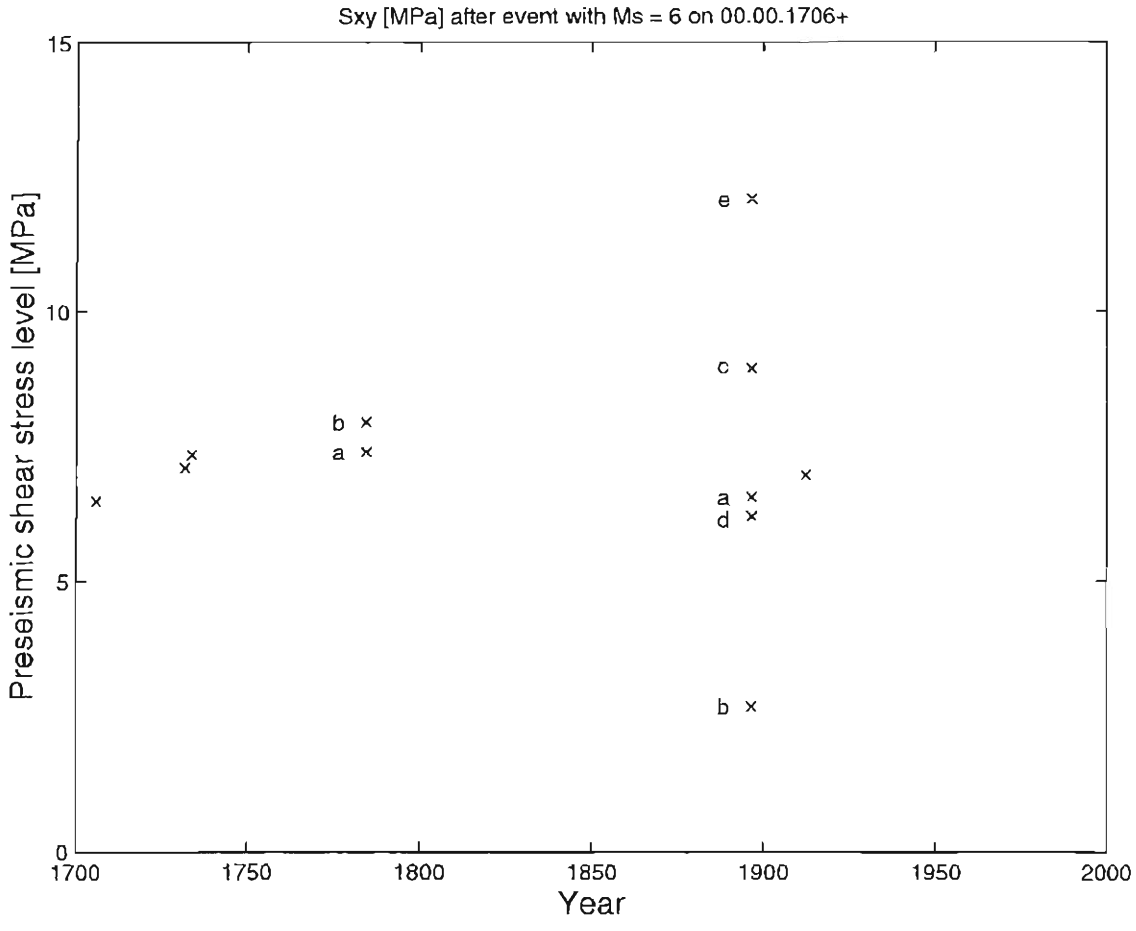

Figure 64. *Cross plot of the pre-seismic shear stress level at the site of the impending earthquakes vs. occurrence time. Here in the "short rupture model", the stress values at 5 to 35 test-points near the surface trace of the rupture plane were averaged. — Letters "a" through "e" denote the events in one year in temporal sequence.*

assumed to reach only 7 km depth and enter than an inelastic, hot region not capable of supporting stresses for time periods of years. Deeper penetration of the brittle layer there would homogenize the stress field between rift tips at some average value. Entailed is the following: In the models introduced here, high initial stresses at the tips are needed to obtain high enough stresses in the center of the SISZ (see section about the initial stress field above). Further, high tensional stresses at the rifts mean high initial stress in 1706 compared to the annual increase by plate motion, as long as the rifting speed is kept constant. Indeed, if one compares the situation in 1912 with that in 1999 (e.g. Figure 59 with Figure 65) the stress build-up by plate motion is very low. It would mean that the stress release by earthquakes in a series of events as it was observed and is modelled here, would be followed by a period of quiescence until the stress level of 1706 is reached again.

On the other hand, there are some indications that the present stress release indeed mainly takes place at the ends of the SISZ: Interestingly, in 1987, there was a strong earthquake (M_S=5.8) at 63.91°N, 19.78°W (198, -9) near Vatnafjöll (see Figure 51) at the east end of the SISZ. This event was not included in the modelling as its magnitude was below M=6. Nevertheless, it occurred in a region of high stress in the models, as shown in Figures 65 and 66 (the time difference of 12 years (between 1987 and 1999) does not mean a big difference in the stress level in the present models. In 1998, there were 2 stronger events at the Hengill triple junction at the western end of the SISZ: June 4 (M=5.1) and November 13 (M=5) both accompanied by a lot of smaller events.

Considering this conflicting information, another (extreme) model will be computed during the next months using a much deeper width of the brittle layer at the rifts with the consequences of lower stresses at the ends of the SISZ and a stronger influence of the plate motion over that of the initial stress amplitudes.

3.7.2.4 Task 2: Pin-pointing of stress concentrations in space and time

The models yields stress concentrations for today at the western (about 21.4°W, 64°N) and eastern end (about 18.8°E, 64°N) of the SISZ and some smaller spots inside the SISZ around (150 to 160, ± 10) in model coordinates, i.e. around (20°W, 64°N). As the stress build-up by plate motion is very low in these models, the uncertainty in time is very large in the so-called "improved model" and still large in the "short rupture model" (compare the stress field in 1999 with that of 1912, Figure 59 with 65 and Figure 63 with 66).

The high stresses at the ends of the SISZ are debatable. On one hand, there was no earthquake above M=6 in both areas since 1706, on the other hand, the recent seismicity in both areas is high with events M≥5 (1987 in the east at Vatnafjöll and in 1998 in the west, near Hengill).

3.7.2.5 Task 3: Search for characteristic preseismic stress level

As a simple assumption, one might expect, that earthquakes in a certain fault zone usually occur at about the same critical shear stress level. Here, we try to find out, if such an expectation matches the known facts about the earthquakes and the stress field in the SISZ.

In all models, the pre-seismic stress level for most main shocks is high and fairly stable. This indicates that the rather simple model can already explain the main features of the behaviour of the SISZ. This is especially astonishing, when the fact is kept in mind, that most (all but one) events used are not instrumentally recorded. Even though the earthquake rupture planes strike N-S, the stress changes calculated here affect the whole

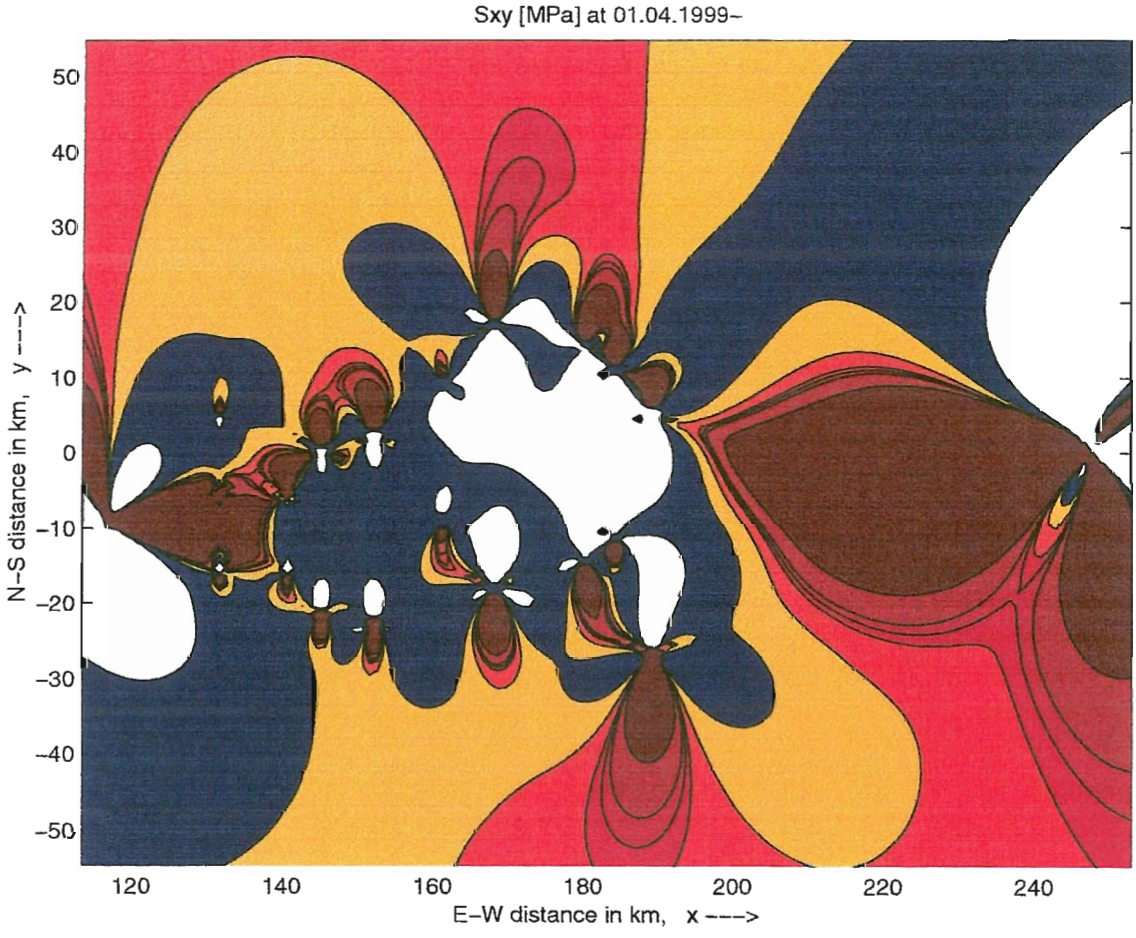

Figure 65. *Extrapolation of the shear stress distribution from 1912 to 1999 ("improved model").*

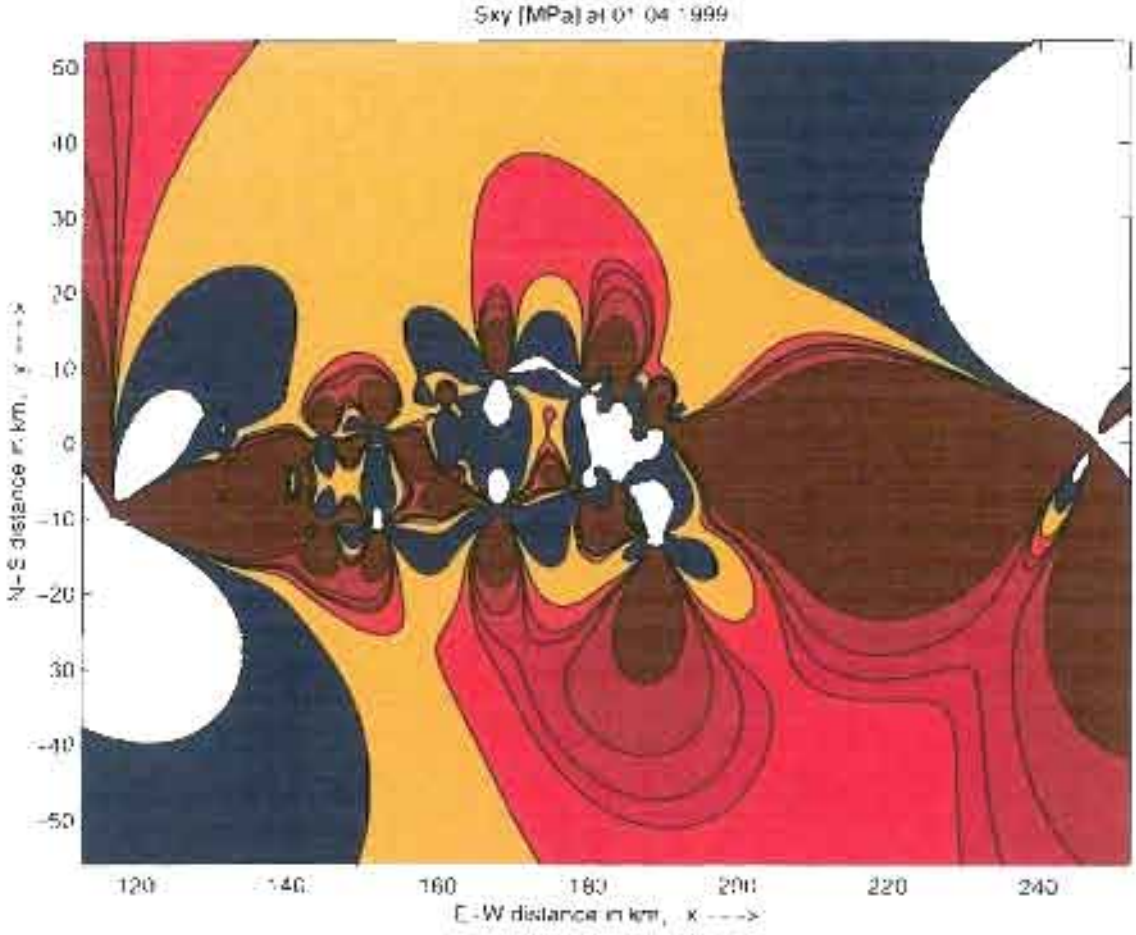

Figure 66: Extrapolation of the shear stress distribution from 1912 to 1999 ("short rupture model")

area of the SISZ.

The tendency with time towards slightly lower values, is an indication that the stress increase due to rifting might have been assumed too low, i.e. the spreading rate between 1706 and 1912 might be higher than 2 cm/year. Moreover, the initial unknown stress field of 1706 could be reduced in the eastern part and the central part, where the first events did not occur before 1732 and 1734, respectively.

A closer look, yields that for the "improved model" the stress level before the earthquakes is between 1.9 and 2.9 MPa, if only the main shocks and no aftershocks are considered (Figure 60). However, in this model, there are 4 events with pre-seismic stress level not much above the background stress, which would not be expected. In the "short rupture model" (same seismic moment as before, but half of the rupture lengths and twice of the co-seismic displacements) the stress level is higher and the pre-event stress level varies between 6.5 and 7.4 MPa for the main shocks (cf. Figure 64). It is more stable than the level in the previous models, if relative values are compared, and for most events, the initial stress level is considerably higher than the background. Only for two main shocks it is near the background (1706 and 1896a) and only for two strong aftershocks it is below (1896b and d). So, the stress field analysis gives some indication that the strong change in rupture lengths used, means to tune the model into the right direction. Nevertheless, the strong variation in model parameters does not lead to totally different results, i.e. the model is rather stable in this respect. To further check the sensitivity of the model results to changes, a model with stronger influence of the permanent stress build-up by plate motion will be calculated next.

In general, the models go beyond the standard earthquake moment release and hazard analysis as they include the spatial location and extension of the events and provide an extrapolation to the present stress situation.

3.7.2.6 Meetings and conferences

A meeting between Maurizio Bonafede and coworkers with Frank Roth took place in March 1999 in Strasbourg, France, parallel to the tenth biennial EUG meeting.

3.7.2.7 Acknowledgements

We thank IMOR.DG for great support on the seismicity of Iceland.

3.7.2.8 References

Roth, F. 1989. A model for the present stress field along the Xian-shui-he fault belt, NW Sichuan, China. In: M.J. Berry (editor), Earthquake hazard assessment and prediction. *Tectonophysics* 167, 103-115.

Einarsson, P., S. Björnsson, G. Foulger, R. Stefánsson & Þ. Skaftadóttir 1981. Seismicity pattern in the South Iceland seismic zone. In: D. Simpson & P. Richards (editors), Earthquake prediction - an international review. *Maurice Ewing Series* 4. American Geophysical Union, 141-151.

Hackman, M.C., G.C.P. King & R. Bilham 1990. The mechanics of the South Iceland seismic zone. *J. Geophys. Res.* 95, 17339-17351.

Bjarnason, I.Þ. & P. Einarsson 1991. Source mechanism of the 1987 Vatnafjöll earthquake in South Iceland. *J. Geophys. Res.* 96, 4313-4324.

Einarsson, P. & K. Sæmundsson 1987. Earthquake epicenters 1982-1985 and volcanic systems in Iceland (map accompanying the festschrift *Í hlutarins eðli*, scale 1:750000). Reykjavík, Menningarsjóður.

DeMets, C., R.G. Gordon, D.F. Argus & S. Stein 1990. Current plate motions. *Geophys. J. Int.* 101, 425-478.

Dziewonski, A.M., A.L.Hales & E.R. Lapwood 1975. Parametrically simple earth models consistent with geophysical data. *Phys. Earth Plan. Int.* 10, 12.

Halldórsson, P., R. Stefánsson, P. Einarsson & S. Björnsson 1984. *Mat á jarðskjálftahættu: Dysnes, Geldinganes, Helguvík, Vatnsleysuvík, Vogastapi og Þorlákshöfn* (earthquake hazard assessment). Veðurstofa Íslands, Raunvísindastofnun Háskólans, Reykjavík.

Stefánsson, R. & P. Halldórsson 1988. Strain release and strain build-up in the South Iceland seismic zone. *Tectonophysics* 152, 267-276.

Stefánsson, R., R. Böðvarsson, R. Slunga, P. Einarsson, S. Jakobsdóttir, H. Bungum, S. Gregersen, J. Havskov, J. Hjelme & H. Korhonen 1993. Earthquake prediction research in the South Iceland seismic zone and the SIL project. *Bull. Seism. Soc. Am.* 83, 696-716.

Kanamori, H. & D.L. Andersson 1975. Theoretical basis of some empirical relations in seismology. *Bull. Seism. Soc. Am.* 65, 1073-1096.

Qian, H. 1986. Recent displacements along Xianshuihe fault belt and its relation with seismic activities. *J. Seism. Res.* 9, 601-614.

Schick, R. 1968. A method for determining source parameters of small magnitude earthquakes. *Zeitschr. f. Geophys.* 36, 205-224.

Papers directly associated with PRENLAB-2

4.1 Subproject 1

Ágústsson, K. 1998. Jarðskjálftahrina á Hellisheiði og í Hengli í maí-júlí 1998. *Greinargerð Veðurstofu Íslands* VÍ-G98040-JA06. Report, Icelandic Meteorological Office, Reykjavík, 35 pp.

Ágústsson, K., A.T. Linde, R. Stefánsson & S. Sacks 1998. Strain changes for the 1987 Vatnafjöll earthquake in South Iceland and possible magmatic triggering. *J. Geophys. Res.* 104, 1151-1161.

Ágústsson, K., S.Th. Rögnvaldsson, B.H. Bergsson & Ragnar Stefánsson 1998. Jarðskjálftamælanet Veðurstofu Íslands og Hitaveitu Suðurnesja - lýsing á mælaneti og fyrstu niðurstöður. *Rit Veðurstofu Íslands* VÍ-R98002-JA02. Research report, Icelandic Meteorological Office, Reykjavík, 17 pp.

Bergerat, F., Á. Guðmundsson, J. Angelier & S.Th. Rögnvaldsson 1998. Seismotectonics of the central part of the South Iceland seismic zone. *Tectonophysics* 298, 319–335.

Böðvarsson, R., S.Th. Rögnvaldsson, R. Slunga & E. Kjartansson 1998. The SIL data acquisition system - at present and beyond year 2000. *Rit Veðurstofu Íslands* VÍ-R98005-JA04. Research report, Icelandic Meteorological Office, Reykjavík, 22 pp.

Böðvarsson, R., S.Th. Rögnvaldsson, R. Slunga & E. Kjartansson 1999. The SIL data acquisition system - at present and beyond year 2000. *Phys. Earth Planet. Inter.* 113, 89-101.

Crampin, S., T. Volti, & R. Stefánsson 1999. A successfully stress-forecast earthquake. *Geophys. J. Int.*, in press.

Rögnvaldsson, S.Th. 1999. Frammistaða SIL kerfisins frá ágúst 1998 til mars 1999. *Greinargerð Veðurstofu Íslands* VÍ-G99004-JA01. Report, Icelandic Meteorological Office, Reykjavík, 14 pp.

Rögnvaldsson, S.Th. 1999. Kort yfir sjálfvirkt ákvarðaðar staðsetningar jarðskjálfta á Íslandi. URL: http://www.vedur.is. June 21, 1999.

Rögnvaldsson, S.Th. & R. Slunga 1999. Kortlagning virkra misgengisflata. URL: http://www.vedur.is/~sr/faults.html. June 21, 1999.

Rögnvaldsson, S.Th., K. Ágústsson, B.H. Bergsson & G. Björnsson 1998. Jarðskjálftamælanet í nágrenni Reykjavíkur - lýsing á mælaneti og fyrstu niðurstöður. *Rit Veðurstofu Íslands* VÍ-R98001-JA01. Research report, Icelandic Meteorological Office, Reykjavík, 15 pp.

Rögnvaldsson, S.Th., Á. Guðmundsson & R. Slunga 1998a. Seismotectonic analysis of the Tjörnes fracture zone - an active transform fault in North Iceland. *J. Geophys. Res.* 103, 30117-30129.

Rögnvaldsson, S.Th., Á. Guðmundsson & R. Slunga 1998b. Seismotectonic analysis of the

Tjörnes fracture zone - an active transform fault in North Iceland. *Rit Veðurstofu Íslands* VÍ-98004-JA03. Research report, Icelandic Meteorological Office, Reykjavík, 23 pp.

Rögnvaldsson, S.Th., G.B. Guðmundsson, K. Ágústsson, S.S. Jakobsdóttir, R. Slunga & R. Stefánsson 1998. Overview of the 1993-1996 seismicity near Hengill. *Rit Veðurstofu Íslands* VÍ-R98006-JA05. Research report, Icelandic Meteorological Office, Reykjavík, 16 pp.

Rögnvaldsson, S.Th., Þ. Árnadóttir, K. Ágústsson, Þ. Skaftadóttir, G.B. Guðmundsson, G. Björnsson, K.S. Vogfjörð, R. Stefánsson, R. Böðvarsson, R. Slunga, S.S. Jakobsdóttir, B. Þorbjarnardóttir, P. Erlendsson, B.H. Bergsson, S. Ragnarsson, P. Halldórsson, B. Thorkelsson & M. Ásgeirsdóttir 1998. Skjálftahrina í Ölfusi í nóvember 1998. *Greinargerð Veðurstofu Íslands* VÍ-G98046-JA09. Report, Icelandic Meteorological Office, Reykjavík, 19 pp.

Rögnvaldsson, S.Th., K.S. Vogfjörð & R. Slunga 1999. Kortlagning brotflata á Hengilssvæði með smáskjálftum. *Rit Veðurstofu Íslands* VÍ-R99002-JA01. Research report, Icelandic Meteorological Office, Reykjavík, 22 pp.

Stefánsson, R. 1998. Earthquake-prediction research in a natural laboratory - PRENLAB. In: C.P. Providakis & M. Yeroyanni (editors), *EU-Japan Workshop on Seismic Risk*. Proceedings of the first expert meeting, Chania, Greece, March 24-26, 1998. European Commission, 113-122.

Stefánsson, R. 1999. A tentative model for the stress build-up and stress release in and around the SISZ.
URL: http://www.vedur.is/ja/prenlab/symp-mar-1999/ragnar/. March 17, 1999.

Stefánsson, R. 1999. Nucleation of earthquakes in the SISZ.
URL: http://www.vedur.is/ja/prenlab/symp-mar-1999/ragnar/index2.html. March 31, 1999.

Stefánsson, R., S.Th. Rögnvaldsson, P. Halldórsson & G.B. Guðmundsson 1998. PRENLAB workshop on the Húsavík earthquake, July 30, 1998. *Greinargerð Veðurstofu Íslands* VÍ-G98032-JA04. Report, Icelandic Meteorological Office, Reykjavík, 5 pp.

Stefánsson, R., F. Bergerat, M. Bonafede, R. Böðvarsson, S. Crampin, P. Einarsson, K. Feigl, Á. Guðmundsson, F. Roth & F. Sigmundsson 1999. Earthquake-prediction research in a natural laboratory - PRENLAB. In: M. Yeroyanni (editor), *Seismic risk in the European Union* II. Proceedings of the review meeting, Brussels, Belgium, November 27-28, 1997. European Commission, 1-39.

Tryggvason, A., S.Th. Rögnvaldsson & Ó.G. Flóvenz 1999. Three-dimensional imaging of the P- and S-wave velocity structure and earthquake locations beneath Southwest Iceland. *J. Geophys. Res.*, submitted.

Vogfjörð K.S. & S.Th. Rögnvaldsson 1999. Identification and modelling of secondary phases in short-period seismograms from local earthquakes in the South Iceland seismic zone. *Geophys. J. Int.*, accepted.

4.2 Subproject 2

Böðvarsson, R., S.Th. Rögnvaldsson, R. Slunga & E. Kjartansson 1999. The SIL data acquisition system - at present and beyond year 2000. *Phys. Earth Planet. Inter.*, 113, 89-101.

Lund, B. & R. Slunga 1999. Stress tensor inversion using detailed microearthquake information and stability constraints: application to Ölfus in Southwest Iceland. *J. Geophys. Res.* 104, 14947-14964.

Shomali, Z.H. & R. Slunga 1999. Body-wave moment tensor inversion of local earthquakes - an application to the South Iceland seismic zone. *Geophys. J. Int.*, submitted.

4.3 Subproject 3

Crampin, S. 1998. Shear-wave splitting in a critical crust: the new promise. Paper presented at the 8^{th} International Workshop on Seismic Anisotrophy, Boussens, France, April 19-24, 1998.

Crampin, S. 1999. Calculable fluid-rock interactions. *J. Geol. Soc.*, in press.

Crampin, S., T. Volti, & R. Stefánsson 1999. A successfully stress-forecast earthquake. *Geophys. J. Int.*, in press.

4.4 Subproject 4

Henneberg, K., F. Roth, H. Sigvaldason, S.Þ. Guðlaugsson, & V. Stefánsson 1998. Ergebnisse von Bohrlochmessungen in der Südisländischen Seismizitätszone in den Jahren 1996 und 1997. Paper presented at the third meeting of the FKPE working group on Borehole Geophysics and Rock Physics, Hannover, Germany, 1998.

Roth F. 1999. Erforschung von Erdbeben auf Island. Invited talk at the Faculty of Geosciences, University of Hamburg, Germany.

Roth F. 1999. Bohrlochmessungen zum Spannungsfeld und zu Aquiferen. Invited talk at the Faculty of Geosciences, Geotechniques and Mining, Technische Universität Bergakademie Freiberg.

Roth, F. & P. Fleckenstein 1999. Report on repeated logging in the framework of PRENLAB-2. Paper presented at the PREN-LAB-2 workshop, Strasbourg, France, March 31, 1999.

4.5 Subproject 5

Einarsson, P., P. Imsland, A.K. Ingimarsson, E.R. Guðmundsdóttir, H. Hallsteinsson, H. Sigurjónsson, J. Guðbjartsson, J. Hendriks, K. Jónsdóttir, K. Ísleifsson, Ó. Hilmarsson, R.H. Sigurðardóttir, S. Hreinsdóttir & V. Roth 1998. Strike-slip faults near Geitafell in the eastern Reykjanes peninsula. In: Abstracts from the spring meeting of the Geoscience Society of Iceland, Reykjavík, Iceland, April 21, 1998. In Icelandic. Paper in preparation 1999.

Gasperi, J., K.L. Feigl, F. Sigmundsson & A. Rigo 1999. Crustal deformation near Hengill volcano, Iceland, 1993-1998: coupling between volcanism and faulting inferred from elastic modelling of satellite radar interferograms, *J. Geophys. Res*, in preparation.

Hreinsdóttir, S., P. Einarsson, F. Sigmundsson & Th. Árnadóttir 1999a. Measurements of continued uplift and expansion at the Hrómundartindur volcanic system. In: Abstracts from the spring meeting of the Geoscience Society of Iceland, Reykjavík, Iceland, April 20, 1999. In Icelandic.

Hreinsdóttir, S., P. Einarsson & F. Sigmundsson 1999b. Crustal deformation at the oblique Reykjanes peninsula plate boundary, SW Iceland, 1993-1998, observed with GPS geodetic measurements. In: Abstracts from the AGU spring meeting, Boston, Massachusetts, May 28 - June 4, 1999.

Johnsson, D.J., F. Sigmundsson & P.T. Delaney 1999. Comment on "Volume of magma accumulation or withdrawal estimated from surface uplift or subsidence, with application to the 1960 collapse of Kilauea volcano" by P.T. Delaney and D.F. McTigue. *Bull. Volc.*, in review.

Jónsdóttir, K., P. Einarsson & V. Hjörleifsdóttir 1999. Fracture systems active in the earthquakes of 1630 and 1784. In: Abstracts from the spring meeting of the Geoscience Society of Iceland, Reykjavík, Iceland, April 20, 1999. In Icelandic.

4.6 Subproject 6

Acocella, V., Á. Guðmundsson & R. Funiciello 1999. The interaction between extensional segments at the Icelandic mid-oceanic ridge. In: Abstracts from the tenth biennial EUG meeting, Strasbourg, France, March 28 - April 1, 1999.

Angelier, J. & F. Bergerat 1998. Stress fields and mechanisms of seismogenic faults: the South Iceland seismic zone as a case example. In: Abstracts from the international workshop on the Resolution of geological analysis and models for earthquake faulting studies, Camerino, June 3-6, 1998.

Angelier, J., F. Bergerat & S.Th. Rögnvaldsson 1998. Seismogenic stress field in the South Iceland seismic zone. In: *Annales Geophysicae.* Abstracts from the XXIII EGS General Assembly, Nice, France, April 20-24, 1998.

Angelier, J., F. Bergerat & C. Homberg 1999a. Variable coupling explains complex tectonic regimes near oceanic transform fault: Flateyjarskagi, Iceland. *Geology*, submitted.

Angelier, J., F. Bergerat & C. Homberg 1999b. Variations in mechanical coupling as a source of apparent polyphase tectonism: the case of the Tjörnes transform zone, North Iceland. In: *Annales Geophysicae.* Abstracts from the XXIV EGS General Assembly, The Hague, The Netherlands, April 19-23, 1999.

Angelier, J., F. Bergerat & S.Th. Rögnvaldsson 1999a. Using inversion of large population of earthquake focal mechanisms to derive the regional seismotectonic field: Iceland. In: Abstracts from the tenth biennial EUG meeting, Strasbourg, France, March 28 - April 1, 1999.

Angelier, J., F. Bergerat & S.Th. Rögnvaldsson 1999b. Perturbation of plate-scale extension across oceanic rift and transform faults revealed by inversion of earthquake focal mechanisms in Iceland. In: *Annales Geophysicae.* Abstracts from the XXIV EGS General Assembly, The Hague, The Netherlands, April 19-23, 1999.

Belardinelli, M.E., M. Bonafede & Á. Guðmundsson 1999. Multiscale surface faulting generated by strike-slip earthquakes in Iceland. In: *Annales Geophysicae.* Abstracts from the XXIV EGS General Assembly, The Hague, The Netherlands, April 19-23, 1999.

Berg, S.S., A. Braathen & Á. Guðmundsson 1999. North-South trending fracture zones in the Sunnfjord region, western Norway. In: Abstracts from the tenth biennial EUG meeting, Strasbourg, France, March 28 - April 1, 1999.

Bergerat, F. & J. Angelier 1998a. Neotectonic evidences from field studies of recent faulting in the South Iceland seismic zone (SISZ). In: *Annales Geophysicae.* Abstracts from the XXIII EGS General Assembly, Nice, France, April 20-24, 1998.

Bergerat, F. & J. Angelier 1998b. Seismotectonics in Southern Iceland: Neotectonic evidences from field studies of recent faulting. In: Abstracts from the international workshop on the Resolution of geological analysis and models for earthquake faulting studies, Camerino, June 3-6, 1998.

Bergerat, F., Á. Guðmundsson, J. Angelier, & S.Th. Rögnvaldsson 1998. Seismotectonics of the central part of the South Iceland seismic zone. *Tectonophysics* 298, 319-335.

Bergerat, F. & J. Angelier 1999a. The South Iceland seismic zone: tectonic and seismotectonic analyses revealing the evolution from rifting to transform motion. *Journ. Geodynamics*, accepted.

Bergerat, F. & J. Angelier 1999b. Fault and stress patterns at different stages of development of oceanic transform zones: examples in Iceland. In: *Annales Geophysicae.* Abstracts from the XXIV EGS General Assembly, The Hague, The Netherlands, April 19-23, 1999.

Bergerat, F., J. Angelier, & C. Homberg 1999. Field studies of recent faulting along the Húsavík-Flatey fault (Tjörnes transform zone Northern Iceland): complex tectonic regimes and variable coupling. In: Abstracts from the tenth biennial EUG meeting, Strasbourg, France, March 28 - April 1, 1999.

Bergerat, F., J. Angelier & S. Verrier 1999. Tectonic stress regimes, rift extension and transform motion: the South Iceland seismic zone. *Geodin. Acta*, in press.

Guðmundsson, Á. 1998a. Development of permeability in fault zones. In: *Annales Geophysicae.* Abstracts from the XXIII EGS General Assembly, Nice, France, April 20-24, 1998.

Guðmundsson, Á. 1998b. Rift-zone and off-rift earthquakes in Iceland. In: *Annales Geophysicae.* Abstracts from the XXIII EGS General Assembly, Nice, France, April 20-24, 1998.

Guðmundsson, Á. 1998c. Extensional veins used to estimate overpressure and depth of origin of fluids in fault zones. Tectonic Study Group Meeting, Trondheim, Norway. Geological Society of Norway.

Guðmundsson, Á. 1999a. Fluid overpressure and flow in fault zones: field measurements and models. Workshop on Fluids and Fractures in the Lithosphere, Tectonic Study Group of Nancy, France. Geological Society of France.

Guðmundsson, Á. 1999b. Extensional veins used to estimate overpressure and depth of origin of fluids in fault zones. In: Abstracts from the tenth biennial EUG meeting, Strasbourg, France, March 28 - April 1, 1999.

Guðmundsson, Á. 1999c. Fluid pressure and stress for large earthquakes. In: *Annales Geophysicae.* Abstracts from the XXIV EGS General Assembly, The Hague, The Netherlands, April 19-23, 1999.

Guðmundsson, Á. 1999d. Injection and arrest of water-filled fractures. In: *Annales Geophysicae.* Abstracts from the XXIV EGS General Assembly, The Hague, The Netherlands, April 19-23, 1999.

Guðmundsson, Á. 1999e. Flow of groundwater into and along fault zones. In: *Annales Geophysicae.* Abstracts from the XXIV EGS General Assembly, The Hague, The Netherlands, April 19-23, 1999.

Guðmundsson, Á. 1999f. Postglacial crustal doming, stresses and fracture formation with application to Norway. *Tectonophysics*, in press.

Guðmundsson, Á. 1999g. Fluid overpressure and stress drop in fault zones. *Geophys. Res. Lett.* 26, 115-118.

Guðmundsson, Á. & C. Homberg 1999. Evolution of stress fields and faulting in seismic zones. *Pure Appl. Geophys.* 154, in press.

Henriot, O., T. Villemin & F. Jouanne 1998. Surface deformation at the Tjörnes rift-transform junction (North Iceland) computed from SAR images. In: *Annales Geophysicae*. Abstracts from the XXIII EGS General Assembly, Nice, France, April 20-24, 1998.

Henriot, O., T. Villemin & F. Jouanne 1999. Seismic risk in northern Iceland (2): deformation maps of Tjörnes peninsula computed from INSAR. In: Abstracts from the tenth biennial EUG meeting, Strasbourg, France, March 28 - April 1, 1999.

Jouanne, F., T. Villemin & GPS-TFZ TEAM 1999. Seismic risk at the rift-transform junction in North Iceland. *Geophys. Res. Lett.*, submitted.

Rögnvaldsson, S.Th., Á. Guðmundsson & R. Slunga 1998. Seismotectonic analysis of the Tjörnes fracture zone - an active transform fault in North Iceland. *J. Geophys. Res.*, 103, 30117-30129.

Villemin, T., F. Jouanne & GPS-TFZ TEAM 1998. 1995-1997 surface deformation along the Húsavík-Flatey transform fault and around its junction with the northern volcanic zone in Iceland. In: *Annales Geophysicae*. Abstracts from the XXIII EGS General Assembly, Nice, France, April 20-24, 1998.

Villemin, T., V. Ferber & M. Colombet 1999. Fault and fissure pattern in a volcanic rift zone: the Krafla fissure swarm in northern Iceland as a case example. *Journal of Structural Geology*, submitted.

Villemin, T., O. Henriot & F. Jouanne 1999. Seismic risk in northern Iceland (1): Locking of the Húsavík fault deduced from GPS. In: Abstracts from the tenth biennial EUG meeting, Strasbourg, France, March 28 - April 1, 1999.

Villemin, T., G. Ouillon & V. Ferber 1999. Processes of fractures pattern evolution deduced from field data: the Krafla fissure swarm and the last rifting episode in North Iceland. *J. Geophys. Res.*, submitted.

4.7 Subproject 7

Belardinelli M.E., M. Bonafede & Á. Guðmundsson, 1999. Secondary earthquake fractures generated by a strike-slip fault in the South Iceland seismic zone. *J. Geophys. Res.*, submitted.

Bonafede M. & N. Cenni 1998. A porous flow model of magma migration within Mt. Etna: the influence of extended sources and permeability anisotropy. *J. Volcanol. Geotherm. Res.* 81, 51-68.

Bonafede M. & M. Mazzanti 1998a. Modelling gravity variations consistent with ground deformation in the Campi Flegrei Caldera. *J. Volcanol. Geotherm. Res.* 81, 137-157.

Bonafede M. & M. Mazzanti 1998b. Residual gravity variations in volcanic areas: constraints to the interpretation of the uplift episodes at Campi Flegrei - Italy. *Physics and Chemistry of the Earth and Solar System*, submitted.

Bonafede M. & A. Neri 1999. Effects induced by an earthquake on its fault plane: a boundary element study. *Geophys. J. Int.*, submitted.

Bonafede M. & B. Parenti 1999. Crack models of strike-slip faults in a layered elastic half-space. In preparation.

Bonafede M. & E. Rivalta 1999a. The tensile dislocation problem in a layered elastic medium. *Geophys. J. Int.* 136, 341-356.

Bonafede M. & E. Rivalta 1999b. On tensile cracks close to and across the interface between two welded elastic half-spaces. *Geophys. J. Int.* 138, in press.

Roth, F. 1998. Modellrechnungen zu den plattentektonischen, insbesondere seismotektonischen Spannungen auf Island (Model calculations on plate tectonic and especially seismotectonic stresses on Iceland). Paper presented at the 4th workshop of the FKPE-working group on Borehole Geophysics and Rock Physics, Hannover, Germany, 1998.

Roth, F. 1999a. Stress changes in space and time at the South Iceland seismic zone - model calculations. Poster presented at the workshop on Recurrence of Great Interplate Earthquakes and its Mechanism, Kochi, Shikoku, Japan, January 20-22, 1999. Japan Science and Technology Agency.

Roth, F. 1999b. Entwicklung des tektonischen Spannungsfeldes im Süden Islands - Modellierung einer Erdbebenserie (Development of the tectonic stress field in the South of Iceland - modelling of an earthquake series). Paper presented at the 59th Annual Meeting of the German Geophysical Society, Braunschweig, Germany.

Roth, F. 1999c. Stress changes in space and time at the South Iceland seismic zone - model calculations In: Abstracts from the tenth biennial EUG meeting, Strasbourg, France, March 28 - April 1, 1999.

Roth, F. 1999d. Erforschung von Erdbeben auf Island (Research about earthquakes on Iceland). Paper presented at the Institute of Geophysics, University Hamburg, on invitation of the Faculty of Geosciences.

Roth, F. 1999e. Stress changes in space and time at the South Iceland seismic zone - model calculations. Expanded abstract in the proceedings of the workshop on Recurrence of Great Interplate Earthquakes and its Mechanism, Kochi, Shikoku, Japan, January 20-22, 1999. Japan Science and Technology Agency.